

**MCAT Institute
Final Report
94-003**

Computational Study Of Generic Hypersonic Vehicle Flow Field

Johnny R. Narayan

May 1994

NCC2-715

**MCAT Institute
3933 Blue Gum Drive
San Jose, CA 95127**

WORK STATEMENT

**ORIGINAL CONTAINS
COLOR ILLUSTRATIONS**

The co-operative agreement was initiated for achieving the following:

1. Carry out a tip-to-tail computation of the flow field of a generic hypersonic vehicle in the power-on configuration. The main focus of the task was to establish and demonstrate a solution procedure/strategy that would be useful for solving the entire flow field associated with an airbreathing hypersonic vehicle. The plan was to utilize available Computational Fluid Dynamics (CFD) codes for this purpose rather than generating a new specialized CFD solver. This would need modifications to the codes to enhance their capabilities in terms of accurate models for physical features such as turbulence, finite rate chemistry, improved boundary conditions etc.
2. Develop and demonstrate a turbulence-chemistry interactions model applicable for high-speed reacting flows involving finite rate chemistry.

The following sections describe the milestones achieved, work in progress and suggestions for future work pertaining to the items described above. In this report, bibliographical references to the physical models such as the turbulence models, thermodynamic models, finite rate chemistry models etc. and CFD codes used are omitted. However, these references can easily be obtained from the attached publications pertaining to the present task.

HYPERSONIC TIP-TO-TAIL COMPUTATION

The geometry of the generic hypersonic vehicle configuration was provided by Dr. Tom Edwards of the Computational Aerosciences Branch, Fluid Dynamics Division at NASA Ames Research Center. The geometric data included body definitions and preliminary grids for the forebody (nose cone excluded), midsection (propulsion system excluded) and afterbody sections. This data was to be augmented by the nose section geometry (blunt conical section mated with the non circular cross section of the forebody initial plane) along with a grid and a detailed supersonic combustion ramjet (scramjet) geometry (inlet and combustor) which should be merged with the nozzle portion of the afterbody geometry. The solutions were to be obtained by using a Navier-Stokes (NS) code such as **TUFF** for the nose portion, a Parabolized Navier Stokes (PNS) solver such as the **UPS** and **STUFF** codes for the forebody, a NS solver with finite rate hydrogen-air chemistry capability such as **TUFF** and **SPARK** for the scramjet and a suitable solver (NS or PNS) for the afterbody and external nozzle flows. Proper interfacing was to be maintained between the solutions of the different sections.

NOSE SECTION

The nose is assumed to be a blunt one in the present computations in keeping with the accepted designs for an airbreathing hypersonic vehicle. As mentioned above, the nose section is a blunt-nosed cone at zero angle of attack. An axisymmetric grid was generated for the nose section using the graphic utility **VG** available on workstation **win35**. The **TUFF** code was used to solve the flow field upto the axial location corresponding to the first plane of the forebody geometry. Finite rate nonequilibrium air-chemistry model was used along with a two-equation turbulence (k-epsilon) model. The flow Mach number was 15 and the Reynolds number based on unit length was 1,700,000. The surface of the body was assumed to be maintained at a constant temperature of 243.4 K. No-slip boundary conditions were used at the body surface. The solutions were then interpolated onto the first plane of the forebody grid.

FOREBODY

Computations were carried out using the PNS solvers **STUFF** and **UPS** in order to ascertain that these codes were equivalent as far as the present application was concerned. The nose-section solution was used along with the forebody grid for this purpose. The solutions were obtained for the flow field around the entire forebody upto the inlet location. Baldwin-Lomax turbulence model was used since the version of the **UPS** code used does not have the two-

equation turbulence model capability. The solutions were compared (temperature, velocities and pressure) and found to be in excellent agreement. Since the **TUFF** and **STUFF** codes have similar structure and physical models, it was decided to use them for the NS and PNS applications, respectively, unless conditions dictated the utilization of a different code such as **SPARK**. This would be extremely useful in interfacing solutions between different sections of the vehicle.

Since the nose section was a conical body with circular cross section, it was necessary to generate a series of cross sections at designated intervals which changed in shape from a circle to that of the first cross section of the forebody grid. A three dimensional grid that bridged the last plane of the nose section with the first plane of the forebody was then generated using these surface definitions (cross sections) and was combined with the given forebody grid to form the new three dimensional grid for the forebody flow field solutions. These solutions were obtained by using the space marching PNS solver **STUFF**. The nose-section solutions were used as initial data for this purpose. The two-equation (k-epsilon) turbulence model including low-Reynolds number terms to account for the near-wall flow field was used and the finite rate air-chemistry model of the nose section was maintained. Even though the turbulence field was not one of the primary targets in these computations, turbulence modeling at the two-equation level was maintained in anticipation of the inlet/combustor flow simulations which require the use of the physically more realistic two-equation model rather than the simple and easy to use algebraic Baldwin-Lomax model. As a result, the computations required more computer resources. Typical results (composite since the full computational data at all the x-locations could not be stored) are shown in the figures at the end of the report. Computationally, there were no unforeseen difficulties in obtaining these solutions. This task was completed in September, 1992.

INLET

The inlet computations represent the critical (bottleneck) part of the entire tip-to-tail solutions. The difficulty was associated with the proper choice of a realistic inlet configuration at the same time minimizing the computational effort which utilized the available resources in an efficient manner. The geometric restrictions imposed by the limited length of the entire scramjet propulsion system to achieve the power requirements for the hypersonic flight is a major factor to be considered here. The mixing between the incoming airflow and the injected fuel dominates the flow field and the mixing efficiency plays a major role in determining the dimensions and geometry of the inlet. Also, physical aspects of the flow such as inlet unstart, flow spillage at

the cowl location to maintain the proper air flow etc. are key factors that must be dealt with in the solutions. The solutions are computationally intensive, requiring an enormous amount of computational resources. Since the incoming forebody flow is three dimensional, the inlet flow solutions also require fully three dimensional analyses.

The computational effort was divided into a series of tasks. First, an inlet configuration had to be selected. Since the present work was meant to be a demonstration type with the purpose of establishing a solution procedure/strategy for carrying out tip-to-tail computations, it was decided to use a multi-module scramjet inlet for the present task. This would conform to the widely accepted inlet configurations being used in research and development efforts carried out at a majority of establishments working in the area of hypersonic flight. In order to reduce the computational effort thus minimizing the demand for computational resources, a three-module configuration that spans the entire undersurface of the vehicle was chosen for the present task. The next task was concerned with the selection of the geometric configuration of each inlet module. Once again, taking into account the realistic configurations and keeping with the aim of minimizing computational effort, a swept-back twin strutted module with side-wall compression was chosen for the present task. A sweep angle of 30 degrees was chosen along with a strut angle of 6 degrees. A schematic view of the inlet module is given in the figures.

The above mentioned choice for the inlet geometry immediately introduced a new problem. This problem was associated with the choice of the particular CFD solver to be used for the solutions. The multiple-module configuration with the cowl plate located downstream of the strut tip introduced a variety of boundary conditions at different locations in the flow field. For example, a typical module has solid walls on three of the six boundary surfaces that define its geometry (omitting for the time being factors such as injection at solid walls). The inlet and exit boundaries pose no serious problems also. However, the fourth boundary that is aligned with the cowl plate surface involves both no-slip and flow-through conditions which are not easy to implement in the CFD codes under consideration. Also, due to the presence of the struts inside the flow region, an enormous grid (single, 3-D) would be required to have any chance at obtaining a realistic solution. The grid needed would be impractical to be used with a NS solver. As a result, a multi-block NS solver that includes all the physical models used for the computing the flow field around the forebody was needed. The multi-block version of the TUFF code became available at that time and hence was selected as the CFD solver for the inlet flow analysis. However, the problems associated with mixed boundary conditions, alluded to earlier, still remained requiring modification of the multi-block TUFF code to account for mixed boundary conditions. These modifications were incorporated in the solver which required

considerable resources in terms of manpower as well as computational resources for validation. The changes led to a system by which different boundary conditions (from among the original options provided in the solver) could be specified at every grid point on the six boundary surfaces.

The fuel of choice for the present case is hydrogen. However, the chemistry model in the TUFF code was for hydrocarbon-air combustion. This led to further modifications to the code whereby a hydrogen-air (finite rate) chemistry model involving nine species (hydrogen, oxygen, water, OH, H, O and nitrogen) and 20 reaction steps (suggested by the NASP Technical Committee) was incorporated. Also, thermodynamic models valid over a wider range of temperature than before was incorporated (by the author of the code). Even though chemical reactions involving combustion are not expected in the inlet, the chemistry model is included for the inlet flow solutions so as to be consistent with the combustor solutions which would follow.

The solution domain is divided into adjoining blocks/zones with distinct boundary conditions. This is done in such a way that the occurrence of mixed boundary conditions along the boundaries is kept to a minimum. A multi-block grid involving 7 blocks was generated for the solutions. A schematic of the block arrangement is shown in the figures along with a representation of the grid system. The solution of the flow in the inlet represents the most computationally intensive part of the entire solution process. The flow is both external and internal involving strong and weak shocks/expansions in the domain. The precompressed air from the forebody (undersurface, mainly) enters the multiple module inlet and undergoes further changes due to the geometry of the inlet. There is flow spillage at the cowl requiring to pay extra attention to the grid there.

Solution of the inlet flow was carried out over a long period of real time. One of the reasons for this was the fact that the computer resources ran out in 1992 about four months before the start of the next account year, virtually stopping the computationally intensive inlet flow solutions for about four months. Only peripheral work could be done at that time. The solutions were finally completed by July 1993. Representative results are included at the end of the report.

COMBUSTOR

The outflow from the inlet were to be used for the solution of the flow field beyond the cowl lip location (all internal flow, wall bounded) into the combustor. The grid for this section

(throat+combustor) is already generated. In order to save computational resources, it was decided to carry out the solution corresponding to only one of the modules (rather than all the three). However, the grid for all the three modules has already been generated in case a full configuration solution is needed. The throat flow solution is completed and is to be used for the combustor flow solution.

The combustor geometry involves a backward facing step at the end of the strut wall extension in order to facilitate injection of hydrogen into the air flow. A 7-species, 7-reaction steps finite rate chemistry model will be used for the combustor flow simulations. The turbulence model is still the two-equation model described before.

TURBULENCE -CHEMISTRY INTERACTION MODEL

The numerical simulation of the hypersonic propulsion system for the generic hypersonic vehicle is the major focus of this entire work. Supersonic combustion ramjet (scramjet) is such a propulsion system as mentioned in the previous section. Hence the main thrust of the present task has been to establish a solution procedure for the scramjet flow. The scramjet flow is compressible, turbulent and reacting. The fuel used is hydrogen and the combustion process proceeds at a finite rate. As a result, the solution procedure must be capable of addressing such flows. The codes chosen for the present work are the TUFF and the SPARK codes. The modifications done to the codes (by the principal investigator on SPARK and TUFF and by Dr. Gregory Molvik on TUFF) are: 1) added the two-equation k -epsilon turbulence model (with low-Re correction terms), 2) added two-equation k -omega turbulence model, 3) added two compressibility correction models for high-speed applications, 4) added a 9-species, 20-reaction steps finite rate hydrogen-air chemistry model and 5) developed and incorporated a turbulence-chemistry interaction model (SPARK only at present). These modifications were carried out over the duration of the period mentioned in the beginning. So far, six technical papers have been presented (OR to be presented in the near future) in national and international meetings and one journal publication has been completed based on the work done under this section of the task. Copies of the important publications (not all of them because the paper presented at two international meetings were already published in USA) are attached at the end of this report. Since these publications contain all the relevant technical details of the models, test cases etc. those details will not be given in the main body of the report.

Since the reaction mechanism in the scramjet is highly dependent upon the mixing between the fuel and oxidizer streams and the reaction zone is mainly confined (initially) to this mixing region, it is logical to validate the solution procedure on reacting mixing layer configurations. This is the strategy followed in the present study. First a two-dimensional nonreacting mixing layer configuration was computed using all the relevant codes. They produced nearly identical results thus proving the basic consistency of the solution procedures. The same geometry was used for the mixing and reaction between the fuel and oxidizer streams at high speeds. Since any validation procedure must include comparison with experimental data, a search was made to secure this data. Useful experimental data in the area of high speed reacting flows is extremely rare and available data sets are nowhere near being adequate for a thorough validation effort. Available experimental data correspond to two basic configurations: 1) two-dimensional (Burrows-Kurkov experiment) and 2) Coaxial jet case where two coflowing jets (inner one is hydrogen and the outer one is vitiated air) . Both these cases were used for the validation effort as detailed in the attached publications. Representative figures are given in this regard.

The flow field in the combustor is extremely complex. There are interactions between the many different physical aspects of the flow, such as the interaction between the turbulence field and the mean flow, interaction between heat release and mean flow and the interactions between turbulence and chemistry. Of these, the last one forms the basis for the present work. A turbulence-chemistry interactions model was developed in cooperation with the scientists at NASA Langley research center (please see attached publications) and this model was demonstrated by means of the two-dimensional reacting mixing layer case mentioned in the beginning of this section. This model represents the first step in the effort to achieve an accurate model for depicting the turbulence-chemistry interactions. The mixing rate is heavily dependent upon the turbulence field and if the turbulence field is affected by the chemistry, then it will affect the physical aspects of the flow such as ignition (since mixing is affected). Also, from a practical point of view, the length of the combustor is a very important parameter in the design of the hypersonic vehicle because the propulsion system is highly integrated with the vehicle airframe. If the mixing process is affected by the interactions mentioned above, then it could lead to impractical dimensions of the combustor. On the other hand, these interactions may have a positive effect and help to come up with a more compact geometry for the propulsion system than before. The main point here is the fact that the solution procedure must have the capability to include these interactions in the computations. The present work provides such a capability and the model is being improved.

The task under the cooperative agreement was designed to last a longer period of time than the duration corresponding to this report. As a result, the full tip-to-tail computational demonstration on a realistic configuration could not be completed. For example, the combustor flow calculations are just beginning and the nozzle flow computations are yet to begin. So this final report refers only to the work completed by the principal investigator during the past three years. However, the solution strategy is in place and the tools (e.g.. TUFF, grid) are identified and readied. Should the need arise, it should be a straight forward process to go from where the current work is today to the completion of the full tip-to-tail computations. The principal investigator extends the offer to help in initiating such a task should the need arise.

ACKNOWLEDGMENTS

The PI would like to acknowledge the invaluable contributions (suggestions, code development and computations) from Dr. Gregory A. Molvik during this task. Also, the contributions from Dr. Thomas Edwards, Dr. Scott Lawrence (both of NASA Ames) and Dr.Ganesh Wadawadigi of U.of Texas at Arlington are acknowledged and appreciated. The PI is grateful to the MCAT Institute for providing the vehicle to carry out this research effort. Finally, the PI would like to acknowledge the opportunity and assistance provided by the Applied Computational Aerosciences branch (Dr.Terry Holst, branch chief) of the Fluid Dynamics division at NASA Ames Research Center.

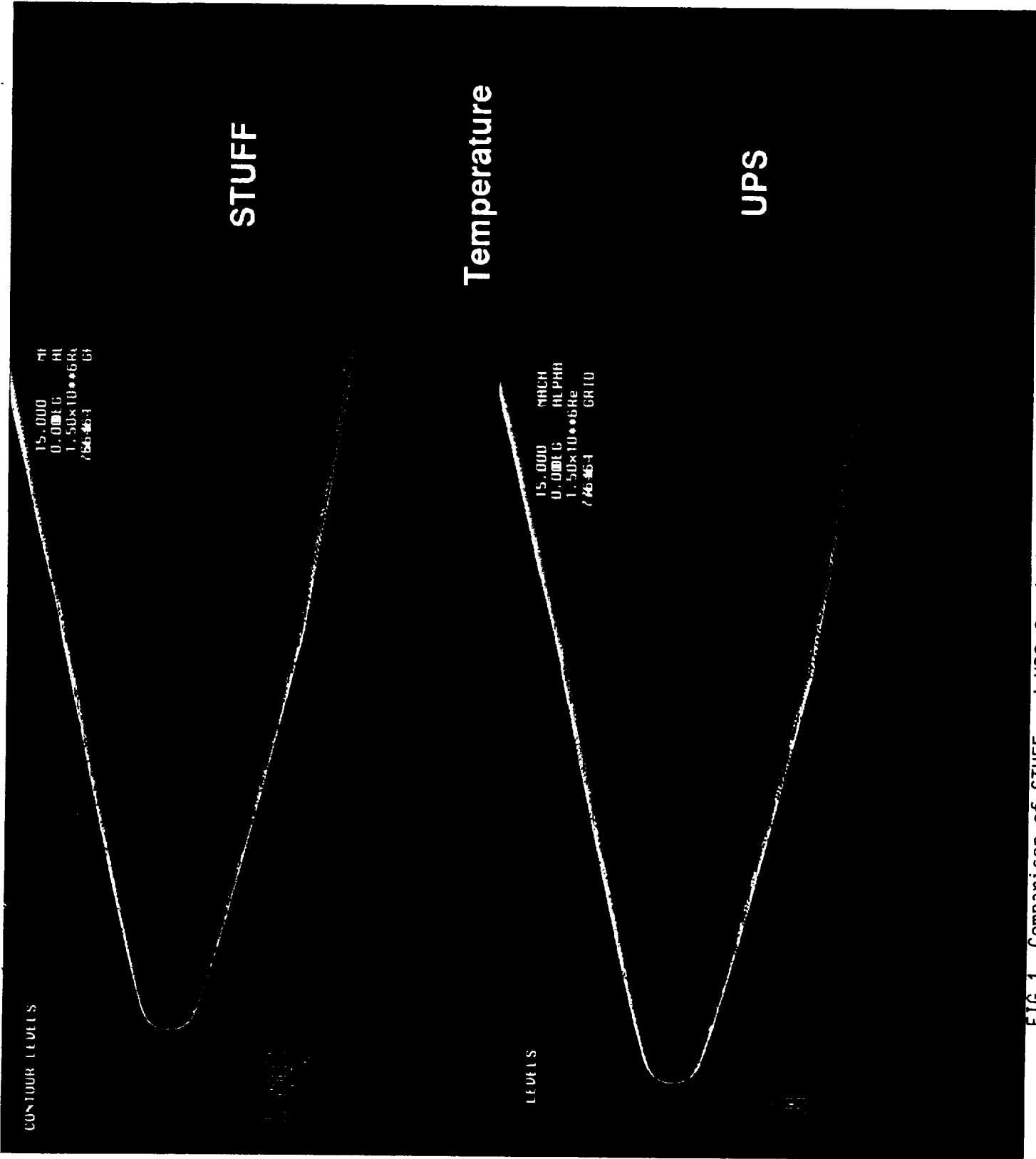


FIG.1 Comparison of STUFF and UPS forebody solutions (zoom view)

STUFF

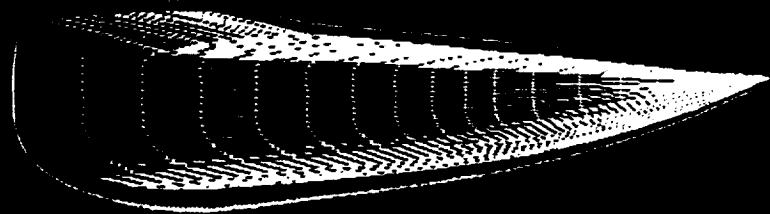
Temperature

UPS

FIG. 2 Comparison of STUFF and UPS forebody solutions

Forebody Solution

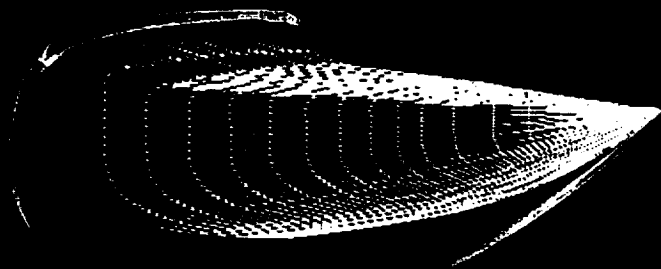
CONTOUR LEVELS



CONTOUR LEVELS

CONTOUR LEVELS

Temperature



Pressure

Mach Number = 15

FIG.3 Forebody temperature and pressure contours

Generic Hypersonic Inlet Geometry



FIG. 4 Generic hypersonic inlet geometry

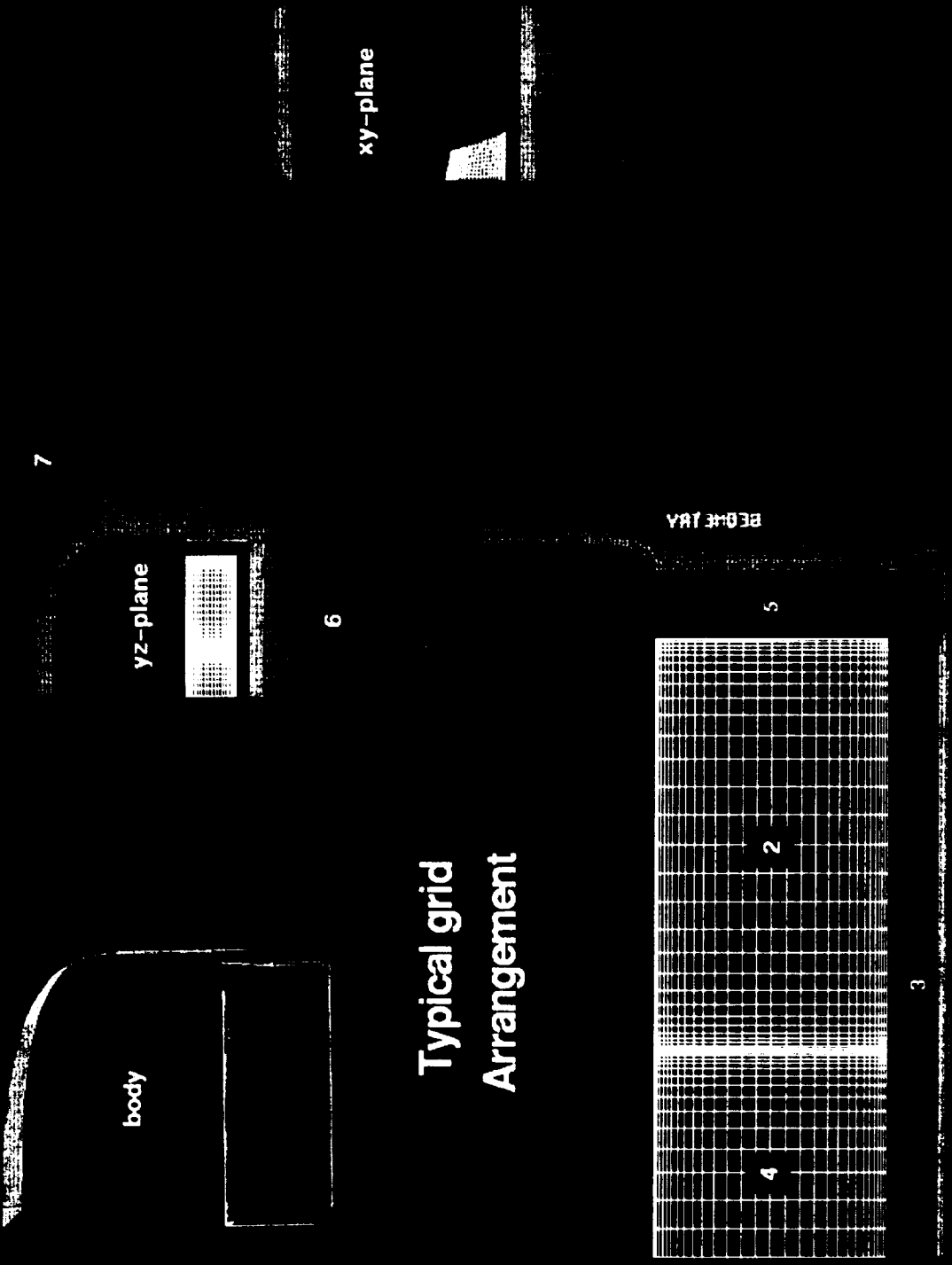


FIG. 5 Grid for hypersonic inlet geometry

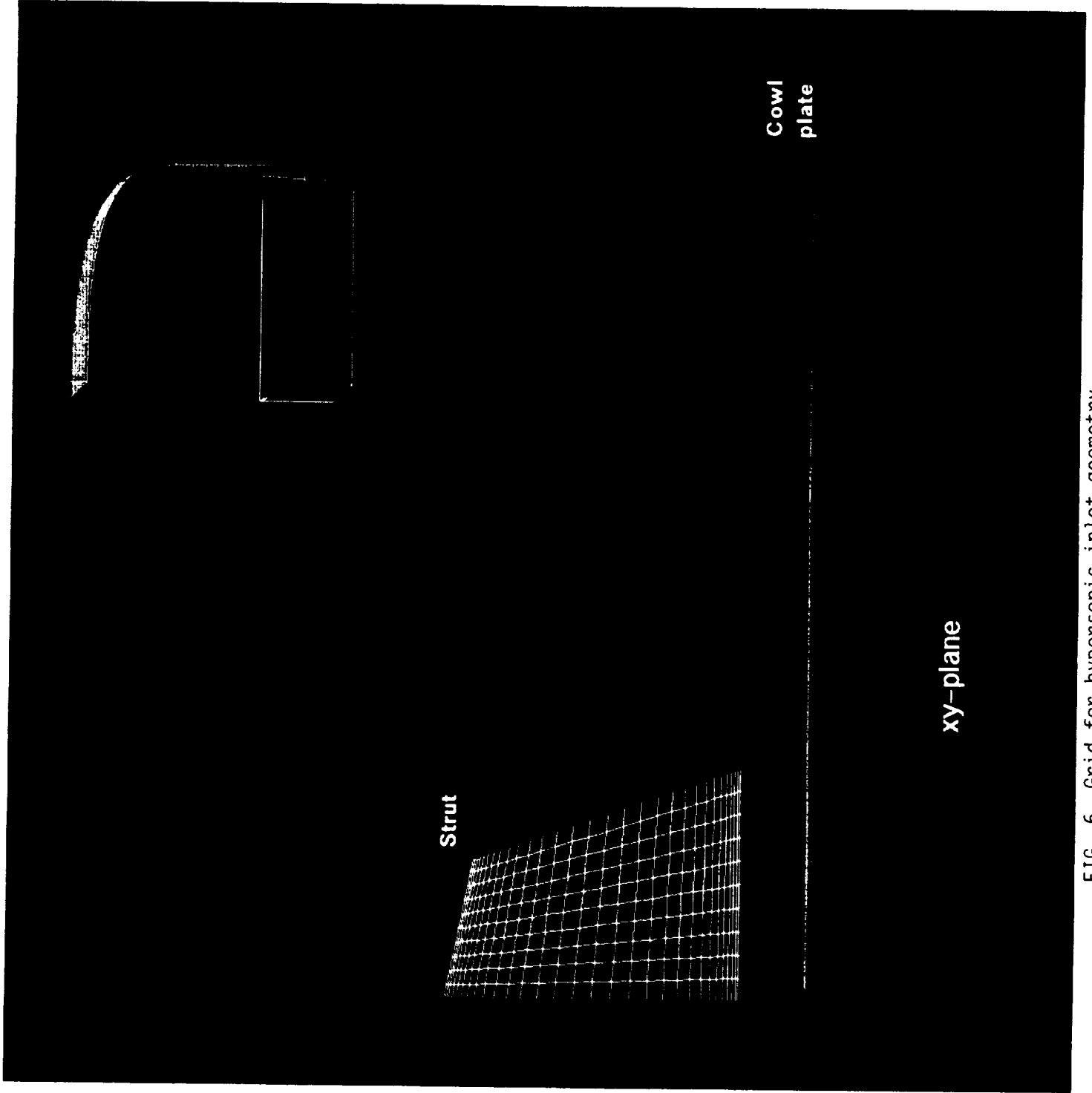


FIG. 6 Grid for hypersonic inlet geometry

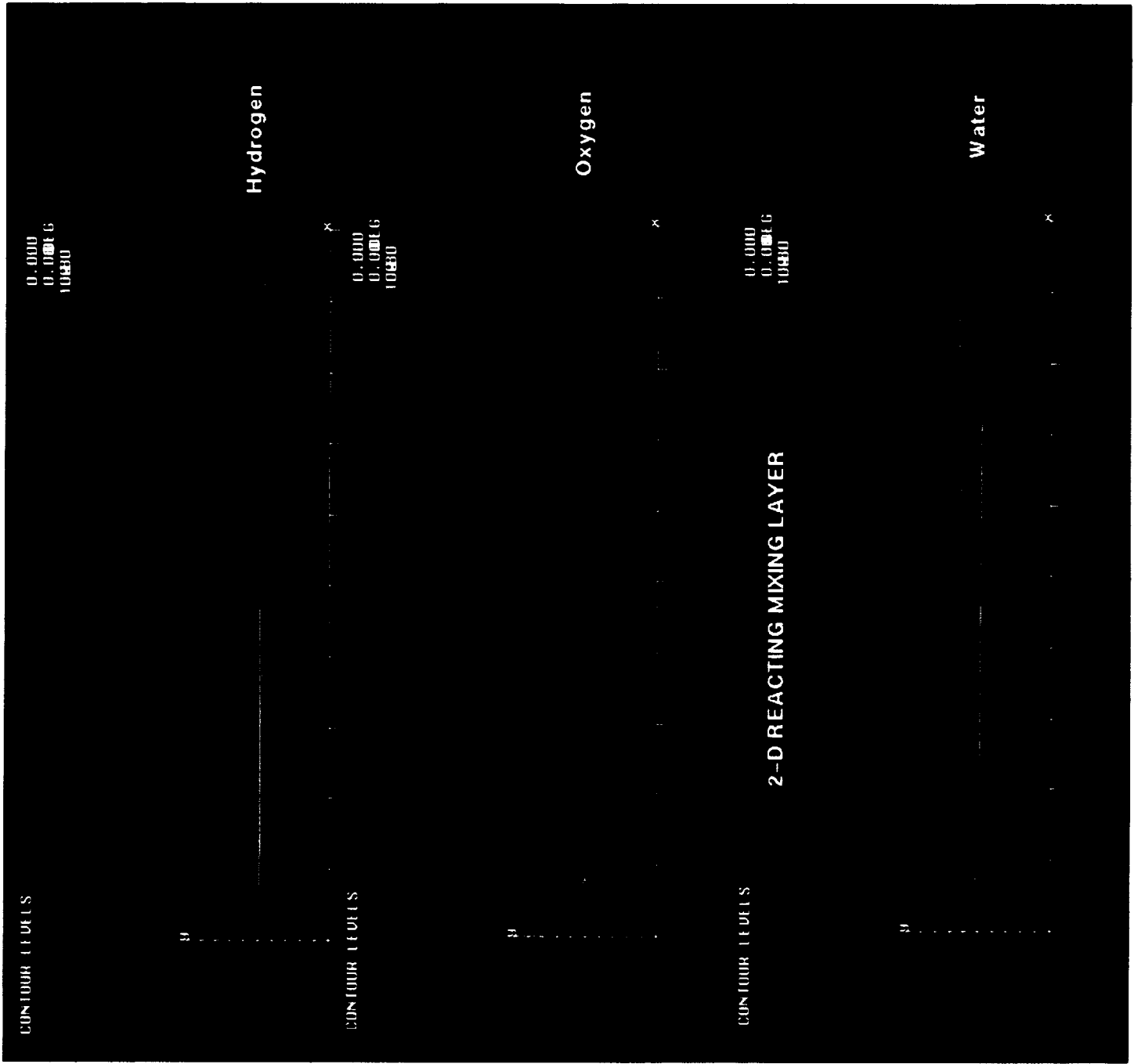


FIG. 7 2-D reacting mixing layer results

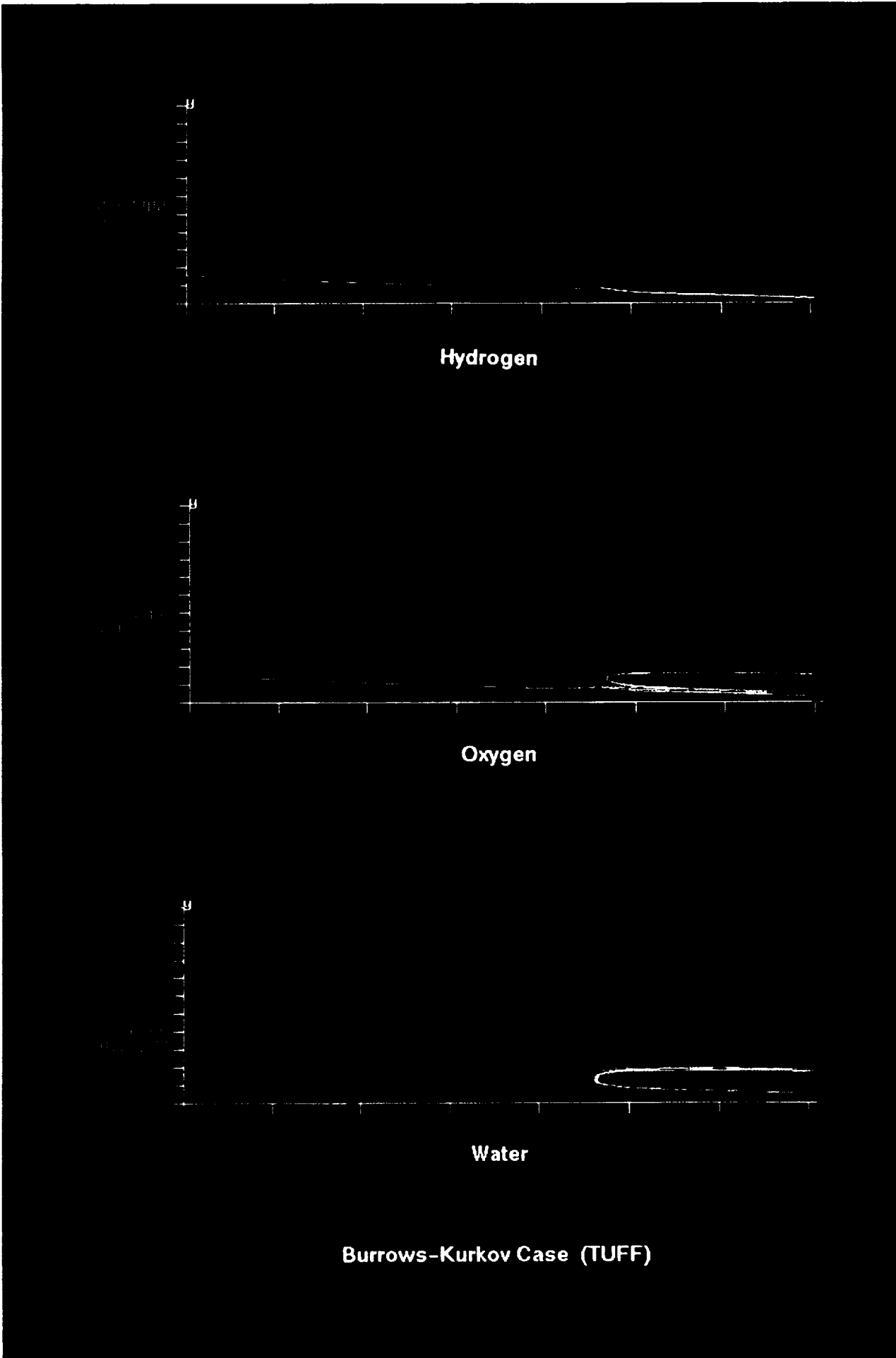


FIG. 8 Burrows Kurkov test case results

APPENDIX - A

AIAA-94-2311

NIS

**Effect of Turbulence - Chemistry
Interactions In Compressible Reacting Flows**

**Johnny R. Narayan
MCAT Institute
Moffett Field
California**

EFFECT OF TURBULENCE-CHEMISTRY INTERACTIONS IN COMPRESSIBLE REACTING FLOWS

J.R. Narayan*

MCAT Institute, NASA ARC, Moffett Field, CA.

ABSTRACT

The objective of this work is to investigate the effect of the interactions between the turbulent scalar field and chemistry in compressible, reacting turbulent flows. A model for these interactions has been proposed. In the thermochemistry model, the effects of temperature and species concentration fluctuations on the species mass production rates are decoupled. The effect of temperature fluctuations is modelled via a moment model and the effect of concentration fluctuations is accounted for using an assumed β -pdf model. A two equation (k - ω) model with compressibility correction is used to calculate the turbulent velocity field. Preliminary results for the case of a two-dimensional reacting mixing layer are presented. Computations are carried out using the Navier-Stokes solver SPARK, with a finite rate chemistry model for hydrogen-air combustion.

NOMENCLATURE

A, b	coefficients in Arrhenius rate equation
C_1, C_2	turbulence model constants
E	total internal energy
f_n	mass fraction of species n
g	scalar variance (enthalpy, mass fraction)
H	source vector
H	total enthalpy
h	static enthalpy
k	turbulent kinetic energy
k_f, k_b	forward and backward reaction rate constants
L	number of reaction steps
M_n	Molecular weight of species n
M_t	Turbulent Mach number
N	number of chemical species
Pr, Pr_t	laminar and turbulent Prandtl numbers
p	pressure
Re_c, Re_T	turbulence model coefficients
Re_k, Re_ω	turbulence model coefficients
Sc, Sc_t	laminar and turbulent Schmidt numbers
T	temperature
T_a	Activation Temperature
t	time

Δt	time step
U	dependent variable vector
\vec{U}	velocity vector
\dot{w}_n	production rate of species n
x	streamwise coordinate
x_j	j^{th} coordinate
y	transverse coordinate
α, α^*	turbulence model coefficients
α_0, α_0^*	turbulence model coefficients
δ_{ij}	Kronecker delta
ϵ	turbulence energy dissipation rate
ϵ_c	compressible dissipation rate
ϵ_g	dissipation rate in g -equation
η	compressibility correction coefficient
γ	ratio of specific heats
ω	specific dissipation rate
μ	laminar viscosity
μ_t	turbulent viscosity
ν	kinematic viscosity
ρ	density
$\sigma_d, \sigma_k, \sigma_\omega$	turbulence model constants
τ_{ij}	stress tensor
Φ_j	flux vector in j^{th} direction
Subscripts	
t	turbulent quantity

INTRODUCTION

Advanced air-breathing propulsion systems such as the supersonic combustion ramjet (scramjet) have been studied for a long time as candidates for high-speed propulsion. Mixing between fuel and oxidizer, heat release, presence of shocks and the chemical reactions are some of the major aspects of such flows. Computations and experiments of the flow fields in the combustors of such systems reveal a complex interplay of these physical phenomena. The effect of turbulent mixing on chemical reaction is an example of such an effect which must be addressed in designing such a propulsion system. One such effect, the turbulence-chemistry interaction, is the subject of our present study. Design parameters such as the mode of fuel injection, flame stabilization, ignition delay, combustion efficiency etc. may be influenced by these interactions.

*Senior Research Scientist, Senior Member AIAA.

There are many factors that affect the successful evaluation of the combustor flow. The flow field in the combustor is turbulent and compressible. A further complication is introduced by the high heat release in the combustor. Today, an ideal procedure for the study of such problems (in the absence of exact analytical solutions to the governing equations) will be a combination of an accurate numerical solver coupled with experimental data to (i) validate the numerical solver and (ii) to provide valuable comparison data for the particular combustor configuration being studied. The calculation method must be capable of addressing high-speed, turbulent, reacting, compressible fluid flows involving high energy release. There is a glut of useful numerical solvers applicable for a wide variety of flows including all speed regimes. The capabilities of the computational fluid dynamics (CFD) codes depend upon the sophistication and accuracy of the models used to simulate the various physical processes involved. There has been a lot of progress made in the development of accurate turbulence models in the recent years. Finite rate chemistry including nonequilibrium thermodynamics is another area where significant progress has been made. Computational algorithms which are fast and accurate are being improved everyday. Computers which can run these codes are also being improved. However, every one of these areas is still under development and as a result there is no single CFD code which includes the accurate models and algorithms in all the areas. Limitations such as the maximum grid size, temperature range of applicability of thermodynamics models, number of steps in a finite rate reaction model, near-wall applicability of the turbulence model etc. still affect the usefulness of these CFD codes. On the other hand, experimental study of such problems is not possible at present due to the lack of adequate facilities. Fortunately, many of the major issues can be addressed using current CFD tools.

The focus of the present work is on the turbulence model(s) used for reacting, compressible flows. Specifically, the interaction between the turbulence field and the chemical kinetics is of interest. The effect of turbulence on phenomena such as mixing between two streams, boundary layer etc. has been studied extensively and it is an ongoing process. However, there is not enough work done in the area of turbulence-chemistry interactions to either emphasize or neglect the importance of such interactions. The main reason for this is the fact that it is extremely difficult to measure these interactions quantitatively. Recently, there have been efforts aimed at establishing pdf-based models for coupling the turbulence field with the thermochemical field in numerical simulations. References [1], [2], [3], [4] and [5] are just a few of the many reports

available in this area. There has also been a concerted effort to generate validation data bases through direct numerical simulations. Even though there is a lot of publications in this area, this effort is still in its early stages.

In a computational analysis of flow fields the choice of turbulence model(s) is dictated by two conflicting requirements. The model should (i) be reasonably accurate with good physical justification; and, (ii) be computationally feasible for complex flow geometries. The turbulence model used in the present instance is a two-equation ($k - \omega$) model [6, 7], modified to account for compressibility. The effect of compressibility in turbulent flows is an important aspect of high speed turbulent flows. There has been a significant effort aimed at developing models to account for these effects [8, 10]. These models have been used to predict shear layer growth rates with some success [11, 12]. The model used in the present computations is the one developed by Zemen [10]. On the thermochemistry front, the effects of temperature and species fluctuations are decoupled. For the temperature-turbulence interaction, a moment model is used [1]. The chemical species fluctuations are accounted for using an assumed multivariate- β -pdf model [1, 2, 3]. The thermochemistry models used here are independent of the model for the turbulent velocity field. These models require the solution of the evolution equations for all the mean flow thermo-chemical variables, turbulent kinetic energy (k), specific dissipation rate (ω), enthalpy variance and turbulent scalar energy (sum of all the species variances). The CFD code used is SPARK [13], developed at NASA Langley Research Center.

Mixing plays a major role in high speed combustor flows. The reaction zone is mainly confined to mixing layers that exist between fuel and oxidizer streams. Efficient mixing of fuel and oxidizer is very important for the design of combustor size. Mixing layers ranging from subsonic to supersonic speeds have been studied extensively over the years [1, 11, 14, 15, 16, 17, 18, 19, 20]. However, most of those studies use oversimplified models for turbulence-chemistry interactions. In the present work, a two-dimensional, compressible, reacting, mixing layer (hydrogen-air) is computed with the aforementioned, more realistic turbulence-chemistry interaction model. The reaction model (hydrogen-air) used is described in Ref. [21] (9 species and 20 reaction steps) and is given in Table 1. Experimental data from compressible, reacting mixing layers is still scarce which hinders the validation of the calculation procedure. As a consequence, the comparison of results is confined to those obtained with and without the interaction model.

The governing and secondary equations used in the

computations have all been described in detail in the references cited above. Only an abbreviated equation set will be given in the present paper. The computations were performed on the supercomputers of NAS and NASA Ames Research Center (C-90).

GOVERNING EQUATIONS

The continuity equation, Navier-Stokes equations, energy equation and species continuity equations govern the instantaneous evolution of the flow variables [1, 15, 22]. Density-weighted averaging [23] is used to derive the mean flow equations from these equations. The dependent variables, with the exception of density and pressure, are written as

$$\phi = \tilde{\phi} + \phi'' \quad (1)$$

where the ϕ'' is the fluctuating component of the variable under consideration and its Favre-mean $\tilde{\phi}$ is defined as

$$\tilde{\phi} \equiv \frac{\overline{\rho\phi}}{\bar{\rho}} \quad (2)$$

In this equation, the overbar indicates conventional time-averaging. Density and pressure are split in the conventional sense as,

$$\rho = \bar{\rho} + \rho' \quad \text{and} \quad p = \bar{p} + p' \quad (3)$$

The averaged continuity and momentum equations are

$$\frac{\partial \bar{\rho}}{\partial t} + \frac{\partial \bar{\rho} \tilde{U}_i}{\partial x_i} = 0 \quad (4)$$

$$\frac{\partial \bar{\rho} \tilde{U}_i}{\partial t} + \frac{\partial \bar{\rho} \tilde{U}_i \tilde{U}_j}{\partial x_j} = - \frac{\partial \bar{p}}{\partial x_i} - \frac{\partial \overline{\rho u_i'' u_j''}}{\partial x_j} + \frac{\partial \tau_{ij}}{\partial x_j} \quad (5)$$

where

$$\tau_{ij} = \mu \left(\frac{\partial u_i}{\partial x_j} + \frac{\partial u_j}{\partial x_i} \right) - \frac{2}{3} \frac{\partial u_k}{\partial x_k} \delta_{ij} \quad (6)$$

with repeated indices indicating summation.

The two turbulence variables for which we carry evolution equations are the turbulent kinetic energy (k) and the specific dissipation rate (ω) [6] defined as

$$k \equiv \frac{\overline{\rho u_i'' u_i''}}{2\bar{\rho}} \quad (7)$$

$$\omega = \epsilon / (C_2 k) \quad (8)$$

where

$$C_2 = \frac{9}{100} \frac{\frac{5}{18} + \left(\frac{Re_\tau}{Re_c}\right)^4}{1 + \left(\frac{Re_\tau}{Re_c}\right)^4} \quad (9)$$

with

$$Re_\tau = \frac{\bar{\rho} k}{\omega \bar{\mu}} \quad (10)$$

and

$$\epsilon \equiv \frac{\overline{\rho \nu \frac{\partial u_i''}{\partial x_j} \frac{\partial u_i''}{\partial x_j}}}{\bar{\rho}} \quad (11)$$

The constant $Re_c = 6$.

Closure of the averaged equations is achieved by invoking the Boussinesq approximation which relates the turbulent stresses to the mean strain rate. The Reynolds stress tensor is written as,

$$\begin{aligned} - \overline{\rho u_i'' u_j''} &= \bar{\mu}_t S_{ij} - \frac{2}{3} \bar{\rho} k \delta_{ij} \\ S_{ij} &= \frac{\partial \tilde{U}_i}{\partial x_j} + \frac{\partial \tilde{U}_j}{\partial x_i} - \frac{2}{3} \frac{\partial \tilde{U}_k}{\partial x_k} \delta_{ij} \end{aligned} \quad (12)$$

where $\bar{\mu}_t$ is the turbulent/eddy viscosity defined as

$$\bar{\mu}_t = \alpha^* \bar{\rho} \frac{k}{\omega} \quad (13)$$

with

$$\alpha^* = \frac{\alpha_0^* + \frac{Re_\tau}{Re_c}}{1 + \frac{Re_\tau}{Re_c}} \quad (14)$$

and

$$\alpha_0^* = C_1/3, \quad Re_c = 8, \quad C_1 = \frac{3}{4} \quad (15)$$

The mean continuity equation (4) does not require any modeling. The modelled momentum equation is,

$$\begin{aligned} \frac{\partial \bar{\rho} \tilde{U}_i}{\partial t} + \frac{\partial \bar{\rho} \tilde{U}_i \tilde{U}_j}{\partial x_j} &= - \frac{\partial \bar{p}}{\partial x_i} + \frac{2}{3} \frac{\partial \bar{\rho} k}{\partial x_j} \delta_{ij} \\ &- \frac{\partial}{\partial x_j} [(\bar{\mu} + \bar{\mu}_t) S_{ij}] \end{aligned} \quad (16)$$

There has been a considerable amount of activity in the area of modeling the compressibility effects [8, 10]. In these models, the compressible dissipation terms are expressed as functions of the turbulent kinetic energy dissipation rate and the local turbulent Mach number. The compressibility effects are represented by a component of the dissipation rate (ϵ_c) given as

$$\begin{aligned} \epsilon_c &= K_c \epsilon \\ K_c &= \eta F(M_t) \\ M_t &= \frac{2k}{a^2} \end{aligned} \quad (17)$$

where a is the local speed of sound and $F(M_t)$ is a function of the local turbulent Mach number (M_t). As

mentioned before, the model used in the present work was proposed by Zemen [10] where $F(M_t)$ is given by

$$\begin{aligned} F(M_t) &= 1 - \exp[-(\frac{M_t - M_{t_0}}{0.6})^2], \quad M_t \geq M_{t_0} \\ &= 0, \quad M_t < M_{t_0} \end{aligned} \quad (18)$$

with $M_{t_0}=0.1$ and $\eta=0.75$. The modelled turbulent kinetic energy equation is [1, 9]

$$\begin{aligned} \frac{\partial \bar{\rho}k}{\partial t} + \frac{\partial \bar{\rho}k\bar{U}_j}{\partial x_j} &= P_k - \bar{\rho}\omega k(1 + K_c) \\ &+ \frac{\partial}{\partial x_j} [(\bar{\mu} + \frac{\bar{\mu}_t}{\sigma_k}) \frac{\partial k}{\partial x_j}] \end{aligned} \quad (19)$$

where

$$P_k = -\overline{\rho u_i'' u_j''} \frac{\partial \bar{U}_i}{\partial x_j} \quad (20)$$

The modelled ω -equation used in the present analysis [6] is given below. This equation does not include any compressibility corrections.

$$\begin{aligned} \frac{\partial \bar{\rho}\omega}{\partial t} + \frac{\partial \bar{\rho}\omega\bar{U}_j}{\partial x_j} &= \alpha \frac{\omega}{k} P_k - C_1 \bar{\rho}\omega^2 + \sigma_d \bar{\rho} D_{k\omega} \\ &+ \frac{\partial}{\partial x_j} [(\bar{\mu} + \frac{\bar{\mu}_t}{\sigma_\omega}) \frac{\partial \omega}{\partial x_j}] \end{aligned} \quad (21)$$

where

$$D_{k\omega} = \frac{\partial k}{\partial x_j} \frac{\partial \omega}{\partial x_j} \quad (22)$$

and

$$\alpha = \frac{1}{2\alpha^*} \frac{\alpha_0 + \frac{Re\tau}{R_\omega}}{1 + \frac{Re\tau}{R_\omega}} \quad (23)$$

The turbulence constants are

$$\begin{aligned} \alpha_0 &= 0.1, \quad R_\omega = 2.2, \quad \sigma_k = 1.0, \quad \sigma_\omega = 1.67, \\ Pr &= 0.72, \quad Pr_t = 1.0, \quad Sc = 0.22, \quad Sc_t = 1.0 \end{aligned}$$

and

$$\begin{aligned} \sigma_d &= 0.0, \quad D_{k\omega} \leq 0 \\ &= 0.3, \quad D_{k\omega} > 0 \end{aligned}$$

The mass-averaged total energy can be written in terms of the total enthalpy as

$$\bar{E} = \bar{H} - \frac{\bar{p}}{\bar{\rho}} \quad (24)$$

The correlations between the fluctuating velocity and the scalar fluctuations are modelled using a gradient-diffusion hypothesis. A typical model is of the form

$$-\overline{\rho u_i'' \phi''} = \frac{\bar{\mu}_t}{\sigma_\phi} \left(\frac{\partial \bar{\phi}}{\partial x_i} \right) \quad (25)$$

where σ_ϕ is a coefficient which, normally, is a constant. For $\phi = f_n$ (n represents the species), $\sigma_\phi = Sc_t$, and for the static enthalpy, ($\phi = h$), $\sigma_\phi = Pr_t$.

Using the above definition, and omitting the body force contribution, the time-averaged and modelled energy equation [1] is

$$\begin{aligned} \frac{\partial \bar{\rho}\bar{E}}{\partial t} + \frac{\partial \bar{\rho}\bar{E}\bar{U}_j}{\partial x_j} &= \frac{\partial}{\partial x_j} (\bar{\tau}_{ij} - \bar{p} \delta_{ij} - \overline{\rho u_i'' u_j''}) \bar{U}_i \\ &+ \frac{\partial}{\partial x_j} \left[\left(\frac{\bar{\mu}}{Pr} + \frac{\bar{\mu}_t}{Pr_t} \right) \frac{\partial \bar{h}}{\partial x_j} + \left(\bar{\mu} + \frac{\bar{\mu}_t}{\sigma_k} \right) \frac{\partial k}{\partial x_j} \right] \end{aligned} \quad (26)$$

where σ_k is a coefficient that appears in the turbulent kinetic energy equation. The modeled species continuity equation is

$$\frac{\partial \bar{\rho}\bar{f}_n}{\partial t} + \frac{\partial \bar{\rho}\bar{f}_n\bar{U}_j}{\partial x_j} = \bar{w}_n - \frac{\partial}{\partial x_j} \left[\left(\frac{\bar{\mu}}{Sc} + \frac{\bar{\mu}_t}{Sc_t} \right) \frac{\partial \bar{f}_n}{\partial x_j} \right] \quad (27)$$

In the above, the mean species production rate due to chemical reaction (\bar{w}_n) needs to be modelled. This term is a function of both the temperature and species concentrations. In the absence of a model for the interaction between the turbulent temperature and concentration fields, this term is evaluated using the mean values of local temperature and species concentrations. In a finite-rate system involving L reaction steps and N species, the instantaneous production rate of a species n can be represented (law of mass action) in the following general form:

$$\begin{aligned} \dot{w}_n &= M_n \sum_{l=1}^L (\nu_{nl}'' - \nu_{nl}') \times \\ &\{ k_{fl} \rho^{m_l} \prod_{s=1}^N \left(\frac{f_s}{M_s} \right)^{\nu_{sl}'} - k_{bl} \rho^{n_l} \prod_{s=1}^N \left(\frac{f_s}{M_s} \right)^{\nu_{sl}''} \}, \end{aligned} \quad (28)$$

where

$$m_l = \sum_{s=1}^N \nu_{sl}', \quad n_l = \sum_{s=1}^N \nu_{sl}''$$

In the above equations, ν_{sl}' and ν_{sl}'' are the number of molecules of the scalar s involved in the l -th reaction step in the forward and backward directions, respectively. The forward and backward rate-constants of the reaction l are given by k_{fl} and k_{bl} respectively. The reaction rates are usually strong functions of the temperature:

$$k_{fl} = A_l T^{b_l} \exp\left[-\frac{T_{a_l}}{T}\right] \quad (29)$$

where A_l , b_l and T_{a_l} are numerical constants specific to the given reaction step l .

Turbulence-chemistry interaction model

The interactions between the temperature and concentration fields (turbulent) may be of importance in many applications. The following section describes a model for such interactions. Practical combustor flows involve multiple scalar mixing and reactions. In order to calculate the mean species production rate using the pdf approach, a model for the joint pdf of temperature and various species is required. Such a joint pdf is difficult to specify and as a preliminary step we effect the simplification that temperature and species fluctuations are uncorrelated. This permits us to deal with the temperature and species fluctuations separately.

Equation (29) can be written as

$$k_{f_l} = A_l (\tilde{T} + T'')^{b_l} \exp\left[-\frac{T_{a_l}}{(\tilde{T} + T'')}\right] \quad (30)$$

Assuming that $\frac{T''}{\tilde{T}} < 1$, the term $(\tilde{T} + T'')$ can be expanded in a series and the resultant modified reaction rate term is written as,

$$\widetilde{k}_{f_l} = (1 + m) A_l \tilde{T}^{b_l} \exp\left[-\frac{T_{a_l}}{\tilde{T}}\right] \quad (31)$$

where

$$m = [(b_l - 1) \left(\frac{b_l}{2} + \frac{T_{a_l}}{\tilde{T}}\right) + \frac{1}{2} \left(\frac{T_{a_l}}{\tilde{T}}\right)^2] \frac{\widetilde{T''T''}}{\tilde{T}^2} \quad (32)$$

Terms of order higher than two in $\frac{T''}{\tilde{T}}$ are neglected from the series expansion in the present analysis since accurate models for these higher order terms do not exist. The factor m represents the effect of temperature fluctuations on the mean reaction rate. The temperature variance is calculated from

$$\widetilde{T''T''} = \frac{\widetilde{h''h''}}{C_p^2} \quad (33)$$

in the present work. Other pdf-based models for the temperature effects exist [5] which will be explored in the future.

For reacting flows involving multiple chemical species, Girimaji suggests [2, 3] the use of a multivariate β -pdf model to account for the effects of the scalar fluctuations on the species production rates. This model is briefly outlined below. The parameters of the multivariate β -pdf for the N -scalar mixing process $(\beta_1, \dots, \beta_N)$ are functions of the mean mass fractions $\overline{f_n}$ and turbulent scalar energy Q :

$$\beta_n = \overline{f_n} \left(\frac{1 - S}{Q} - 1 \right) \quad (34)$$

where

$$S = \sum_{n=1}^N \overline{f_n}^2, \quad Q = \sum_{n=1}^N \overline{f_n'' f_n''}. \quad (35)$$

Decoupling the effects of temperature and species concentrations, the mean species production rate can be written as,

$$\overline{w_n} = M_n \sum_{l=1}^L (\nu_{nl}'' - \nu_{nl}') \times \quad (36)$$

$$\left\{ \widetilde{k}_{f_l} \rho^{m_l} \left(\prod_{s=1}^N M_s^{-\nu_{sl}'} \right) I_{f_l} - \overline{k}_{b_l} \rho^{n_l} \left(\prod_{s=1}^N M_s^{-\nu_{sl}''} \right) I_{b_l} \right\}$$

where

$$I_{f_l} \equiv \left\langle \prod_{s=1}^N f_s^{\nu_{sl}'} \right\rangle, \quad I_{b_l} \equiv \left\langle \prod_{s=1}^N f_s^{\nu_{sl}''} \right\rangle$$

In the above, angular brackets represent conventional time averaging. The modelled expression for I_{f_l} using the multivariate β -pdf is [2],

$$I_{f_l} = \prod_{s=1}^N \prod_{r=1}^{\nu_{sl}'} (\beta_s + \nu_{sl}' - r) / \prod_{p=1}^{m_l} (B + m_l - p) \quad (37)$$

Similarly, the expression for I_{b_l} is,

$$I_{b_l} = \prod_{s=1}^N \prod_{r=1}^{\nu_{sl}''} (\beta_s + \nu_{sl}'' - r) / \prod_{p=1}^{n_l} (B + n_l - p) \quad (38)$$

where

$$B = \beta_1 + \beta_2 + \dots + \beta_N \quad (39)$$

The production of turbulent scalar energy due to chemical reaction can be decomposed as

$$\sum_{n=1}^N \overline{w_n f_n''} = \sum_{n=1}^N \overline{w_n f_n} - \sum_{n=1}^N \overline{w_n} \widetilde{f_n}. \quad (40)$$

Only the first term on the right hand side of the above equation needs further modeling. This term can be written as, using the assumptions above,

$$\sum_{n=1}^N \overline{w_n f_n} = \sum_{n=1}^N M_n \sum_{l=1}^L (\nu_{nl}'' - \nu_{nl}') \times \quad (41)$$

$$\left\{ \overline{k}_{f_l} \rho^{m_l} \left(\prod_{s=1}^N M_s^{-\nu_{sl}'} \right) J_{f_{l,n}} - \overline{k}_{b_l} \rho^{n_l} \left(\prod_{s=1}^N M_s^{-\nu_{sl}''} \right) J_{b_{l,n}} \right\}$$

where

$$J_{f_{l,n}} \equiv \left\langle f_n \prod_{s=1}^N f_s^{\nu_{sl}'} \right\rangle, \quad J_{b_{l,n}} \equiv \left\langle f_n \prod_{s=1}^N f_s^{\nu_{sl}''} \right\rangle$$

The terms $J_{f_{l,n}}$ and $J_{b_{l,n}}$ are also moments of the scalar joint-pdf. The modelled expression for these moments are [2],

$$J_{f_{l,n}} = I_{f_l} \frac{\beta_n + \nu_{nl}'}{B + m_l} \quad (42)$$

$$J_{b_{l,n}} = I_{b_l} \frac{\beta_n + \nu_{nl}''}{B + n_l}$$

Substitution of equation (42) into equation (41) leads to the model for the source/sink of turbulent scalar energy. The main advantage of this choice of the assumed-pdf model is that the chemistry related models are obtained analytically and no numerical integration in the species space is necessary.

The turbulence-thermochemistry interaction models require the enthalpy variance and the turbulent scalar energy distributions. The modeled equations for enthalpy variance ($\overline{h''h''}$) and turbulent scalar energy (Q) are of a form similar to that of the turbulent kinetic energy:

$$\frac{\partial \bar{\rho}g}{\partial t} + \frac{\partial \bar{\rho}g\bar{U}_j}{\partial x_j} = -\overline{2\rho u_j'G''} \frac{\partial \bar{G}}{\partial x_j} - 2\bar{\rho}\epsilon_g + \frac{\partial}{\partial x_j} \left[\left(\frac{\bar{\mu}}{\sigma} + \frac{\bar{\mu}_t}{\sigma_g} \right) \frac{\partial g}{\partial x_j} \right] + \Psi. \quad (43)$$

For $g = \overline{h''h''}$, $G = h$, $\Psi=0$, $\sigma = Pr$ and $\sigma_g = Pr_t$. For $g = \sum_{n=1}^N \bar{f}_n'' \bar{f}_n''$, $G = f_n$, $\Psi = 2\sum_{n=1}^N \bar{w}_n \bar{f}_n''$, $\sigma = Sc$ and $\sigma_g = Sc_t$. The dissipation term in the above equation is assumed to be

$$\epsilon_g = C_g \frac{\epsilon}{k} g = C_g C_2 \omega g \quad (44)$$

The model for $\sum_{n=1}^N \bar{w}_n \bar{f}_n''$, is given in equations (40)-(42). The constants C_g are assigned a value of 0.5.

Solution of the modeled governing equations

The equations are discretized and integrated in space and time to obtain steady state solutions using an elliptic solver SPARK [13]. The governing equations are written in vector form as follows.

$$\frac{\partial \mathbf{U}}{\partial t} + \frac{\partial \Phi_j}{\partial x_j} = \mathbf{H} \quad (45)$$

where \mathbf{U} is the vector of dependent variables, Φ_j are flux vectors containing convective and diffusive terms (repeated indices indicate summation), and \mathbf{H} is the source vector containing production/dissipation terms. The temporally discrete form of equation (45) is

$$\mathbf{U}^{n+1} = \mathbf{U}^n - \Delta t \left[\frac{\partial \Phi_j^n}{\partial x_j} - \mathbf{H}^{n+1} \right] \quad (46)$$

where n is the old time level and $n+1$ is the new time level.

The source terms in the k - and ω -equations are decoupled by suitable manipulation of the ω term in the present analysis in order to alleviate the computational stiffness introduced by these terms. For example, in the k -equation, the dissipation term is written as,

$$C_2 \bar{\rho} \omega k = C_2 \bar{\rho} k \omega^* \quad (47)$$

The term ω^* is taken from the most recent calculation step. The source terms of the ω -equation are also manipulated in a similar manner. These nonlinear turbulence source terms are treated in a pointwise-implicit manner while solving the turbulence equations by rewriting equation (46) as,

$$(\mathbf{I} - \Delta t \frac{\partial \mathbf{H}}{\partial \mathbf{U}}) (\mathbf{U}^{n+1} - \mathbf{U}^n) = -\Delta t \left[\frac{\partial \Phi_j^n}{\partial x_j} - \mathbf{H}^n \right] \quad (48)$$

The discretized equations are solved by means of a fourth-order compact scheme.

RESULTS AND DISCUSSION

Choosing a flow configuration to demonstrate the effect of turbulence-chemistry interactions is a difficult task due to the lack of guidelines based on prior data (experimental or otherwise). Since the present work is part of a larger task of establishing a solution procedure for high speed propulsion systems (scramjets), the initial choice fell on a two-dimensional high speed reacting mixing layer. Non-reacting and reacting high speed mixing layers have already been computed using the computational procedure described above [14]. Available experimental data were used to validate the prediction procedure. The β -pdf model to account for the effect of species concentration fluctuations on the mean production rate of species was also introduced in conjunction with the $k-\epsilon$ turbulence model before [1]. The main aim of the present work is to introduce the results obtained by coupling the β -pdf model with an improved version of the $k-\omega$ model [6].

A schematic of the flow problem is given in Figure 1. The two streams are, air ($U=1606$ m/sec, $T=1600$ K with $f_{H_2}=0.0$, $f_{O_2}=0.267$ and $f_{N_2}=0.733$) and hydrogen ($U=1250$ m/sec, $T=254$ K with $f_{H_2}=1.0$, $f_{O_2}=0.0$ and $f_{N_2}=0.0$). The two streams are supersonic with the air stream Mach number of 2.07 and hydrogen stream Mach number of 1.03. The inlet mean velocity is assumed to have a hyperbolic tangent profile, thus imitating the flow that exists downstream of the splitter plate trailing edge. A constant turbulence intensity level is used in the free stream for arriving at the initial distribution of turbulent kinetic energy and the specific dissipation rate. The pressures are matched between the two streams ($P=1$ atm.). A 13-step, 8-species H_2 - Air reaction model (Table 1) has been used for the finite-rate chemistry system considered here. A 101 X 81 grid (101 points in flow direction, 81 points in the transverse direction) was used for the calculations. The length of the flow domain is 0.25 m and its width is 0.05 m. In all the figures shown in this report, y refers to the lateral distance measured from the outer edge of the lower stream. The title g refers to calculations that include the interaction model.

As a first step, the difference made by the temperature fluctuations model (28) is explored. Figure 2 shows the factor $(1 + m)$ as a function of y for representative reaction steps at the exit plane of the flow domain. The need for including the temperature fluctuations is evident in the figure. The forward reaction rate changes by as much as 400 percent (reaction step 1) due to the effect of this model. The species production rate is a strong function of the reaction rate (32) and hence will be affected by the inclusion of this model.

The effect of the turbulence-chemistry interactions model on the species production rate is shown in the next few figures. Figure 3 shows the production rates of the major species involved (H_2 , O_2 , H_2O , OH) as functions of y at the exit plane. Computational results obtained with $(k-\omega-g)$ and without $(k-\omega)$ the effect of these interactions are shown in the figure. It is seen that the net change in the production rate in the shear layer/reaction zone is reduced by the effect of these interactions for the species H_2 , O_2 and H_2O . For the species OH , the effect of these interactions seems to be to reverse the rate of production from the case where the interactions are not included. While it is not conclusive whether the turbulence-chemistry interactions increase or decrease the production rates of individual species, it is important to note that these interactions do have a significant effect on progress of the chemical reactions.

Figures 4 show the distribution of the streamwise velocity and static temperature as a function of y at the exit plane. The effect of the interactions seems to be felt more at the edges of the mixing layer/reaction zone than anywhere else. In the Going back to figure 3, the production rate seems to be sensitive to the temperature gradients rather than the temperature itself. Turbulence affects the distribution of temperature both directly (thermodynamic energy equation) and indirectly (via the shear layer effect). This effect is transmitted through the interactions model and is seen in the chemical production rate profiles. Figure 5 shows the effect of the interactions on the species distributions. The effect seems to be more pronounced in the case of the products (H_2O , OH) than the primary reactants (H_2 , O_2). The changes are larger in regions of higher gradients (on the fuel stream side for H_2 and air stream side for O_2 , for example).

One of the unknown yet crucial factors associated with the present work is the lack of prior knowledge as to the effect of turbulence on chemical reactions and the reverse effect of the chemical reactions (heat release, concentration change) on the turbulent field. Which of these effects is dominant is a debatable issue. Based on the results shown in this report as well

as other similar computations (not shown) carried out by the author, it is not possible to come up with a definite answer to this question. It is also not established whether the type of flow configuration (mixing layer, jet, boundary layer) has any significance in this discussion. So far, all computations using the proposed model have been done for reacting mixing layer (2-D and coaxial jets) involving the mixing and reaction between fuel and oxidizer streams. It is not certain whether a premixed reacting flow configuration will show a more pronounced effect of these interactions than the non-premixed cases studied so far. Also the effect of the interactions near a solid wall is an area worth exploring.

An interesting aspect of the analysis is that the particular turbulence model chosen ($k - \epsilon$ as opposed to $k - \omega$, for example) seems to have an effect on the overall predictions [1]. Since the g -equations, which provide the variances needed to construct the interactions model, are strongly coupled (via their production terms) with the turbulence model equations it is also essential to differentiate between the effects of the turbulence model and the turbulence-chemistry interaction model. This brings up the importance of the accuracy of the turbulence model which was one of the main reasons for carrying out this task using the $k - \omega$ turbulence model. It is crucial to keep the shortcomings of the model in perspective while attempting to validate the results. The assumptions made in arriving at the model, such as the decoupling of temperature and concentration effects, are as important as the model itself in some cases.

On the positive side, this effort represents a significant push in the right direction in this very important area of turbulent reacting flows. The model is simple to use and is easily adaptable to other types of turbulence closures such as the Reynolds stress models. More improvements can certainly be done in terms of using more realistic models for the temperature and concentration fluctuations such as a pdf-based model for temperature effects (as opposed to the moment model employed here), a joint-pdf model to represent the effects of both the temperature and the concentration fields etc. However, in order for the model to be useful for practical applications, it must be kept in a form which promotes ease of use as well as computational economy. This is the main reason for resorting to a two-equation level turbulence model in the present work. A concerted validation effort is crucial to ensure the success of the modelling efforts. One debilitating factor in this regard is the nonexistence of useful experimental data. It is extremely difficult, if not almost impossible, to obtain such experimental data using present day equipment. An alternative seems to be direct numerical simulations (DNS) which

has shown promising signs in relatively simpler flow configurations. In spite of the major advances made in the area of DNS in recent years, it still is a developing field and is far from providing useful data for validation purposes in cases such as the present work.

CONCLUSIONS

A turbulence-chemistry interaction model has been proposed in conjunction with a recent version of the two-equation $k - \omega$ model of turbulence for use in chemically reacting flows. Preliminary computations carried out with the model for the case of a two-dimensional, high speed, reacting mixing layer indicate that these interactions have a significant effect on the flow predictions. The species production rates of individual species seem to be affected by these interactions. It is not possible, yet, to quantify the effects of these interactions based on available data. More detailed analysis of the various aspects of the model developmental process need to be done.

ACKNOWLEDGMENTS

This work was supported by the Applied Computational Fluids Branch of the Fluid Dynamics Division at NASA Ames Research Center under Cooperative agreement number NCC 2-715. The author would like to acknowledge the valuable role played by Dr. S.S. Girimaji of ICASE, NASA Langley Research Center in the development of the model.

References

- [1] Narayan, J. R. and Girimaji, S. S., "Turbulent Reacting Flow Computations Including Turbulence-Chemistry Interactions." AIAA-92-0342, 1992.
- [2] Girimaji, S. S., "A Simple Recipe for Modeling Reaction-rates in Flows with Turbulent-Combustion", AIAA-91-1792, 1991.
- [3] Girimaji, S. S., "Assumed β -pdf model for turbulent mixing: Validation and Extension to Multiple Scalar Mixing", *Combustion Science & Technology*, Vol.78, 1991, pp 177-196.
- [4] Pope, S. B., "Computations of Turbulent Combustion: Progress and Challenges", *Proc. 23rd Symposium (Int.) on Combustion*, The combustion Institute, Pittsburgh, PA, 1990, pp 591-612.
- [5] Frankel, S.H., Drummond, J.P. and Hassan, H.A., "A Hybrid Reynolds Averaged/pdf Closure Model for Supersonic Turbulent Combustion", AIAA-90-1573, 1990.
- [6] Wilcox, D.C., "A Two-Equation Turbulence Model for Wall-Bounded and Free-Shear Flows", AIAA Paper 93-2905, 1993.
- [7] Mentor, F. R., "Zonal Two Equation $k-\omega$ Turbulence Models for Aerodynamic Flows", AIAA Paper 93-2906, 1993.
- [8] Sarkar, S., Erlebacher, G., Hussaini, M. Y., and Kreiss, H. O., "The Analysis and Modeling of Dilatational Terms in Compressible Turbulence", *NASA CR 181959*, 1989.
- [9] Jones, W.P. and Launder, B.E., "The Prediction of Laminarization with a Two-Equation Model of Turbulence", *Int. J. Heat Mass Transfer*, Vol.15, 1972, pp 301-314.
- [10] Zeman, O., "Compressible Turbulence Subjected to Shear and Rapid Compression", Eighth Symposium on Turbulent Shear Flows, Munich, Germany, 1991.
- [11] Narayan, J. R., "A Two-Equation Turbulence Model for Compressible Reacting Flows." AIAA-91-0755, 1991.
- [12] Wilcox, D.C., "Progress in Hypersonic Turbulence Modeling", AIAA-91-1785, 1991.
- [13] Carpenter, M. H., "Three-Dimensional Computations of Cross-Flow Injection and Combustion in a Supersonic Flow", AIAA-89-1870, 1989.
- [14] Narayan, J. R., Sekar, B., "Computation of Turbulent High Speed Mixing Layers Using a Two-Equation Turbulence Model." *Proceedings of the CFD Symposium on Aeropropulsion*, NASA Lewis Research Center, Cleveland, Ohio, April 24-26, 1990.
- [15] Drummond, J. P., Carpenter, M. H. and Riggins, D. W., "Mixing and Mixing Enhancement in Supersonic Reacting Flows", *High Speed Propulsion Systems: Contributions to Thermodynamic Analysis*, ed. E. T. Curran and S. N. B. Murthy, American Institute of Astronautics and Aeronautics, Washington, D. C., 1990.
- [16] Drummond, J. P., "A Two-Dimensional Numerical Simulation of a Supersonic, Chemically Reacting Mixing Layer", *NASA TM 4055*, 1988.
- [17] "Free Turbulent Shear Flows", *NASA SP-321*, Vol.1, 1972.
- [18] Brown, G. L. and Roshko, A., "On Density Effects and Large Structure in Turbulent Mixing Layers", *J. Fluid Mech.*, vol. 64, pt. 4, 1974, pp. 775-816.

- [19] Papamoschou, D. and Roshko, A., "The Compressible Turbulent Shear Layer : An Experimental Study", *J.Fluid Mechanics*, v.197, 1988, pp 453-477.
- [20] "Seventh Symposium on Turbulent Shear Flows", Vol.1 and 2, Stanford University, Stanford, California, 1989.
- [21] Oldenberg, R. et al., "Hypersonic Combustion Kinetics - Status Report of the Rate Constant Committee, NASP High-Speed Propulsion Technology Team", *NASA TM 1107*, 1990.
- [22] Williams, F. A., *Combustion Theory*. Addison-Wesley Publishing Company, Inc., Reading, MA, pp. 358-429, 1965.
- [23] Favre, A., "Statistical Equations of Turbulent Gases", *Institut de Mechanique Statistique de la Turbulence, Marseille*.

Table 1. $H_2 - Air$ Reaction System

No.	Reaction
1	$H + O_2 \rightleftharpoons O + OH$
2	$OH + H_2 \rightleftharpoons H_2O + H$
3	$O + H_2 \rightleftharpoons OH + H$
4	$OH + OH \rightleftharpoons H_2O + O$
5	$H + OH + M \rightleftharpoons H_2O + M$
6	$H + H + M \rightleftharpoons H_2 + M$
7	$O + O + M \rightleftharpoons O_2 + M$
8	$H + O + M \rightleftharpoons OH + M$
9	$H + O_2 + M \rightleftharpoons HO_2 + M$
10	$OH + HO_2 \rightleftharpoons H_2O + O_2$
11	$H + HO_2 \rightleftharpoons H_2 + O_2$
12	$H + HO_2 \rightleftharpoons OH + OH$
13	$O + HO_2 \rightleftharpoons OH + O_2$
14	$HO_2 + HO_2 \rightleftharpoons H_2O_2 + O_2$
15	$H + H_2O_2 \rightleftharpoons H_2 + HO_2$
16	$OH + H_2O_2 \rightleftharpoons H_2O + HO_2$
17	$H + H_2O_2 \rightleftharpoons H_2O + OH$
18	$O + H_2O_2 \rightleftharpoons HO_2 + OH$
19	$OH + OH + M \rightleftharpoons H_2O_2 + M$
20	$OH + OH \rightleftharpoons H_2 + O_2$

Species : $H_2, O_2, H_2O, OH, H, O, HO_2, H_2O_2$ and N_2 (inert)
 M is a third body (all species included)

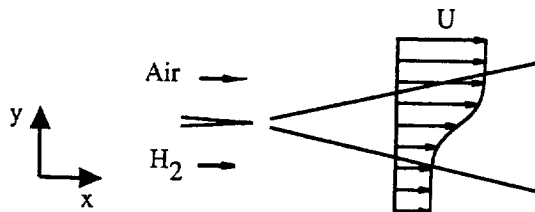


Fig. 1 Mixing Layer - schematic

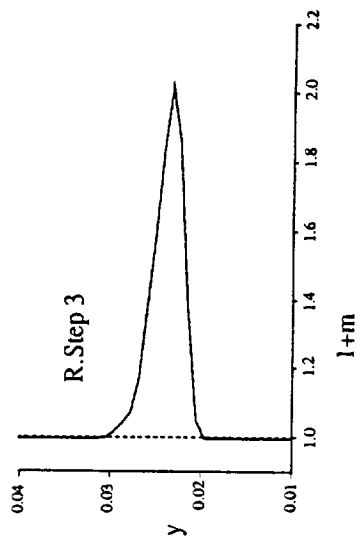
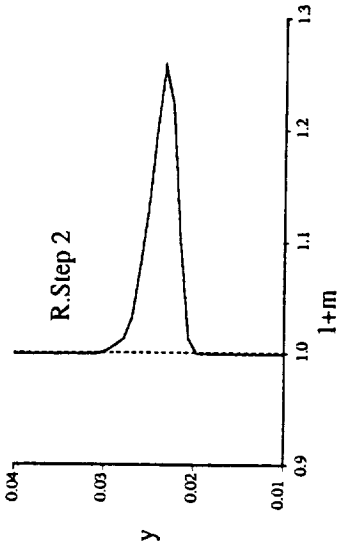
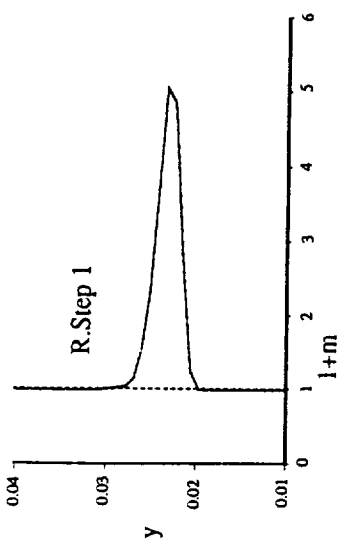
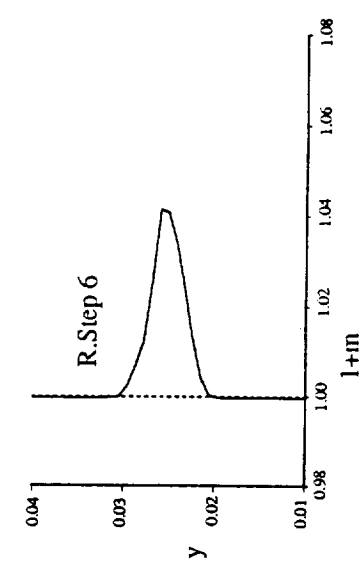
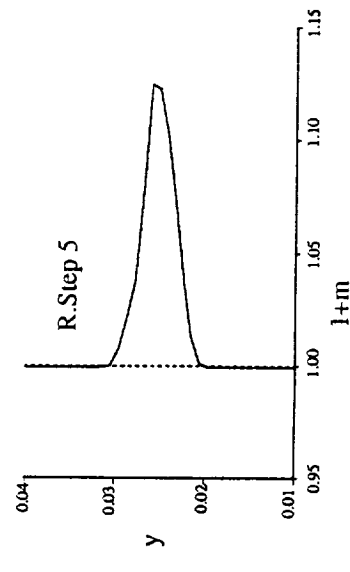
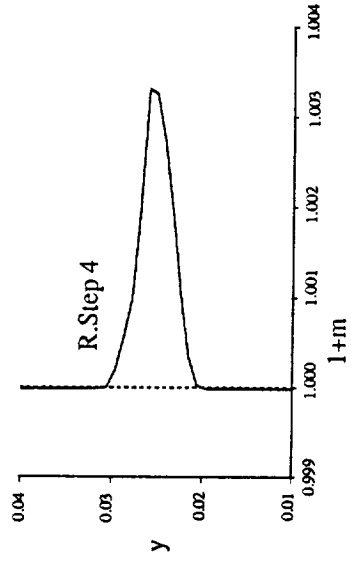


Fig. 2 Effect of Temperature Fluctuations

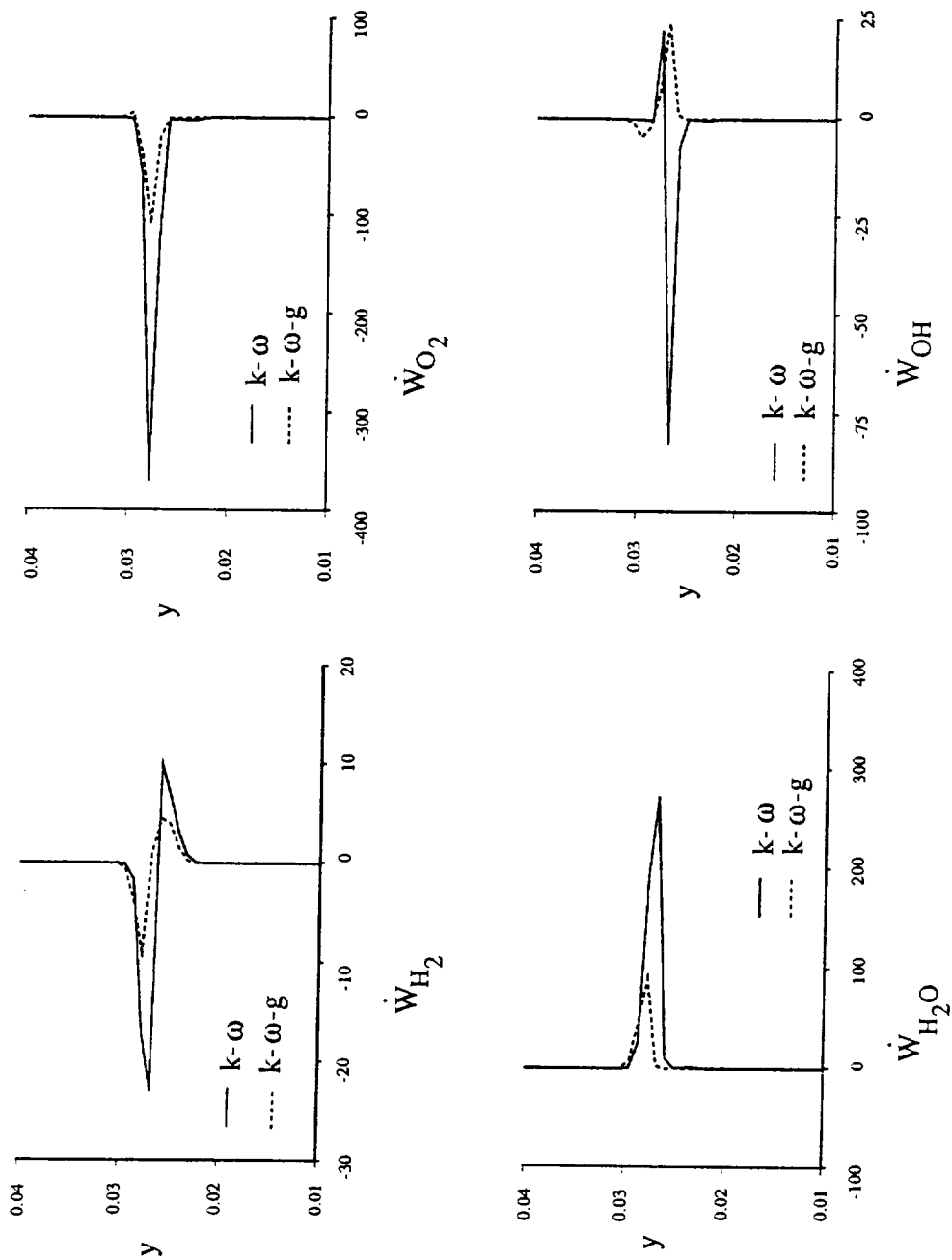


Fig. 3 Effect of Turbulence-Chemistry interactions on species production rate

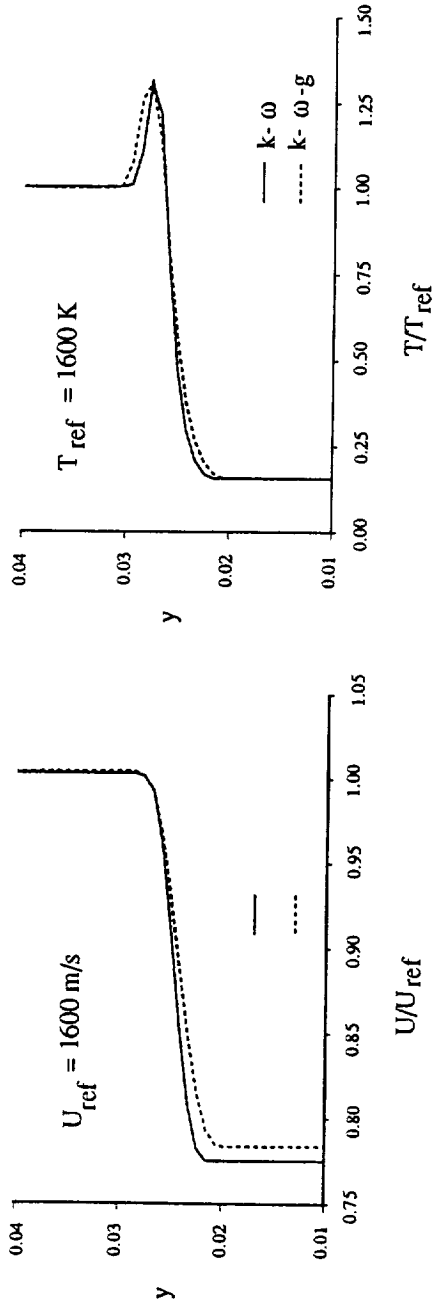


Fig. 4 Effect of interaction model - velocity & temperature

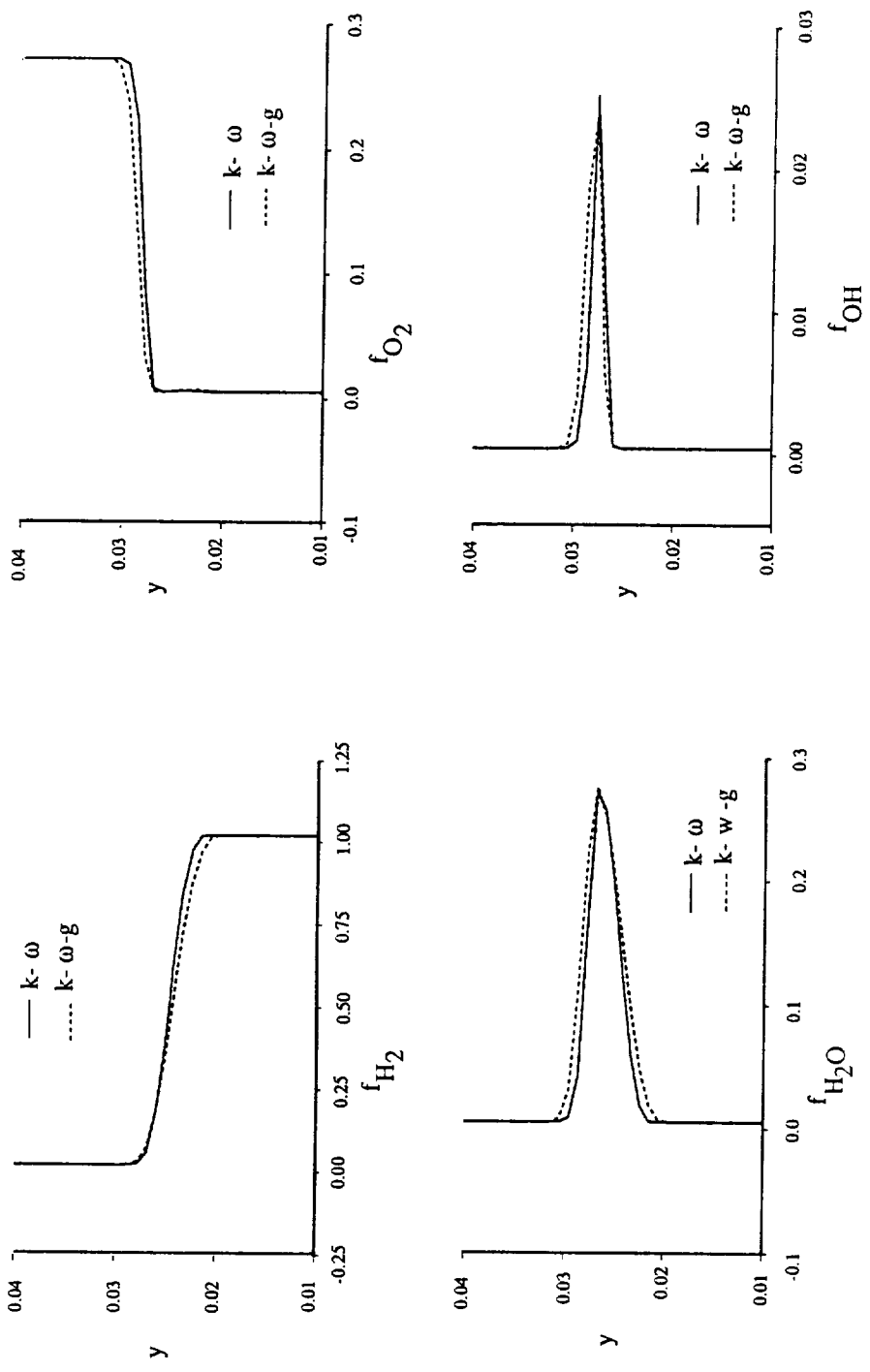


Fig. 5 Effect of interaction model on species mass fractions

APPENDIX - B

AIAA-94-2313

N/S

**Computation Of High Speed Turbulent
Reacting Flows Relevent To Scramjet
Combusters**

**Johnny Narayan and Gregory Molvik
MCAT Institute
Moffett Field, California**

and

**G.Wadawadigi
University of Texas at Arlington
Arlington, Texas**

COMPUTATION OF HIGH-SPEED TURBULENT REACTING FLOWS RELEVANT TO SCRAMJET COMBUSTORS

J.R. Narayan*

MCAT Institute, Moffett Field, CA.

G. Wadawadigi†

U. of Texas at Arlington, Arlington , Texas.

and

G. Molvik‡

MCAT Institute, Moffett Field, CA.

ABSTRACT

Computations are done on flow configurations that resemble the reaction zone in the scramjet combustor flows. Compressible, reacting, turbulent flow solutions are obtained. A two equation ($k-\epsilon$) model with compressibility correction is used to calculate the flow field. A finite rate (8-species, 13-reaction steps) chemistry model for hydrogen-air combustion has been used. Computations are carried out using the Navier-Stokes solver TUFF. Predictions are compared with available experimental data and also those obtained by using the code UPS.

NOMENCLATURE

A, b	coefficients in Arrhenius rate equation
C_1, C_2, C_μ	turbulence model constants
E	total internal energy
f_n	mass fraction of species n
H	total enthalpy
h	static enthalpy
k	turbulent kinetic energy
k_f, k_b	forward and backward reaction rate constants
L	number of reaction steps
M_n	Molecular weight of species n
M_t	Turbulent Mach number
N	number of chemical species
Pr, Pr_t	laminar and turbulent Prandtl numbers
p	pressure
Sc, Sc_t	laminar and turbulent Schmidt numbers
T	temperature
T_a	Activation Temperature
t	time
\vec{U}	velocity vector
\dot{w}_n	production rate of species n
x	streamwise coordinate

x_j	j^{th} coordinate
y	transverse coordinate
δ_{ij}	Kronecker delta
ϵ	turbulence energy dissipation rate
ϵ_c	compressible dissipation rate
η	compressibility correction coefficient
γ	ratio of specific heats
ω	specific dissipation rate
μ	laminar viscosity
μ_t	turbulent viscosity
ν	kinematic viscosity
ρ	density
$\sigma_k, \sigma_\epsilon$	turbulence model constants
τ_{ij}	stress tensor
Φ_j	flux vector in j^{th} direction
Subscripts	
t	turbulent quantity

INTRODUCTION

Hypersonic travel requires propulsion systems which are different from the conventional ones used in most of the modern aircraft. The supersonic combustion ramjet (scramjet) is a system considered to be suitable for high speed applications. There has been a tremendous amount of activity in the area of scramjet research in recent years ([1] - [11]). Some of the related topics include inlet configuration, mixing layers, mixing enhancement, combustor configuration, finite rate chemistry models and chemical kinetics. The fuel used in the scramjet varies depending upon the application. For example, hypersonic waveriders using hydrocarbon fuels have been designed [12] for applications in the moderate hypersonic speed regimes. For Mach numbers of the order of 15 and above, hydrogen is generally considered to be the fuel of choice. In the present work, hydrogen is the fuel used in the computations.

The present work represents a computational ef-

*Senior Research Scientist, Senior Member AIAA.

†PostDoctoral Fellow, Member AIAA.

‡Senior Research Scientist, Member AIAA.

fort in establishing a solution procedure for hypersonic propulsion applications. The entire task of establishing the solutions procedure must then be divided into smaller tasks dealing with subsets such as turbulence modelling, chemical kinetics, geometry etc. One such task is the topic for the present study. Here, the relevant flow features of the combustor, namely the mixing and chemical reaction between the fuel and oxidizer streams, is addressed. The flow field in a scramjet is complex. It is turbulent and compressible involving high heat release. The solution procedure should address all aspects of the flow field adequately. It should be capable of accurately modelling the turbulent field, taking into account the effects of compressibility, and addressing the changes associated with heat release. Also, the interactions between the distinct physical aspects of the flow such as the effect of heat release on turbulence, the interaction between turbulence and chemistry etc. must be properly addressed. Significant progress has been made in addressing these areas via accurate and realistic modelling in recent years [6].

Remarkable advances have been made in the area of turbulence modelling, accounting for a variety of factors that affect the flow field. Compressibility correction models to account for the effects of compressibility, near-wall turbulence models to deal with the transition from fully turbulent to zero turbulence, viscous dominated flow field near no-slip boundaries and modifications to models to account for flow curvature are some examples. A wide variety of turbulence models, including algebraic (zero-equation), one-equation, two-equation, Reynolds stress and large eddy simulation models, are available (for example references [13] - [15]) depending upon the sophistication and accuracy desired and the limits imposed by numerical solution procedures.

Thermodynamic and chemical kinetic models [16] applicable to the scramjet flows have been undergoing continuous improvements in recent years. Accurate modelling of thermodynamic variables as functions of temperature which are valid over a wide range of temperatures is an example. In flows such as the one associated with the scramjet, the time scales associated with fluid dynamics and chemical reaction (not to mention the turbulence scales) require that the combustion process be modelled via a finite rate chemistry mechanism. Such a mechanism should account not only for the major species (reactants and products) involved in the chemical reactions but also the intermediate transient ones which play a vital role in the reaction progress process. Accurate models for the chemical reactions in the scramjet combustor, thus, is a crucial aspect of the solution procedure.

The design of the combustor is strongly dependent

upon factors such as the mixing between fuel and oxidizer streams, presence of shocks in the flow field, boundary layer effects, flow separation, extent of chemical reaction within the combustor and so on. The numerical solution procedure should have the capability of addressing all of these factors while maintaining the required accuracy and robustness. There is a glut of useful numerical solvers applicable for a wide variety of flows including all speed regimes. Computational algorithms which are fast and accurate are being improved everyday.

Even though there are a wide variety of sophisticated and physically accurate thermodynamic, chemical kinetic and turbulence models available it is not always possible to use the most accurate and elaborate versions in a numerical simulation due to the limitations imposed by computer memory requirements, computational economy, ease of use and adaptability to practical problems. Solutions often are required, especially in the engineering industry which is the end user for such solvers, in a short time using computers that may not be the fastest available. As a result, compromises must be struck between physical accuracy and computational feasibility and it is this aspect which differentiates between various solvers that exist today.

In the present study, an attempt is made to establish a solution procedure for scramjet combustor flow predictions from the perspective of the discussion above. The models chosen to represent the turbulent and chemistry fields reflect the compromise between physical accuracy and computational economy mentioned above. The code chosen for the computations is the TUFF [17] code and the solutions are compared with those obtained with the UPS [18, 20] code. The turbulence model chosen is the two-equation $k - \epsilon$ turbulence model with low Reynolds number modifications [13]. However, the Baldwin-Lomax algebraic model is also available as an option. The compressibility effects are included via the compressibility correction model proposed by Zeman [19]. The fuel used is hydrogen although the numerical solver can easily be modified for hydrocarbon fuels. A 9-species, 20-reaction steps chemical kinetics model for hydrogen-air combustion [16] is available. For the computations presented in this report, an abbreviated version (8-species, 13-steps) of this model has been used.

Mixing plays a major role in high speed combustor flows. The reaction zone is mainly confined to mixing layers that exist between fuel and oxidizer streams. Two flow configurations are chosen for the study. The first is the well known Burrows-Kurkov experiment [21] in which hydrogen and vitiated air streams (two-dimensional) mix and react. The second

case is that of an axisymmetric configuration [22, 23] where two coaxial jets (fuel and oxidizer) mix and react. Experimental data from compressible, reacting mixing layers is still scarce which hinders the validation of the calculation procedure. The available data from the above two experiments are used to compare with the predictions. The governing and secondary equations used in the computations have all been described in detail in the references cited above. Only an abbreviated equation set will be given in the present paper. The computations were performed on the supercomputers of NAS and NASA Ames Research Center (C-90).

GOVERNING EQUATIONS

The equations used for computations are described in detail in references [6, 7, 10] and [24]. Only the forms of the modelled equations used in the present study are given here. Density-weighted averaging is used to derive the mean flow equations from the instantaneous conservation equations. The dependent variables, with the exception of density and pressure, are written as

$$\phi = \bar{\phi} + \phi'' \quad (1)$$

where the ϕ'' is the fluctuating component of the variable under consideration and its Favre-mean $\bar{\phi}$ is defined as

$$\bar{\phi} \equiv \frac{\overline{\rho\phi}}{\bar{\rho}} \quad (2)$$

In this equation, the overbar indicates conventional time-averaging. Density and pressure are split in the conventional sense as,

$$\rho = \bar{\rho} + \rho' \quad \text{and} \quad p = \bar{p} + p' \quad (3)$$

The averaged continuity and momentum equations are

$$\frac{\partial \bar{\rho}}{\partial t} + \frac{\partial \bar{\rho} \bar{U}_i}{\partial x_i} = 0 \quad (4)$$

$$\frac{\partial \bar{\rho} \bar{U}_i}{\partial t} + \frac{\partial \bar{\rho} \bar{U}_i \bar{U}_j}{\partial x_j} = - \frac{\partial \bar{p}}{\partial x_i} - \frac{\partial \overline{\rho u_i'' u_j''}}{\partial x_j} + \frac{\partial \bar{\tau}_{ij}}{\partial x_j} \quad (5)$$

where

$$\tau_{ij} = \mu \left(\frac{\partial u_i}{\partial x_j} + \frac{\partial u_j}{\partial x_i} \right) - \frac{2}{3} \frac{\partial u_k}{\partial x_k} \delta_{ij} \quad (6)$$

with repeated indices indicating summation.

In the two-equation turbulence model, the two turbulence variables are the turbulent kinetic energy (k) and the dissipation rate (ϵ) [13] defined as

$$k \equiv \frac{\overline{\rho u_i'' u_i''}}{2\bar{\rho}} \quad (7)$$

and

$$\epsilon \equiv \frac{\overline{\rho \nu \frac{\partial u_i''}{\partial x_j} \frac{\partial u_i''}{\partial x_j}}}{\bar{\rho}} \quad (8)$$

Boussinesq approximation is used to obtain closure of the averaged equations. Here the Reynolds stress tensor is written as,

$$S_{ij} = - \frac{\overline{\rho u_i'' u_j''}}{\bar{\rho}} = \bar{\mu}_t S_{ij} - \frac{2}{3} \bar{\rho} k \delta_{ij} \quad (9)$$

where μ_t is the turbulent/eddy viscosity defined as

$$\bar{\mu}_t = C_\mu \bar{\rho} \frac{k^2}{\epsilon} \quad (10)$$

with $C_\mu=0.09$.

The modelled momentum equation, then, is,

$$\frac{\partial \bar{\rho} \bar{U}_i}{\partial t} + \frac{\partial \bar{\rho} \bar{U}_i \bar{U}_j}{\partial x_j} = - \frac{\partial \bar{p}}{\partial x_i} + \frac{2}{3} \frac{\partial \bar{\rho} k}{\partial x_j} \delta_{ij} - \frac{\partial}{\partial x_j} [(\bar{\mu} + \bar{\mu}_t) S_{ij}] \quad (11)$$

The effects of compressibility are included via the model proposed by Zeman [19]. Here, the compressible dissipation terms are expressed as functions of the turbulent kinetic energy dissipation rate and the local turbulent Mach number. The compressibility effects are represented by a component of the dissipation rate (ϵ_c) given as

$$\begin{aligned} \epsilon_c &= K_c \epsilon \\ K_c &= \eta F(M_t) \\ M_t &= \frac{2k}{a^2} \end{aligned} \quad (12)$$

where a is the local speed of sound and $F(M_t)$ is a function of the local turbulent Mach number (M_t). $F(M_t)$ is given by

$$\begin{aligned} F(M_t) &= 1 - \exp\left[-\left(\frac{M_t - M_{t_0}}{0.6}\right)^2\right], \quad M_t \geq M_{t_0} \\ &= 0, \quad M_t < M_{t_0} \end{aligned}$$

with $M_{t_0}=0.1$ and $\eta=0.75$. The modelled turbulent kinetic energy equation is [6, 13]

$$\begin{aligned} \frac{\partial \bar{\rho} k}{\partial t} + \frac{\partial \bar{\rho} k \bar{U}_j}{\partial x_j} &= P_k - \bar{\rho} \epsilon (1 + K_c) \\ &+ \frac{\partial}{\partial x_j} \left[\left(\bar{\mu} + \frac{\bar{\mu}_t}{\sigma_k} \right) \frac{\partial k}{\partial x_j} \right] \end{aligned} \quad (13)$$

where

$$P_k = - \overline{\rho u_i'' u_j''} \frac{\partial \widetilde{U}_i}{\partial x_j} \quad (14)$$

The modelled ϵ -equation used (no compressibility corrections) in the present analysis [13] is given below.

$$\begin{aligned} \frac{\partial \bar{\rho} \epsilon}{\partial t} + \frac{\partial \bar{\rho} \epsilon \widetilde{U}_j}{\partial x_j} &= (C_1 P_k - C_2 \bar{\rho} \epsilon) \frac{\epsilon}{k} \\ &+ \frac{\partial}{\partial x_j} \left[\left(\bar{\mu} + \frac{\bar{\mu}_t}{\sigma_\epsilon} \right) \frac{\partial \epsilon}{\partial x_j} \right] \end{aligned} \quad (15)$$

where P_k is the production term in the turbulent kinetic energy equation. The model constants used in the analysis are $C_1=1.44$, $C_2=1.92$, $\sigma_k=1.0$, $\sigma_\epsilon=1.3$, $Pr=0.72$, $Pr_t=1.0$, $Sc=0.22$ and $Sc_t=1.0$.

The mass-averaged total energy can be written in terms of the total enthalpy as

$$\widetilde{E} = \widetilde{H} - \frac{\bar{p}}{\bar{\rho}} \quad (16)$$

The correlations between the fluctuating velocity and the scalar fluctuations are modelled using a gradient-diffusion hypothesis. A typical model is of the form

$$- \overline{\rho u_i'' \phi''} = \frac{\bar{\mu}_t}{\sigma_\phi} \left(\frac{\partial \widetilde{\phi}}{\partial x_i} \right) \quad (17)$$

where σ_ϕ is a coefficient which, normally, is a constant. For $\phi = f_n$ (n represents the species), $\sigma_\phi = Sc_t$, and for the static enthalpy, ($\phi = h$), $\sigma_\phi = Pr_t$. Using the above definition, and omitting the body force contribution, the time-averaged and modelled energy equation [6] is

$$\begin{aligned} \frac{\partial \bar{\rho} \widetilde{E}}{\partial t} + \frac{\partial \bar{\rho} \widetilde{E} \widetilde{U}_j}{\partial x_j} &= \frac{\partial}{\partial x_j} \left(\bar{\tau}_{ij} - \bar{p} \delta_{ij} - \overline{\rho u_i'' u_j''} \right) \widetilde{U}_i \\ &+ \frac{\partial}{\partial x_j} \left[\left(\frac{\bar{\mu}}{Pr} + \frac{\bar{\mu}_t}{Pr_t} \right) \frac{\partial \widetilde{h}}{\partial x_j} + \left(\bar{\mu} + \frac{\bar{\mu}_t}{\sigma_k} \right) \frac{\partial k}{\partial x_j} \right] \end{aligned} \quad (18)$$

where σ_k comes from the turbulent kinetic energy equation. The modelled species continuity equation is

$$\frac{\partial \bar{\rho} \widetilde{f}_n}{\partial t} + \frac{\partial \bar{\rho} \widetilde{f}_n \widetilde{U}_j}{\partial x_j} = \bar{w}_n - \frac{\partial}{\partial x_j} \left[\left(\frac{\bar{\mu}}{Sc} + \frac{\bar{\mu}_t}{Sc_t} \right) \frac{\partial \widetilde{f}_n}{\partial x_j} \right] \quad (19)$$

The modelled form of the mean species production rate due to chemical reaction (\bar{w}_n) is given, for a finite-rate system involving L reaction steps and N species, in the following general form:

$$\begin{aligned} \bar{w}_n &= M_n \sum_{l=1}^L (\nu_{nl}'' - \nu_{nl}') \times \\ &\left\{ k_{fl} \rho^{m_l} \prod_{s=1}^N \left(\frac{f_s}{M_s} \right)^{\nu_{sl}'} - k_{bl} \rho^{n_l} \prod_{s=1}^N \left(\frac{f_s}{M_s} \right)^{\nu_{sl}''} \right\}, \end{aligned} \quad (20)$$

where

$$m_l = \sum_{s=1}^N \nu_{sl}', \quad n_l = \sum_{s=1}^N \nu_{sl}''$$

where, ν_{sl}' and ν_{sl}'' are the number of molecules of the scalar s involved in the l -th reaction step in the forward and backward directions, respectively. The forward and backward rate-constants of the reaction l are given by k_{fl} and k_{bl} respectively.

$$k_{fl} = A_l T^{b_l} \exp\left[-\frac{T_{a_l}}{T}\right] \quad (21)$$

where A_l , b_l and T_{a_l} are numerical constants specific to the given reaction step l . k_{bl} is determined from the equilibrium constant for the l -th reaction step and k_{fl} .

Solution of the modeled equations

The equations are discretized and integrated in space and time to obtain steady state solutions using the finite-volume based numerical solver TUFF [17]. The TUFF code contains many desirable features for the computation of three-dimensional, hypersonic flow fields. It has non-equilibrium, equilibrium and perfect gas capabilities along with an incompressible option. It employs a finite-volume philosophy to ensure that the schemes are fully conservative. The upwind inviscid fluxes are obtained by employing a new temporal Riemann solver that fully accounts for the gas model used. This property allows the flow field discontinuities such as shocks and contact surfaces to be captured by the numerical scheme without smearing. Total Variation Diminishing (TVD) techniques are included to allow extension of the schemes to higher orders of accuracy without introducing spurious oscillations. The schemes employ a strong coupling between the fluid dynamic and species conservation equations and are made fully implicit to eliminate the step-size restriction of explicit schemes. This is necessary since step-sizes in a viscous, chemically reacting calculation can be excessively small for an explicit scheme, and the resulting computer times prohibitively large. A fully conservative zonal scheme has been implemented to allow solutions of very complex problems. The schemes are made implicit by fully linearizing all of the fluxes and source terms and by employing a modified Newton iteration to eliminate any linearization and approximate factorization errors that might occur. Approximate factorization is then employed to avoid solving many enormous banded matrices. As mentioned before, the options for turbulence models include both zero and two equation models (both $k - \epsilon$ and $k - \omega$). For more details about the solution procedure the reader is directed to the reference cited above [17].

RESULTS AND DISCUSSION

Two reacting flow configurations have been chosen for the present study. As mentioned before, the Navier Stokes solver TUFF has been used for the computations. The first one is the case of coaxial jets [22, 23] where a hydrogen jet flows (inner jet) coaxially with an outer vitiated air (mass fractions: oxygen=0.246, water=0.209 and nitrogen=0.545) jet. A schematic of the flow problem is given in Figure 1. The two streams are, air ($U=1380$ m/sec, $T=1180$ K with $p=107000$ N/m²) and hydrogen ($U=1774$ m/sec, $T=545$ K with $p=112000$ N/m²). The air stream is supersonic with a Mach number of 1.97 and the hydrogen stream Mach number is 1.00. The inlet mean velocity is assumed to have a step profile with the two jets having uniform speeds at the specified values (no experimental data available). The velocity in the lip region of the inner jet tube wall (finite wall thickness) is assumed to be zero. The inlet temperature profile is derived based on the experimental data given for a location just downstream of it (shown later). The inlet species mass fraction distributions are also chosen based on the experimental data provided at the same downstream location. A constant turbulence intensity level is used in the free stream for arriving at the initial distribution of turbulent kinetic energy and the dissipation rate. A 13-step, 8-species $H_2 - Air$ reaction model (Table 1) has been used for the finite-rate chemistry system considered here. A 81 X 91 grid (81 points in flow direction, 91 points in the radial direction) was used for the calculations. The inner jet/tube diameter ($D=0.00236$ m) is used as a reference length. The total length of the flow domain is equal to $43.1 D$. The outer boundary (radial) of the flow domain is taken to be at $y=17 D$. A more detailed description of the flow parameters is given in Table 2. The region outside the limits of the air jet is assumed to be still air at a temperature of 273 K. The two-equation ($k-\epsilon$) turbulence model is used along with the finite rate H_2-Air chemistry model mentioned above. In all the figures shown in this report, y refers to the radial distance measured from the axis of the coaxial system of jets.

Figures 2 - 3 show the results of the computations. Figure 2 shows the computed and experimental distributions of species mole fractions. The figure is designed in a two-column format. The left side column represents the inlet (first x-location) data and the right side column is the data at the exit plane ($x/D=43.1 D$). As seen in these figures, the inlet data agreement between the computations and experiment is not perfect, especially around the jet edges, and this might affect the computed distributions at downstream locations. The comparison between predictions and experiment at the downstream location

($x/D=43.1 D$) is good given the above mismatch between the two data at the inlet. The development of the reaction zone after ignition is not predicted well. The experimental data indicates that the reaction zone (depicted by the water mole fraction distribution) spreads more quickly than the predictions indicate. The predictions show the reaction zone to be off-center whereas the experimental data shows the reaction zone to be closer to the axis of symmetry. However, there is very good qualitative agreement between the data with the peak values of the reaction products predicted very well. The flow domain was seen to have a wave-like structure as shown by the predicted profiles. The worst agreement seems to be for the case of oxygen. However, when the initial profiles of oxygen are compared one finds that there too is the worst agreement between computations and experiment which may be reason for the problem downstream. Figure 3 shows the comparison of static temperature data. The agreement between predictions and experiment is good qualitatively displaying similar trends. The uncertainty associated with the accuracy of the experimental data is unknown. There are considerable differences between the data presented by the two references [22, 23], especially in the temperature profiles. Overall, there is good qualitative agreement between the predictions and experiment.

The second test case considered is the Burrows-Kurkov experiment [21]. The flow configuration is two-dimensional. A schematic diagram of the configuration is given in figure 4. No-slip walls bound both the upper and lower regions ($y=0$ and $y=y_{max}$). The lower wall is inclined to form an expansion surface. Hydrogen is injected along this surface into a vitiated air stream. The two streams mix and react downstream of the injection location (inlet). The hydrogen stream is injected at a velocity of 1216 m/sec and a temperature of 254 K. The airstream comes in at a speed of 1764 m/sec and a temperature of 1270 K. Full details about the flow parameters and geometry are given in Table 3. In this case, the reference length used in the hydrogen jet width at inlet, h ($h=0.004$ m). The models for turbulence and chemistry are identical to the ones used for the coaxial jet case. The grid size is 81 X 121 (81 grid points in the axial (x) direction and 121 grid points in the transverse direction). The total length of the solution domain is 0.356 m ($x/h=89$). Available inlet data have been used for the first-plane profiles which improved the predictions remarkably over the solutions obtained with uniform profiles. The solutions are compared with the available experimental data at this location (exit) in figures 5-7. The solutions carried out with the space marching PNS code UPS [20] using the Baldwin-Lomax turbulence model are also given for comparison.

Figure 5 shows the comparison between the predicted distributions of the species mole fractions and the corresponding experimental data. As seen in these figures, there is excellent agreement between the TUFF predictions and experiment. The predictions by the UPS code do not agree very well but still there is very good qualitative agreement with the experimental data. Figure 6 compares the predicted profiles of exit plane total temperature and Mach number with the experimental data. There is good qualitative agreement in the case of temperature and very good overall agreement in the case of the Mach number distribution. Figure 7 shows the comparison between the predictions and experiment of the lower wall (hydrogen jet side) pressure. Ignition causes the pressure rise in the profile. Ignition seems to be delayed in the case of the predictions accompanied by a more pronounced pressure rise.

High speed reacting flows such as the two cases studied here are complex in spite of their simple geometries. The interactions between the different aspects of the flow such as turbulence, chemical kinetics, heat release etc. are very difficult to understand and, to a large extent, impossible to model accurately. Modern day experimental facilities still cannot make complete measurements in such flows. Only mean values of temperature, velocity, pressure, species concentrations etc. are available, if any. Even then, the uncertainties associated with the data force one to accept them only with certain reservations. Given that, there is almost never a chance for perfect agreement between predictions and experiment in all the areas. While the advances made in measurement techniques improve every day, the fruits of these advancements (ie. accurate measurements) are not realized immediately. As a result, today's computations will have only old data for validation (in the present case, the best data is already four years old) purposes which is certainly the case here. Unless more accurate experimental data with minimum uncertainties are available, the best a computational effort can hope for, in terms of validation, is probably what is seen here.

CONCLUSIONS

Computation of the flow fields of two high-speed, turbulent, reacting flow configurations involving finite-rate chemical kinetics for hydrogen-air combustion have been carried out. A two-equation ($k - \epsilon$) turbulence model with compressibility corrections has been used. The predictions are compared with available experimental data. Good qualitative agreement is present between computations and experiment. More detailed experimental data is necessary.

ACKNOWLEDGMENTS

This work was supported by the Applied Computational Fluids Branch of the Fluid Dynamics Division at NASA Ames Research Center under the Cooperative agreement number NCC 2-715.

References

- [1] Marvin, J. G., "A CFD Validation Roadmap For Hypersonic Flows", NASA Technical Memorandum 103935, 1992.
- [2] Ebrahimi, H. B., "CFD Validation For Scramjet Combustor and Nozzle Flows, Part I", AIAA-93-1840, 1993.
- [3] Vitt, P. H., Riggins, D. W. and McClinton, C. R., "The Validation and Application of Numerical Modelling to Supersonic Mixing and Reacting Flows", AIAA-92-0626, 1992.
- [4] Riggins, D. W. and McClinton, C. R., "A Computational Investigation of Mixing and Reacting Flows in Supersonic Combustors", AIAA-92-0626, 1992.
- [5] Eklund, D. R. and Northam, G. B., "A Numerical Study of the Effects of Geometry on the Performance of a Supersonic Combustor." AIAA-92-0624, 1992.
- [6] Narayan, J. R. and Girimaji, S. S., "Turbulent Reacting Flow Computations Including Turbulence-Chemistry Interactions." AIAA-92-0342, 1992.
- [7] Narayan, J. R., "A Two-Equation Turbulence Model for Compressible Reacting Flows." AIAA-91-0755, 1991.
- [8] Eklund, D. R., "Calculation of Supersonic Turbulent Reacting Coaxial Jets." AIAA Journal, Vol.28, No.9, 1990, pp 1633-1641.
- [9] Carpenter, M. H., "Three-Dimensional Computations of Cross-Flow Injection and Combustion in a Supersonic Flow", AIAA-89-1870, 1989.
- [10] Drummond, J. P., Carpenter, M. H. and Riggins, D. W., "Mixing and Mixing Enhancement in Supersonic Reacting Flows", *High Speed Propulsion Systems: Contributions to Thermodynamic Analysis*, ed. E. T. Curran and S. N. B. Murthy, American Institute of Astronautics and Aeronautics, Washington, D. C., 1990.
- [11] Drummond, J. P., "A Two-Dimensional Numerical Simulation of a Supersonic, Chemically Reacting Mixing Layer", NASA TM 4055, 1988.

- [12] Molvik, G. A. Bowles, J.V. and Huynh, L. C., "A Hypersonic Research Vehicle with Hydrocarbon Scramjet Propulsion: Design and Analysis", AIAA Paper 93-5097, 1993.
- [13] Jones, W.P. and Launder, B.E., "The Prediction of Laminarization with a Two-Equation Model of Turbulence", *Int. J. Heat Mass Transfer*, Vol.15, 1972, pp 301-314.
- [14] Launder, B.E., Reece, G.J. and Rodi, W., "Progress in the Development of a Reynolds Stress Turbulence Closure", *J. Fluid Mech.*, Vol.68, 1975, pp 537-566.
- [15] Wilcox, D.C., "A Two-Equation Turbulence Model for Wall-Bounded and Free-Shear Flows", AIAA Paper 93-2905, 1993.
- [16] Oldenberg, R. et al., "Hypersonic Combustion Kinetics - Status Report of the Rate Constant Committee, NASP High-Speed Propulsion Technology Team", *NASA TM 1107*, 1990.
- [17] Molvik, G. A. and Merkle, C. L., "A Set of Strongly Coupled Upwind Algorithms for Computing Flows in Chemical Nonequilibrium", AIAA Paper 89-0199, 1989.
- [18] Lawrence, S. L., Chaussee, D. S. and Tannehill, J. C., "Application of an Upwind Algorithm to the Three-Dimensional Parabolized Navier-Stokes Equations", AIAA 87-1112, 1987.
- [19] Zeman, O., "Compressible Turbulence Subjected to Shear and Rapid Compression", Eighth Symposium on Turbulent Shear Flows, Munich, Germany, 1991.
- [20] Wadawadigi, G. Tannehill, J. C., Buelow, P. E. and Lawrence, S. L., "A Three-Dimensional Upwind PNS Code for Chemically Reacting Scramjet Flowfields", AIAA 92-2898, 1992.
- [21] Burrows, M. C. and Kurkov, A. P., "Analytical and Experimental Study of Supersonic Combustion of Hydrogen in a Vitiated Airstream." NASA TM X-2828, 1973.
- [22] Cheng, T. S., Wehrmeyer, J. A., Pitz, R. W., Jarret, O. and Northam, G. B., "UV Raman Scattering Measurements in a Mach 2 H_2 -Air Flame for Assessment of CFD Models." Proc. of the *Central States Meeting of the Combustion Institute*, Nashville, TN, 1991.
- [23] Jarret, O. Jr., Cutler, A. D., Antcliff, R. R., Chit-somboon, T., Dancey, C. L. and Wang, J. A., "Measurements of Temperature, Density, and Velocity in Supersonic Reacting Flow for CFD Code Validation." Proc. of the *25th JANNAF Combustion Meeting*, Huntsville, Alabama, 1988.
- [24] Williams, F. A., *Combustion Theory*. Addison-Wesley Publishing Company, Inc., Reading, MA, pp. 358-429, 1965.

Table 1. H_2 - Air Reaction System

No.	Reaction
1	$H + O_2 \rightleftharpoons O + OH$
2	$OH + H_2 \rightleftharpoons H_2O + H$
3	$O + H_2 \rightleftharpoons OH + H$
4	$OH + OH \rightleftharpoons H_2O + O$
5	$H + OH + M \rightleftharpoons H_2O + M$
6	$H + H + M \rightleftharpoons H_2 + M$
7	$O + O + M \rightleftharpoons O_2 + M$
8	$H + O + M \rightleftharpoons OH + M$
9	$H + O_2 + M \rightleftharpoons HO_2 + M$
10	$OH + HO_2 \rightleftharpoons H_2O + O_2$
11	$H + HO_2 \rightleftharpoons H_2 + O_2$
12	$H + HO_2 \rightleftharpoons OH + OH$
13	$O + HO_2 \rightleftharpoons OH + O_2$
14	$HO_2 + HO_2 \rightleftharpoons H_2O_2 + O_2$
15	$H + H_2O_2 \rightleftharpoons H_2 + HO_2$
16	$OH + H_2O_2 \rightleftharpoons H_2O + HO_2$
17	$H + H_2O_2 \rightleftharpoons H_2O + OH$
18	$O + H_2O_2 \rightleftharpoons HO_2 + OH$
19	$OH + OH + M \rightleftharpoons H_2O_2 + M$
20	$OH + OH \rightleftharpoons H_2 + O_2$

Species : $H_2, O_2, H_2O, OH, H, O, HO_2, H_2O_2$ and N_2 (inert)

M is a third body (all species included)

Table 2. Conditions for coaxial jet experiment

	H_2	Air
Mach No.	1.0	1.97
Temperature	545 K	1180 K
Pressure	0.112 MPa	0.107 MPa
Velocity	1774 m/s	1380 m/s
f_{H_2}	1.0	0.0
f_{O_2}	0.0	0.246
f_{N_2}	0.0	0.545
f_{H_2O}	0.0	0.209

Fuel injector diameter=0.00236 m

Lip thickness=0.000725 m

Nozzle diameter(air flow)=0.01778 m

Table 3. Conditions for Burrows-Kurkov Experiment

	H_2	Air
Mach No.	1.0	2.44
Temperature	254 K	1270 K
Pressure	0.1 MPa	0.1 MPa
Velocity	1216 m/s	1764 m/s
f_{H_2}	1.0	0.0
f_{O_2}	0.0	0.258
f_{N_2}	0.0	0.486
f_{H_2O}	0.0	0.256

Fuel injector height=0.004 m
 Duct height at inlet=0.0938 m
 Duct height at exit=0.1048 m

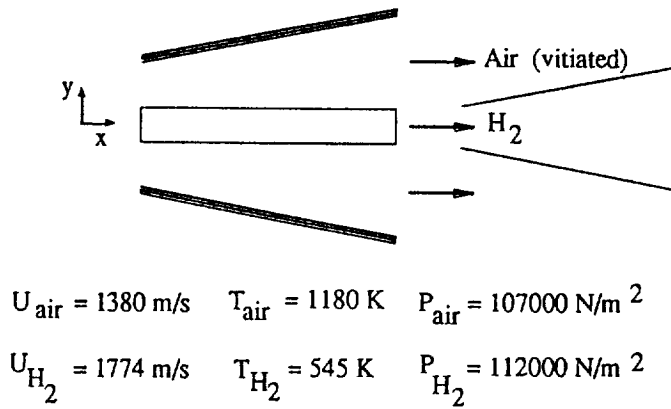


Fig. 1 Coaxial jet case : schematic

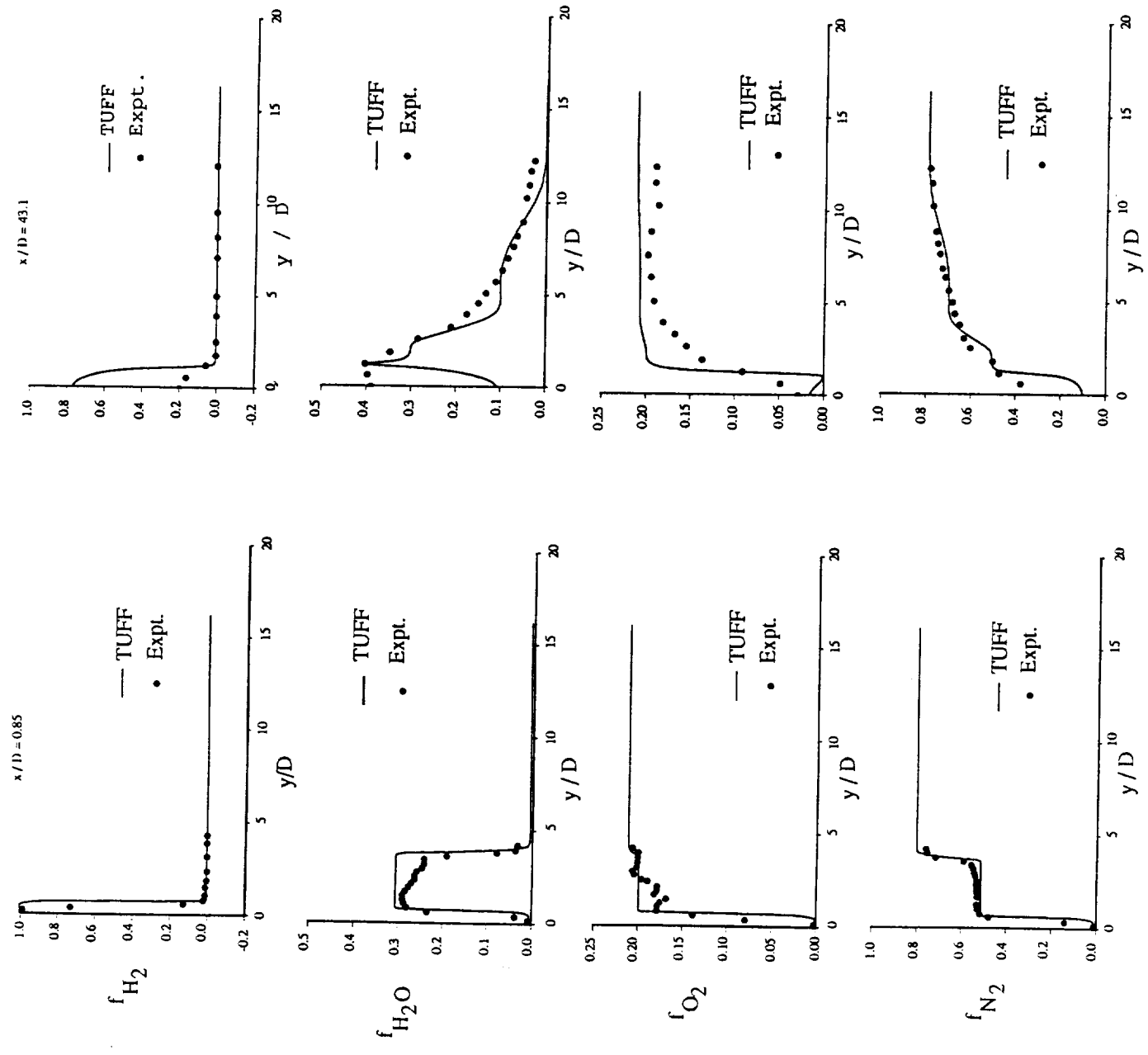
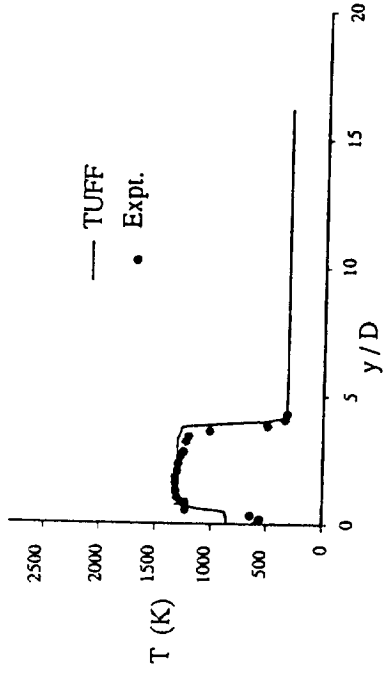


Fig. 2 Coaxial jet case: species mole fractions

$x/D = 0.85$



$x/D = 43.1$

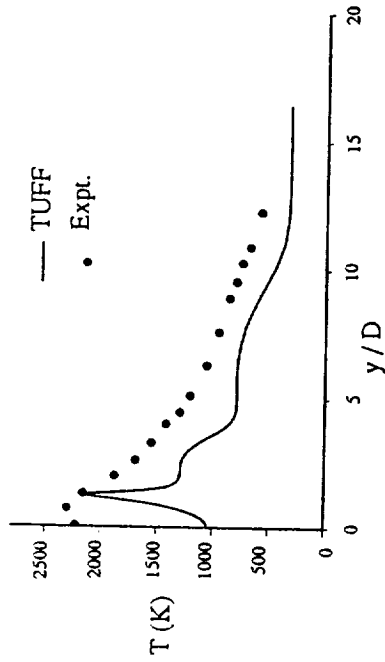


Fig. 3 Coaxial case : static temperature

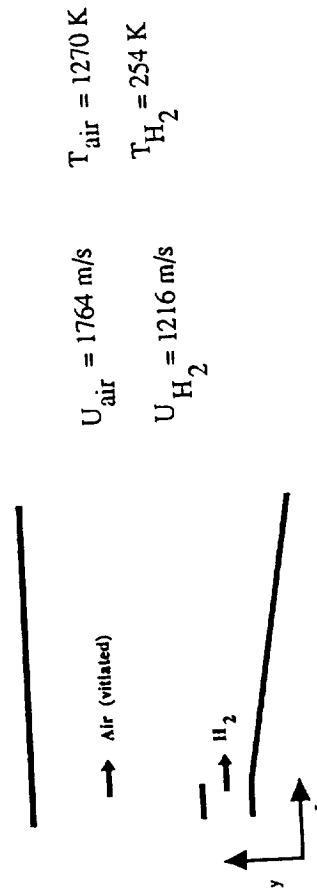
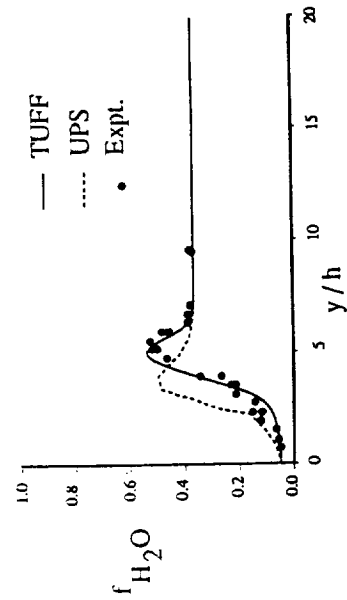
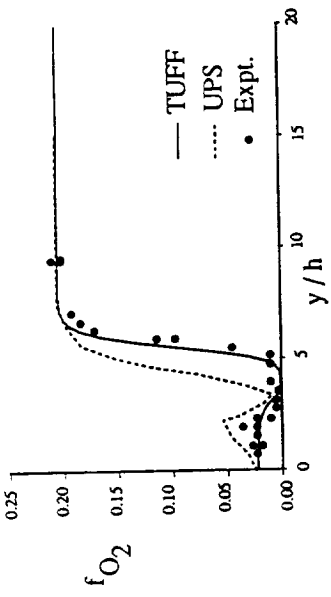


Fig. 4 Burrows-Kurkov expt. : schematic



$h = 0.004 \text{ m}$

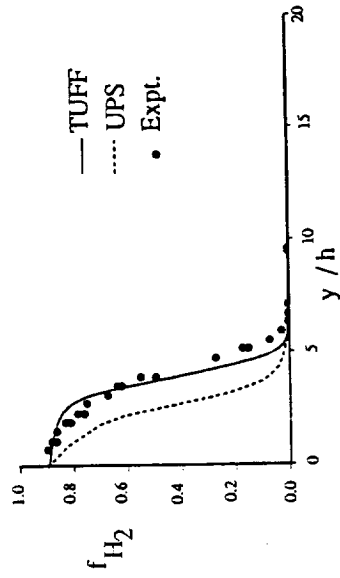
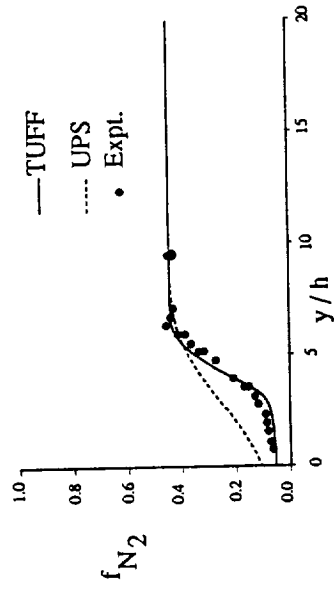


Fig. 5 Burrows-Kurkov expt. : species mole fractions at exit

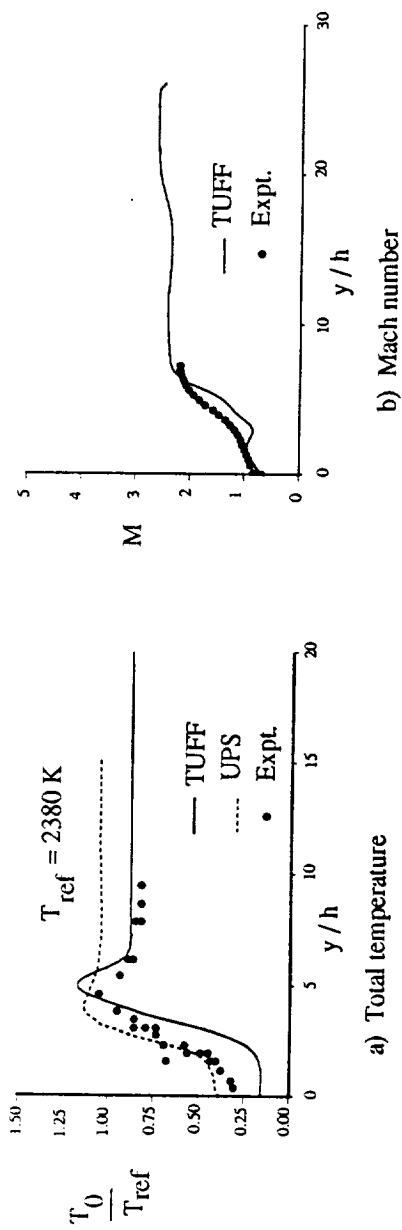


Fig. 6 Burrows-Kurkov Expt. - Temperature and Mach number at exit

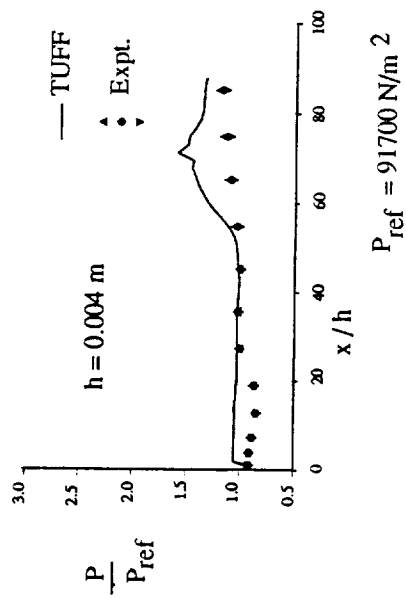


Fig. 7 Burrows-Kurkov expt. : wall pressure

APPENDIX - C

AIAA-94-2948

13 -

**Prediction Of Turbulent Reacting Flows
Related To Hypersonic Airbreathing
Propulsion Systems**

**Johnny Narayan
MCAT Institute
Moffett Field
California**

PREDICTION OF TURBULENT REACTING FLOWS RELATED TO HYPERSONIC AIRBREATHING PROPULSION SYSTEMS

J.R. Narayan*

MCAT Institute, Moffett Field, CA.

ABSTRACT

Computation of scramjet combustor flows is the main thrust of this work. Computations are done on flow configurations that resemble the reaction zone in the scramjet combustors. Compressible, reacting, turbulent flow solutions are obtained. A two equation (k - ϵ) model with compressibility correction is used to calculate the flow field. A finite rate (9-species, 20-reaction steps) chemistry model for hydrogen-air combustion has been used. Computations are carried out using the Navier-Stokes solver TUFF. Predictions are compared with available experimental data and also those obtained by using the codes UPS and SPARK. A turbulence-chemistry interaction model is included. This model represents the first step in the effort to include these interactions in high-speed reacting flows. A two-dimensional reacting mixing layer has been used for demonstration.

NOMENCLATURE

A, b	coefficients in Arrhenius rate equation
C_1, C_2, C_μ	turbulence model constants
C_5, C_6	turbulence model constants
E	total internal energy
f_n	mass fraction of species n
g	scalar variance (enthalpy, mass fraction)
H	total enthalpy
h	static enthalpy
k	turbulent kinetic energy
k_f, k_b	forward and backward reaction rate constants
L	number of reaction steps
M_n	Molecular weight of species n
M_t	Turbulent Mach number
N	number of chemical species
Pr, Pr_t	laminar and turbulent Prandtl numbers
p	pressure
Re_c, Re_T	turbulence model coefficients
R_k, R_ω	turbulence model coefficients
Sc, Sc_t	laminar and turbulent Schmidt numbers
T	temperature
T_a	Activation Temperature
t	time

\vec{U}	velocity vector
\dot{w}_n	production rate of species n
x	streamwise coordinate
x_j	j^{th} coordinate
y	transverse coordinate
α, α^*	turbulence model coefficients
α_0, α_0^*	turbulence model coefficients
σ_d, σ_ω	turbulence model constants
δ_{ij}	Kronecker delta
ϵ	turbulence energy dissipation rate
ϵ_c	compressible dissipation rate
η	compressibility correction coefficient
γ	ratio of specific heats
ω	specific dissipation rate
μ	laminar viscosity
μ_t	turbulent viscosity
ν	kinematic viscosity
ρ	density
$\sigma_k, \sigma_\epsilon$	turbulence model constants
τ_{ij}	stress tensor
Subscripts	
t	turbulent quantity

INTRODUCTION

Propulsion systems for hypersonic applications are required to use the supersonic combustion ramjet (scramjet) due to the flight regime involved. Due to the advent of the National Aerospace Plane (NASP) proposed over a decade ago, there has been a considerable amount of effort directed at developing a scramjet based propulsion system for a number of years. Even though interest in the NASP is waning at present due to various reasons, the research effort in the area of high speed propulsion systems such as the scramjet still is going strong as evidenced by the enormous number of reports published in the literature and national and international meetings. It is not within the scope of the present report to list and describe all the work going on in the area of high speed propulsion. However, references [1] to [11] are some examples of the vast amount of work in this area. The area of high speed propulsion, especially for hypersonic applications, is a complex one encompassing a wide variety of related topics such as inlet configuration, mix-

*Senior Research Scientist, Senior Member AIAA.

ing layers, mixing enhancement, combustor configuration, finite rate chemistry models and chemical kinetics. Both hydrocarbons and hydrogen are considered as fuels depending upon the application. For example, hypersonic waveriders using hydrocarbon fuels have been designed [1] for applications in the moderate hypersonic speed regimes. For Mach numbers of the order of 15 and above, hydrogen is generally considered to be the fuel of choice. The present work represents a computational effort in establishing a solution procedure for high speed propulsion in general and scramjet flows in particular.

The flow field in a scramjet is complex. It is turbulent and compressible involving high heat release. The solution procedure should address all aspects of the flow field adequately. It should be capable of accurately modelling the turbulent field, taking into account the effects of compressibility, address the changes associated with heat release and accurately describe the chemical kinetics mechanism which is vital in high speed combustion. Also, the interactions between the distinct physical aspects of the flow such as the effect of heat release on turbulence, the interaction between turbulence and chemistry etc. must be properly addressed. Progress has been made in addressing these areas via accurate and realistic modelling in recent years [6]. However, a significant amount of work remains to be done before any realistic claims for accurate models in these areas can be made. There have been remarkable advances made in the area of turbulence modelling, accounting for a variety of factors that affect the flow field. Compressibility correction models to account for the effects of compressibility, near-wall turbulence models to deal with the transition from fully turbulent to zero turbulence, viscous dominated flow field near no-slip boundaries and modifications to models to account for flow curvature are some examples. A wide variety of turbulence models, ranging from the algebraic (zero-equation) models to Reynolds stress and large eddy simulation models are available (references [12] - [14] are some examples) depending upon the sophistication and accuracy desired and the limits imposed by numerical solution procedures.

Thermodynamic and chemical kinetic models [15, 16] applicable to the scramjet flows have been undergoing continuous improvements in recent years. Accurate modelling of thermodynamic variables as functions of temperature which are valid over a wide range of temperatures is an example. The design of the combustor is strongly dependent upon factors such as the mixing between fuel and oxidizer streams, presence of shocks in the flow field, boundary layer effects, flow separation, extent of chemical reaction within the combustor and so on. The numerical solution procedure

should have the capability of addressing all of these factors while maintaining the required accuracy and robustness. Computational algorithms which are fast and accurate are being improved everyday and being adapted in present day numerical solvers applicable for a wide variety of flows including all speed regimes. In spite of the existence of a wide variety of sophisticated and physically accurate models in many of the areas associated with high speed propulsion, it is not always possible to use the best models in a numerical simulation due to the limitations imposed by computer resources, computational economy and adaptability to practical problems. Fast turnaround is a key factor in the success of any solver in practical problem solving situations. Compromises must be struck between physical accuracy and computational feasibility.

The present work represents the effort made to establish a solution procedure for high speed propulsion related flows. The models chosen to represent the turbulent and chemistry fields reflect the compromise between physical accuracy and computational economy mentioned above. The code chosen for the computations are the TUFF [17] code and the SPARK code [6, 9]. The solutions are compared with those obtained with the UPS [18, 19] code and available experimental data. The turbulence model chosen is the two-equation ($k - \epsilon$) turbulence model with low Reynolds number modifications [12]. The compressibility effects are included via the compressibility correction model proposed by Zeman [20]. The fuel used is hydrogen and a 9-species, 20-reaction steps chemical kinetics model for hydrogen-air combustion [15] (Table 1) is used (in its abbreviated version).

In the present task, major emphasis is on the turbulence model(s) used for reacting, compressible flows. Specifically, the interaction between the turbulence field and the chemical kinetics is of interest. The effect of turbulence on phenomena such as mixing between two streams, boundary layer etc. has been studied extensively and it is an ongoing process. However, there is not enough work done in the area of turbulence-chemistry interactions in order to either emphasize or neglect the importance of such interactions. The main reason for this is the fact that it is extremely difficult to quantify these interactions experimentally. There have been efforts aimed at establishing pdf-based models for coupling the turbulence field with the thermochemical field in numerical simulations. References [6], [21] and [22] are just a few of the many reports available in this area. There has also been a concerted effort to generate validation data bases through direct numerical simulations which is still in its early stages.

In the present work, on the thermochemistry front, the effects of temperature and species the effects of

temperature and species fluctuations are decoupled. For the temperature-turbulence interaction, a moment model is used [6]. The chemical species fluctuations are accounted for using an assumed multivariate- β -pdf model [6, 21, 22]. The thermochemistry models used here are independent of the model for the turbulent velocity field. These models require the solution of the evolution equations for all the mean flow thermochemical variables, turbulence variables (k and either ω or ϵ), enthalpy variance and turbulent scalar energy (sum of all the species variances). The CFD code used is SPARK [9].

Mixing plays a major role in high speed combustor flows. The reaction zone is mainly confined to mixing layers that exist between fuel and oxidizer streams. Efficient mixing of fuel and oxidizer is very important for the design of combustor size. Mixing layers ranging from subsonic to supersonic speeds have been studied extensively over the years. In the present work, a two-dimensional and axisymmetric compressible, reacting, mixing layer (hydrogen-air) is computed with the aforementioned codes. Experimental data from compressible, reacting mixing layers is still scarce which hinders the validation of the calculation procedure. Three flow configurations are chosen for the study. The first two are chosen to demonstrate the solution procedure without the turbulence-chemistry interaction model and the last case is used exclusively to demonstrate the effect of this model. The first case is the well known Burrows-Kurkov experiment [23] in which hydrogen and vitiated air streams (two-dimensional) mix and react. The second case is that of an axisymmetric configuration [24, 25] where two coaxial jets (fuel and oxidizer) mix and react. The two-equation, ($k-\epsilon$) turbulence model is used for these applications. Available data from the above two experiments are used to compare with the predictions. The last case considered is a two-dimensional, reacting, mixing layer problem. Here, the two-equation, ($k-\omega$) turbulence model [14] has been used. The governing and secondary equations used in the computations have all been described in detail in the references cited above. Only an abbreviated equation set will be given in the present paper. The computations were performed on the supercomputers of NAS and NASA Ames Research Center.

GOVERNING EQUATIONS

The equations used for computations are described in detail in references [6, 7, 10] and [26]. Only the forms of the modelled equations used in the present study are given here. Density-weighted averaging is used to derive the mean flow equations from the instantaneous conservation equations. In the following,

a tilde represents Favre (density-weighted) averaging and a simple overbar represents conventional time averaging. The averaged continuity and momentum equations are

$$\frac{\partial \bar{\rho}}{\partial t} + \frac{\partial \bar{\rho} \widetilde{U}_i}{\partial x_i} = 0 \quad (1)$$

$$\frac{\partial \bar{\rho} \widetilde{U}_i}{\partial t} + \frac{\partial \bar{\rho} \widetilde{U}_i \widetilde{U}_j}{\partial x_j} = - \frac{\partial \bar{p}}{\partial x_i} - \frac{\partial \overline{\rho u_i'' u_j''}}{\partial x_j} + \frac{\partial \tau_{ij}}{\partial x_j} \quad (2)$$

where

$$\tau_{ij} = \mu \left(\frac{\partial u_i}{\partial x_j} + \frac{\partial u_j}{\partial x_i} \right) - \frac{2}{3} \frac{\partial u_k}{\partial x_k} \delta_{ij} \quad (3)$$

with repeated indices indicating summation.

In the two-equation turbulence model, the two turbulence variables are the turbulent kinetic energy (k) and either the dissipation rate ϵ [12] or the specific dissipation rate ω [14]. The definitions of these variables can be found in the cited references. Boussinesq approximation is used to obtain closure of the averaged equations. The Reynolds stress tensor is written as,

$$\begin{aligned} - \overline{\rho u_i'' u_j''} &= \bar{\mu}_t S_{ij} - \frac{2}{3} \bar{\rho} k \delta_{ij} \\ S_{ij} &= \frac{\partial \widetilde{U}_i}{\partial x_j} + \frac{\partial \widetilde{U}_j}{\partial x_i} - \frac{2}{3} \frac{\partial \widetilde{U}_k}{\partial x_k} \delta_{ij} \end{aligned} \quad (4)$$

where μ_t is the turbulent/eddy viscosity defined as

$$\bar{\mu}_t = C_\mu \bar{\rho} \frac{k^2}{\epsilon} \quad (5)$$

with $C_\mu=0.09$, or, with ω defined as,

$$\omega = \epsilon / (C_5 k) \quad (6)$$

where

$$C_5 = \frac{9}{100} \frac{\frac{5}{18} + \left(\frac{Re_T}{R_c}\right)^4}{1 + \left(\frac{Re_T}{R_c}\right)^4} \quad (7)$$

with $R_c=6$ and

$$Re_T = \frac{\bar{\rho} k}{\omega \bar{\mu}} \quad (8)$$

μ_t is given as

$$\bar{\mu}_t = \alpha^* \bar{\rho} \frac{k}{\omega} \quad (9)$$

with

$$\alpha^* = \frac{\alpha_0^* + \frac{Re_T}{R_k}}{1 + \frac{Re_T}{R_k}} \quad (10)$$

and

$$\alpha_0^* = C_6/3, \quad R_k = 8, \quad C_6 = \frac{3}{40} \quad (11)$$

The modelled momentum equation, then, is,

$$\begin{aligned} \frac{\partial \bar{\rho} \widetilde{U}_i}{\partial t} + \frac{\partial \bar{\rho} \widetilde{U}_i \widetilde{U}_j}{\partial x_j} &= - \frac{\partial \bar{p}}{\partial x_i} + \frac{2}{3} \frac{\partial \bar{\rho} k}{\partial x_j} \delta_{ij} \\ &- \frac{\partial}{\partial x_j} [(\bar{\mu} + \bar{\mu}_t) S_{ij}] \end{aligned} \quad (12)$$

The effects of compressibility are included via the model proposed by Zeman [20]. Here, the compressible dissipation terms are expressed as functions of the turbulent kinetic energy dissipation rate and the local turbulent Mach number. The compressibility effects are represented by a component of the dissipation rate (ϵ_c) given as

$$\begin{aligned} \epsilon_c &= K_c \epsilon \\ K_c &= \eta F(M_t) \\ M_t &= \frac{2k}{a^2} \end{aligned} \quad (13)$$

where a is the local speed of sound and $F(M_t)$ is a function of the local turbulent Mach number (M_t). $F(M_t)$ is given by

$$\begin{aligned} F(M_t) &= 1 - \exp[-(\frac{M_t - M_{t0}}{0.6})^2], \quad M_t \geq M_{t0} \\ &= 0, \quad M_t < M_{t0} \end{aligned} \quad (14)$$

with $M_{t0}=0.1$ and $\eta=0.75$. The modelled turbulent kinetic energy equation is [6, 12]

$$\begin{aligned} \frac{\partial \bar{\rho} k}{\partial t} + \frac{\partial \bar{\rho} k \widetilde{U}_j}{\partial x_j} &= P_k - \bar{\rho} \Phi (1 + K_c) \\ &+ \frac{\partial}{\partial x_j} [(\bar{\mu} + \frac{\bar{\mu}_t}{\sigma_k}) \frac{\partial k}{\partial x_j}] \end{aligned} \quad (15)$$

where Φ is either ϵ or ωk and

$$P_k = - \frac{\overline{\rho u_i'' u_j''}}{\partial x_j} \frac{\partial \widetilde{U}_i}{\partial x_j} \quad (16)$$

The modelled ϵ -equation used (no compressibility corrections) in the present analysis [12] is given below.

$$\begin{aligned} \frac{\partial \bar{\rho} \epsilon}{\partial t} + \frac{\partial \bar{\rho} \epsilon \widetilde{U}_j}{\partial x_j} &= (C_1 P_k - C_2 \bar{\rho} \epsilon) \frac{\epsilon}{k} \\ &+ \frac{\partial}{\partial x_j} [(\bar{\mu} + \frac{\bar{\mu}_t}{\sigma_\epsilon}) \frac{\partial \epsilon}{\partial x_j}] \end{aligned} \quad (17)$$

where P_k is the production term in the turbulent kinetic energy equation. The modelled ω -equation [14]

is given below.

$$\begin{aligned} \frac{\partial \bar{\rho} \omega}{\partial t} + \frac{\partial \bar{\rho} \omega \widetilde{U}_j}{\partial x_j} &= \alpha \frac{\omega}{k} P_k - C_6 \bar{\rho} \omega^2 + \sigma_d \frac{\bar{\rho}}{\omega} D_{k\omega} \\ &+ \frac{\partial}{\partial x_j} [(\bar{\mu} + \frac{\bar{\mu}_t}{\sigma_\omega}) \frac{\partial \omega}{\partial x_j}] \end{aligned} \quad (18)$$

where

$$D_{k\omega} = \frac{\partial k}{\partial x_j} \frac{\partial \omega}{\partial x_j} \quad (19)$$

and

$$\alpha = \frac{1}{2\alpha^*} \frac{\alpha_0 + \frac{Re_\tau}{R_\omega}}{1 + \frac{Re_\tau}{R_\omega}} \quad (20)$$

The turbulence constants are $\alpha_0=0.1$, $R_\omega=2.2$, $\sigma_\omega=1.67$, $C_1=1.44$, $C_2=1.92$, $\sigma_k=1.0$, $\sigma_\epsilon=1.3$, $Pr=0.72$, $Pr_t=1.0$, $Sc=0.22$ and $Sc_t=1.0$ and

$$\begin{aligned} \sigma_d &= 0.0, \quad D_{k\omega} \leq 0 \\ &= 0.3, \quad D_{k\omega} > 0 \end{aligned}$$

The mass-averaged total energy can be written in terms of the total enthalpy as

$$\tilde{E} = \tilde{H} - \frac{\bar{p}}{\rho} \quad (21)$$

The correlations between the fluctuating velocity and the scalar fluctuations are modelled using a gradient-diffusion hypothesis. A typical model is of the form

$$- \overline{\rho u_i'' \phi''} = \frac{\bar{\mu}_t}{\sigma_\phi} \left(\frac{\partial \tilde{\phi}}{\partial x_i} \right) \quad (22)$$

where σ_ϕ is a coefficient which, normally, is a constant. For $\phi = f_n$ (n represents the species), $\sigma_\phi = Sc_t$, and for the static enthalpy, ($\phi = h$), $\sigma_\phi = Pr_t$. Using the above definition, and omitting the body force contribution, the time-averaged and modelled energy equation [6] is

$$\begin{aligned} \frac{\partial \bar{\rho} \tilde{E}}{\partial t} + \frac{\partial \bar{\rho} \tilde{E} \widetilde{U}_j}{\partial x_j} &= \frac{\partial}{\partial x_j} (\overline{\tau_{ij}} - \bar{p} \delta_{ij} - \overline{\rho u_i'' u_j''}) \widetilde{U}_i \\ &+ \frac{\partial}{\partial x_j} [(\frac{\bar{\mu}}{Pr} + \frac{\bar{\mu}_t}{Pr_t}) \frac{\partial \tilde{h}}{\partial x_j} + (\bar{\mu} + \frac{\bar{\mu}_t}{\sigma_k}) \frac{\partial k}{\partial x_j}] \end{aligned} \quad (23)$$

where σ_k comes from the turbulent kinetic energy equation. The modelled species continuity equation is

$$\frac{\partial \bar{\rho} \tilde{f}_n}{\partial t} + \frac{\partial \bar{\rho} \tilde{f}_n \widetilde{U}_j}{\partial x_j} = \overline{w_n} - \frac{\partial}{\partial x_j} [(\frac{\bar{\mu}}{Sc} + \frac{\bar{\mu}_t}{Sc_t}) \frac{\partial \tilde{f}_n}{\partial x_j}] \quad (24)$$

The modelled form of the mean species production rate due to chemical reaction ($\overline{w_n}$) is given, for a finite-rate system involving L reaction steps and N species,

in the following general form:

$$\dot{w}_n = M_n \sum_{l=1}^L (\nu''_{nl} - \nu'_{nl}) \times \{k_{f_l} \rho^{m_l} \prod_{s=1}^N (\frac{f_s}{M_s})^{\nu'_{sl}} - k_{b_l} \rho^{n_l} \prod_{s=1}^N (\frac{f_s}{M_s})^{\nu''_{sl}}\}, \quad (25)$$

where

$$m_l = \sum_{s=1}^N \nu'_{sl}, \quad n_l = \sum_{s=1}^N \nu''_{sl}$$

where, ν'_{sl} and ν''_{sl} are the number of molecules of the scalar s involved in the l -th reaction step in the forward and backward directions, respectively. The forward and backward rate-constants of the reaction l are given by k_{f_l} and k_{b_l} respectively.

$$k_{f_l} = A_l T^{b_l} \exp[-\frac{T_{a_l}}{T}] \quad (26)$$

where A_l , b_l and T_{a_l} are numerical constants specific to the given reaction step l . k_{b_l} is determined from the equilibrium constant for the l -th reaction step and k_{f_l} .

Turbulence-chemistry interaction model

Practical combustor flows involve multiple scalar mixing and reactions. In order to calculate the mean species production rate using the probability density function (pdf) approach, a model for the joint pdf of temperature and various species is required. Such a joint pdf is difficult to specify and as a preliminary step we effect the simplification that temperature and species fluctuations are uncorrelated. This permits us to deal with the temperature and species fluctuations separately. Equation (26) can be written as

$$k_{f_l} = A_l (\tilde{T} + T'')^{b_l} \exp[-\frac{T_{a_l}}{(\tilde{T} + T'')}] \quad (27)$$

Assuming that $\frac{T''}{\tilde{T}} < 1$, the term $(\tilde{T} + T'')$ can be expanded in a series and the resultant modified reaction rate term is written as,

$$\tilde{k}_{f_l} = (1 + m) A_l \tilde{T}^{b_l} \exp[-\frac{T_{a_l}}{\tilde{T}}] \quad (28)$$

where

$$m = [(b_l - 1) (\frac{b_l}{2} + \frac{T_{a_l}}{\tilde{T}}) + \frac{1}{2} (\frac{T_{a_l}}{\tilde{T}})^2] \frac{\overline{T''T''}}{\tilde{T}^2} \quad (29)$$

Terms of order higher than two in $\frac{T''}{\tilde{T}}$ are neglected from the series expansion in the present analysis since accurate models for these higher order terms do not

exist. The factor m represents the effect of temperature fluctuations on the mean reaction rate. The temperature variance is calculated from the enthalpy variance [6].

For reacting flows involving multiple chemical species, a multivariate β -pdf model is used to account for the effects of the scalar fluctuations on the species production rates [6]. Relevant features of this model are briefly outlined below. The parameters of the multivariate β -pdf for the N -scalar mixing process $(\beta_1, \dots, \beta_N)$ are functions of the mean mass fractions \bar{f}_n and turbulent scalar energy Q :

$$\beta_n = \bar{f}_n (\frac{1 - S}{Q} - 1) \quad (30)$$

where

$$S = \sum_{n=1}^N \bar{f}_n^2, \quad Q = \sum_{n=1}^N \overline{f''_n f''_n}. \quad (31)$$

Decoupling the effects of temperature and species concentrations, the mean species production rate can be written as,

$$\overline{\dot{w}_n} = M_n \sum_{l=1}^L (\nu''_{nl} - \nu'_{nl}) \times \{ \overline{k_{f_l} \rho^{m_l} (\prod_{s=1}^N M_s^{-\nu'_{sl}})} I_{f_l} - \overline{k_{b_l} \rho^{n_l} (\prod_{s=1}^N M_s^{-\nu''_{sl}})} I_{b_l} \} \quad (32)$$

$$\{ \overline{k_{f_l} \rho^{m_l} (\prod_{s=1}^N M_s^{-\nu'_{sl}})} I_{f_l} - \overline{k_{b_l} \rho^{n_l} (\prod_{s=1}^N M_s^{-\nu''_{sl}})} I_{b_l} \}$$

where

$$I_{f_l} \equiv \langle \prod_{s=1}^N f_s^{\nu'_{sl}} \rangle, \quad I_{b_l} \equiv \langle \prod_{s=1}^N f_s^{\nu''_{sl}} \rangle$$

In the above, angular brackets represent conventional time averaging. The modelled expression for I_{f_l} using the multivariate β -pdf is [21],

$$I_{f_l} = \prod_{s=1}^N \prod_{r=1}^{\nu'_{sl}} (\beta_s + \nu'_{sl} - r) / \prod_{p=1}^{m_l} (B + m_l - p) \quad (33)$$

Similarly, the expression for I_{b_l} is,

$$I_{b_l} = \prod_{s=1}^N \prod_{r=1}^{\nu''_{sl}} (\beta_s + \nu''_{sl} - r) / \prod_{p=1}^{n_l} (B + n_l - p) \quad (34)$$

where

$$B = \beta_1 + \beta_2 + \dots + \beta_N \quad (35)$$

The production of turbulent scalar energy due to chemical reaction can be decomposed as

$$\sum_{n=1}^N \overline{\dot{w}_n f''_n} = \sum_{n=1}^N \overline{\dot{w}_n f_n} - \sum_{n=1}^N \overline{\dot{w}_n} \tilde{f}_n. \quad (36)$$

Only the first term on the right hand side of the above equation needs further modeling and details can be found in reference [6]. The turbulence-thermochemistry interaction models require the enthalpy variance and the turbulent scalar energy distributions. The modeled equations for enthalpy variance ($\widetilde{h''h''}$) and turbulent scalar energy (Q) are of a form similar to that of the turbulent kinetic energy:

$$\begin{aligned} \frac{\partial \bar{\rho}g}{\partial t} + \frac{\partial \bar{\rho}g\widetilde{U}_j}{\partial x_j} &= -2\overline{\rho u_j''G''} \frac{\partial \widetilde{G}}{\partial x_j} - 2\bar{\rho}\epsilon_g \\ &+ \frac{\partial}{\partial x_j} \left[\left(\frac{\bar{\mu}}{\sigma} + \frac{\bar{\mu}_t}{\sigma_g} \right) \frac{\partial g}{\partial x_j} \right] + \Psi. \end{aligned} \quad (37)$$

For $g = \widetilde{h''h''}$, $G = h$, $\Psi=0$, $\sigma = Pr$ and $\sigma_g = Pr_t$. For $g = \sum_{n=1}^N \widetilde{f_n''f_n''}$, $G = f_n$, $\Psi = 2\sum_{n=1}^N \overline{w_n f_n''}$, $\sigma = Sc$ and $\sigma_g = Sc_t$. The dissipation term in the above equation is assumed to be

$$\epsilon_g = C_g \frac{\epsilon}{k} g = C_g C_2 \omega g \quad (38)$$

Solution of the modeled equations

The equations are discretized and integrated in space and time to obtain steady state solutions using either the finite-volume based numerical solver TUFF [17] (for the first two test cases) or the finite difference solver SPARK [9] (for the last case). The TUFF code contains many desirable features for the computation of three-dimensional, hypersonic flow fields. It has non-equilibrium, equilibrium and perfect gas capabilities along with an incompressible option. It employs a finite-volume philosophy to ensure that the schemes are fully conservative. The upwind inviscid fluxes are obtained by employing a new temporal Riemann solver that fully accounts for the gas model used. This property allows the flow field discontinuities such as shocks and contact surfaces to be captured by the numerical scheme without smearing. Total Variation Diminishing (TVD) techniques are included to allow extension of the schemes to higher orders of accuracy without introducing spurious oscillations. The schemes employ a strong coupling between the fluid dynamic and species conservation equations and are made fully implicit to eliminate the step-size restriction of explicit schemes. This is necessary since step-sizes in a viscous, chemically reacting calculation can be excessively small for an explicit scheme, and the resulting computer times prohibitively large. A fully conservative zonal scheme has been implemented to allow solutions of very complex problems. The schemes are made implicit by fully linearizing all of the fluxes and source terms and by employing a modified Newton iteration to eliminate any linearization and approximate factorization errors that might occur. Approximate factorization is then employed to

avoid solving many enormous banded matrices. As mentioned before, the options for turbulence models include both zero and two equation models (both $k-\epsilon$ and $k-\omega$). For more details about the solution procedure the reader is directed to the reference cited above [17]. The SPARK solver is a finite difference elliptic solver using a hybrid McCormack scheme. More details about the solution procedure can be found in references [6] and [9].

RESULTS AND DISCUSSION

The computational effort is divided into two parts. The first part deals with the demonstration and validation process for the solution procedure by application to high speed turbulent reacting flows involving finite rate hydrogen-air chemistry. As mentioned before, the Navier Stokes solver TUFF has been used for the computations. Two reacting flow configurations have been chosen for this part. The first test case considered is the Burrows-Kurkov experiment [23]. The flow configuration is two-dimensional. A schematic diagram of the configuration is given in figure 1. No-slip walls bound both the upper and lower regions ($y=0$ and $y=y_{max}$). The lower wall is inclined to form an expansion surface. Hydrogen is injected into a vitiated air stream. The two streams mix and react downstream of the injection location (inlet). The hydrogen stream is injected at a velocity of 1216 m/sec and a temperature of 254 K. The airstream comes in at a speed of 1764 m/sec and a temperature of 1270 K. Full details about the flow parameters and geometry are given in Table 2. In this case, the reference length used in the hydrogen jet width at inlet, h ($h=0.004$ m). A constant turbulence intensity level is used for arriving at the initial distribution of turbulent kinetic energy and the dissipation rate. A 13-step, 8-species $H_2 - Air$ reaction model (Table 1) has been used for the finite-rate chemistry system considered here. The grid size is 81 X 121 (81 grid points in the axial (x) direction and 121 grid points in the transverse direction). The total length of the solution domain is 0.356 m ($x/h=89$). Available inlet data have been used for the first-plane profiles which improved the predictions remarkably over the solutions obtained with uniform profiles. The solutions are compared with the available experimental data at this location (exit) in figures 2-4. The solutions carried out with the space marching PNS code UPS [19] using the Baldwin-Lomax turbulence model are also given for comparison.

Figure 2 shows the comparison between the predicted distributions of the species mole fractions and the corresponding experimental data. As seen in these figures, there is excellent agreement between the TUFF predictions and experiment. The predictions by

the UPS and SPARK codes do not agree very well but still there is very good qualitative agreement with the experimental data. Figure 3 compares the predicted profiles of exit plane total temperature with the experimental data. There is good qualitative agreement here. Figure 4 shows the comparison between the predictions and experiment of the lower wall (hydrogen jet side) pressure. Ignition causes the pressure rise in the profile. Ignition seems to be delayed in the case of the TUFF predictions accompanied by a more pronounced pressure rise. A point to note here is the fact that the SPARK, UPS and TUFF codes produced nearly identical results for nonreacting mixing layers which is not the case in the present reacting flow simulations.

The second case is that of coaxial jets [24, 25] where a hydrogen jet flows (inner jet) coaxially with an outer vitiated air (mass fractions: oxygen=0.246, water=0.209 and nitrogen=0.545) jet. A schematic of the flow problem is given in Figure 5. The two streams are, air ($U=1380$ m/sec, $T=1180$ K with $p=107000$ N/m²) and hydrogen ($U=1774$ m/sec, $T=545$ K with $p=112000$ N/m²). The air stream is supersonic with a Mach number of 1.97 and the hydrogen stream Mach number is 1.00. The inlet mean velocity is assumed to have a step profile with the two jets having uniform speeds at the specified values (no experimental data available). The velocity in the lip region of the inner jet tube wall (finite wall thickness) is assumed to be zero. The inlet temperature profile is derived based on the experimental data given for a location just downstream of it (shown later). The inlet species mass fraction distributions are also chosen based on the experimental data provided at the same downstream location. The models for turbulence and chemistry are identical to the ones used for the first test case. A 81 X 91 grid (81 points in flow direction, 91 points in the radial direction) was used for the calculations. The inner jet/tube diameter ($D=0.00236$ m) is used as a reference length. The total length of the flow domain is equal to $43.1 D$. The outer boundary (radial) of the flow domain is taken to be at $y=17 D$. A more detailed description of the flow parameters is given in Table 3. The region outside the limits of the air jet is assumed to be still air at a temperature of 273 K. The two-equation ($k - \epsilon$) turbulence model is used along with the finite rate H_2 -Air chemistry model mentioned above. In all the figures shown for this case, y refers to the radial distance measured from the axis of the coaxial system of jets.

Figures 6 - 7 show the results of the computations. Figure 6 shows the computed and experimental distributions of species mole fractions. The figure is designed in a two-column format. The left side column represents the inlet (first x-location) data and the right side column is the data at the exit plane

($x/D=43.1 D$). As seen in these figures, the inlet data agreement between the computations and experiment is not perfect, especially around the jet edges, and this might affect the computed distributions at downstream locations. The comparison between predictions and experiment at the downstream location ($x/D=43.1 D$) is good given the above mismatch between the computational and experimental data at the inlet. The development of the reaction zone after ignition is not predicted well by the TUFF code whereas the SPARK code fares better. The experimental data indicates that the reaction zone (depicted by the water mole fraction distribution) spreads more quickly than the predictions indicate. There seems to be a discrepancy between the locations of peak reaction activity between the predictions (off the axis) and the experiment (closer to axis). However, there is very good qualitative agreement between the data with the peak values of the reaction products predicted very well. The flow domain was seen to have a wave-like structure as shown by the predicted profiles. Figure 7 shows the comparison of static temperature data. The agreement between predictions and experiment is good qualitatively displaying similar trends. The uncertainty associated with the accuracy of the experimental data is unknown. There are considerable differences between the data presented by the two references [24, 25], especially in the temperature profiles. Overall, there is good qualitative agreement between the predictions and experiment.

In the second part, the turbulence-chemistry interaction model is demonstrated using a two-dimensional mixing layer configuration. A schematic of the flow problem is given in figure 8. The two streams are, air ($U =1606$ m/sec, $T =1600$ K with $f_{H_2}=0.0$, $f_{O_2}=0.267$ and $f_{N_2}=0.733$) and hydrogen ($U =1250$ m/sec, $T =254$ K with $f_{H_2}=1.0$, $f_{O_2}=0.0$ and $f_{N_2}=0.0$). The two streams are supersonic with the air stream Mach number of 2.07 and hydrogen stream Mach number of 1.03. The inlet mean velocity is assumed to have a hyperbolic tangent profile. A constant turbulence intensity level is used in the free stream for arriving at the initial distribution of turbulent kinetic energy and the specific dissipation rate. The pressures are matched between the two streams ($P =1$ atm.). A 13-step, 8-species $H_2 - Air$ reaction model (Table 1) has been used for the finite-rate chemistry system considered here. A 101 X 81 grid (101 points in flow direction, 81 points in the transverse direction) was used for the calculations. The length of the flow domain is 0.25 m and its width is 0.05 m. In the figures the title g refers to calculations that include the interaction model.

The difference made by the temperature fluctuations model is shown in figure 9. Here the factor $(1 + m)$ is

plotted as a function of y for the first three reaction steps at the exit plane of the flow domain. The need for including the temperature fluctuations is evident in the figure. The forward reaction rate changes by as much as 400 percent (reaction step 1) due to the effect of this model. The species production rate is a strong function of the reaction rate (29) and hence will be affected by the inclusion of this model. The effect of the turbulence-chemistry interactions model on the species production rate is shown in the next few figures. Figure 10 shows the production rates of the major species involved (H_2 , O_2 , H_2O , OH) as functions of y at the exit plane. Computational results obtained with $(k-\omega-g)$ and without $(k-\omega)$ the effect of these interactions are shown in the figure. It is seen that the interaction between turbulence and chemistry has a significant effect on the net production rate of chemical species. While it is not conclusive whether the turbulence-chemistry interactions increase or decrease the production rates of individual species, it is important to note that these interactions do have a significant effect on progress of the chemical reactions. Figure 11 shows the effect of the interactions on the species distributions. The effect seems to be more pronounced in the case of the products (H_2O , OH) than the primary reactants (H_2 , O_2). The changes are larger in regions of higher gradients (on the fuel stream side for H_2 and air stream side for O_2 , for example).

This effort represents a significant push in the right direction in this very important area of turbulent reacting flows. The model is simple to use and is easily adaptable to other types of turbulence closures such as the Reynolds stress models. More improvements can certainly be done in terms of using more realistic models for the temperature and concentration fluctuations such as a pdf-based model for temperature effects (as opposed to the moment model employed here), a joint-pdf model to represent the effects of both the temperature and the concentration fields etc. However, in order for the model to be useful for practical applications, it must be kept in a form which promotes ease of use as well as computational economy. This is the main reason for resorting to a two-equation level turbulence model in the present work. A concerted validation effort is crucial to ensure the success of the modelling efforts. One debilitating factor in this regard is the nonexistence of useful experimental data. It is extremely difficult, if not almost impossible, to obtain such experimental data using present day equipment. An alternative seems to be direct numerical simulations (DNS) which has shown promising signs in relatively simpler flow configurations.

CONCLUSIONS

A numerical solution procedure applicable to high speed reacting flows has been demonstrated. In the first part, computation of the flow fields of two high-speed, turbulent, reacting flow configurations involving finite-rate chemical kinetics for hydrogen-air combustion have been carried out. A two-equation ($k - \epsilon$) turbulence model with compressibility corrections has been used. The predictions are compared with available experimental data. Good qualitative agreement is present between computations and experiment. More detailed experimental data is necessary. In the second part, a turbulence-chemistry interaction model is introduced and its effect is demonstrated via a two-dimensional turbulent reacting flow problem. The interactions seem to have a significant effect on the species production rate. More detailed analysis is necessary.

ACKNOWLEDGMENTS

This work was supported by the Applied Computational Fluids Branch of the Fluid Dynamics Division at NASA Ames Research Center under the Cooperative agreement number NCC 2-715. The author wishes to acknowledge the contributions of Dr. Gregory Molvik of MCAT Institute, NASA Ames Research Center, California and Dr. Ganesh Wadawadigi of University of Texas at Arlington, Texas. Also, the invaluable contribution to the interaction model by Dr. Sharath Girimaji of ICASE, NASA Langley Research Center is acknowledged and appreciated.

References

- [1] Molvik, G. A. Bowles, J.V. and Huynh, L. C., "A Hypersonic Research Vehicle with Hydrocarbon Scramjet Propulsion: Design and Analysis", AIAA Paper 93-5097, 1993.
- [2] Ebrahimi, H. B., "CFD Validation For Scramjet Combustor and Nozzle Flows, Part I", AIAA-93-1840, 1993.
- [3] Vitt, P. H., Riggins, D. W. and McClinton, C. R., "The Validation and Application of Numerical Modelling to Supersonic Mixing and Reacting Flows", AIAA-92-0626, 1992.
- [4] Riggins, D. W. and McClinton, C. R., "A Computational Investigation of Mixing and Reacting Flows in Supersonic Combustors", AIAA-92-0626, 1992.
- [5] Eklund, D. R. and Northam, G. B., "A Numerical Study of the Effects of Geometry on the Performance of a Supersonic Combustor." AIAA-92-0624, 1992.

- [6] Narayan, J. R. and Girimaji, S. S., "Turbulent Reacting Flow Computations Including Turbulence-Chemistry Interactions." AIAA-92-0342, 1992.
- [7] Narayan, J. R., "A Two-Equation Turbulence Model for Compressible Reacting Flows." AIAA-91-0755, 1991.
- [8] Eklund, D. R., "Calculation of Supersonic Turbulent Reacting Coaxial Jets." AIAA Journal, Vol.28, No.9, 1990, pp 1633-1641.
- [9] Carpenter, M. H., "Three-Dimensional Computations of Cross-Flow Injection and Combustion in a Supersonic Flow", AIAA-89-1870, 1989.
- [10] Drummond, J. P., Carpenter, M. H. and Riggins, D. W., "Mixing and Mixing Enhancement in Supersonic Reacting Flows", *High Speed Propulsion Systems: Contributions to Thermodynamic Analysis*, ed. E. T. Curran and S. N. B. Murthy, American Institute of Astronautics and Aeronautics, Washington, D. C., 1990.
- [11] Drummond, J. P., "A Two-Dimensional Numerical Simulation of a Supersonic, Chemically Reacting Mixing Layer", *NASA TM 4055*, 1988.
- [12] Jones, W.P. and Launder, B.E., "The Prediction of Laminarization with a Two-Equation Model of Turbulence", *Int. J. Heat Mass Transfer*, Vol.15, 1972, pp 301-314.
- [13] Launder, B.E., Reece, G.J. and Rodi, W., "Progress in the Development of a Reynolds Stress Turbulence Closure", *J. Fluid Mech.*, Vol.68, 1975, pp 537-566.
- [14] Wilcox, D.C., "A Two-Equation Turbulence Model for Wall-Bounded and Free-Shear Flows", AIAA Paper 93-2905, 1993.
- [15] Oldenborg, R. et al., "Hypersonic Combustion Kinetics - Status Report of the Rate Constant Committee, NASP High-Speed Propulsion Technology Team", *NASA TM 1107*, 1990.
- [16] Jachimowski, C. J., "An Analytical Study of the Hydrogen-Air Reaction Mechanism with Application to Scramjet Combustion", *NASA TP 2791*, 1988.
- [17] Molvik, G. A. and Merkle, C. L., "A Set of Strongly Coupled Upwind Algorithms for Computing Flows in Chemical Nonequilibrium", AIAA Paper 89-0199, 1989.
- [18] Lawrence, S. L., Chaussee, D. S. and Tannehill, J. C., "Application of an Upwind Algorithm to the Three-Dimensional Parabolized Navier-Stokes Equations", AIAA 87-1112, 1987.
- [19] Wadawadigi, G. Tannehill, J. C., Buelow, P. E. and Lawrence, S. L., "A Three-Dimensional Upwind PNS Code for Chemically Reacting Scramjet Flowfields", AIAA 92-2898, 1992.
- [20] Zeman, O., "Compressible Turbulence Subjected to Shear and Rapid Compression", Eighth Symposium on Turbulent Shear Flows, Munich, Germany, 1991.
- [21] Girimaji, S. S., "A Simple Recipe for Modeling Reaction-rates in Flows with Turbulent-Combustion", AIAA-91-1792, 1991.
- [22] Girimaji, S. S., "Assumed β -pdf model for turbulent mixing: Validation and Extension to Multiple Scalar Mixing", *Combustion Science & Technology*, Vol.78, 1991, pp 177-196.
- [23] Burrows, M. C. and Kurkov, A. P., "Analytical and Experimental Study of Supersonic Combustion of Hydrogen in a Vitiated Airstream." *NASA TM X-2828*, 1973.
- [24] Cheng, T. S., Wehrmeyer, J. A., Pitz, R. W., Jarret, O. and Northam, G. B., "UV Raman Scattering Measurements in a Mach 2 H_2 -Air Flame for Assessment of CFD Models." Proc. of the *Central States Meeting of the Combustion Institute*, Nashville, TN, 1991.
- [25] Jarret, O. Jr., Cutler, A. D., Antcliff, R. R., Chitsonboon, T., Dancey, C. L. and Wang, J. A., "Measurements of Temperature, Density, and Velocity in Supersonic Reacting Flow for CFD Code Validation." Proc. of the *25th JANNAF Combustion Meeting*, Huntsville, Alabama, 1988.
- [26] Williams, F. A., *Combustion Theory*. Addison-Wesley Publishing Company, Inc., Reading, MA, pp. 358-429, 1965.

Table 1. H_2 - Air Reaction System

No.	Reaction
1	$H + O_2 \rightleftharpoons O + OH$
2	$OH + H_2 \rightleftharpoons H_2O + H$
3	$O + H_2 \rightleftharpoons OH + H$
4	$OH + OH \rightleftharpoons H_2O + O$
5	$H + OH + M \rightleftharpoons H_2O + M$
6	$H + H + M \rightleftharpoons H_2 + M$
7	$O + O + M \rightleftharpoons O_2 + M$
8	$H + O + M \rightleftharpoons OH + M$
9	$H + O_2 + M \rightleftharpoons HO_2 + M$
10	$OH + HO_2 \rightleftharpoons H_2O + O_2$
11	$H + HO_2 \rightleftharpoons H_2 + O_2$
12	$H + HO_2 \rightleftharpoons OH + OH$
13	$O + HO_2 \rightleftharpoons OH + O_2$
14	$HO_2 + HO_2 \rightleftharpoons H_2O_2 + O_2$
15	$H + H_2O_2 \rightleftharpoons H_2 + HO_2$
16	$OH + H_2O_2 \rightleftharpoons H_2O + HO_2$
17	$H + H_2O_2 \rightleftharpoons H_2O + OH$
18	$O + H_2O_2 \rightleftharpoons HO_2 + OH$
19	$OH + OH + M \rightleftharpoons H_2O_2 + M$
20	$OH + OH \rightleftharpoons H_2 + O_2$

Species : $H_2, O_2, H_2O, OH, H, O, HO_2, H_2O_2$ and N_2 (inert)
 M is a third body (all species included)

Table 2. Conditions for Burrows-Kurkov Experiment

	H_2	Air
Mach No.	1.0	2.44
Temperature	254 K	1270 K
Pressure	0.1 MPa	0.1 MPa
Velocity	1216 m/s	1764 m/s
f_{H_2}	1.0	0.0
f_{O_2}	0.0	0.258
f_{N_2}	0.0	0.486
f_{H_2O}	0.0	0.256

Fuel injector height=0.004 m
 Duct height at inlet=0.0938 m
 Duct height at exit=0.1048 m

Table 3. Conditions for coaxial jet experiment

	H_2	Air
Mach No.	1.0	1.97
Temperature	545 K	1180 K
Pressure	0.112 MPa	0.107 MPa
Velocity	1774 m/s	1380 m/s
f_{H_2}	1.0	0.0
f_{O_2}	0.0	0.246
f_{N_2}	0.0	0.545
f_{H_2O}	0.0	0.209

Fuel injector diameter=0.00236 m
 Lip thickness=0.000725 m
 Nozzle diameter(air flow)=0.01778 m

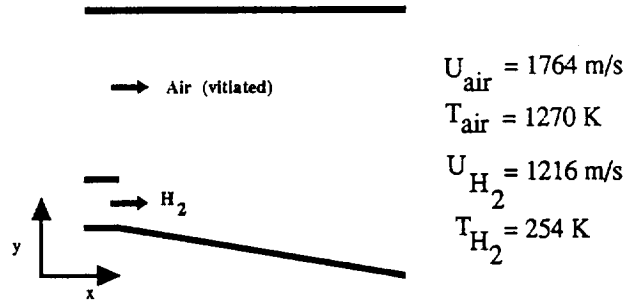


Fig.1 Burrows-Kurkov experiment : schematic

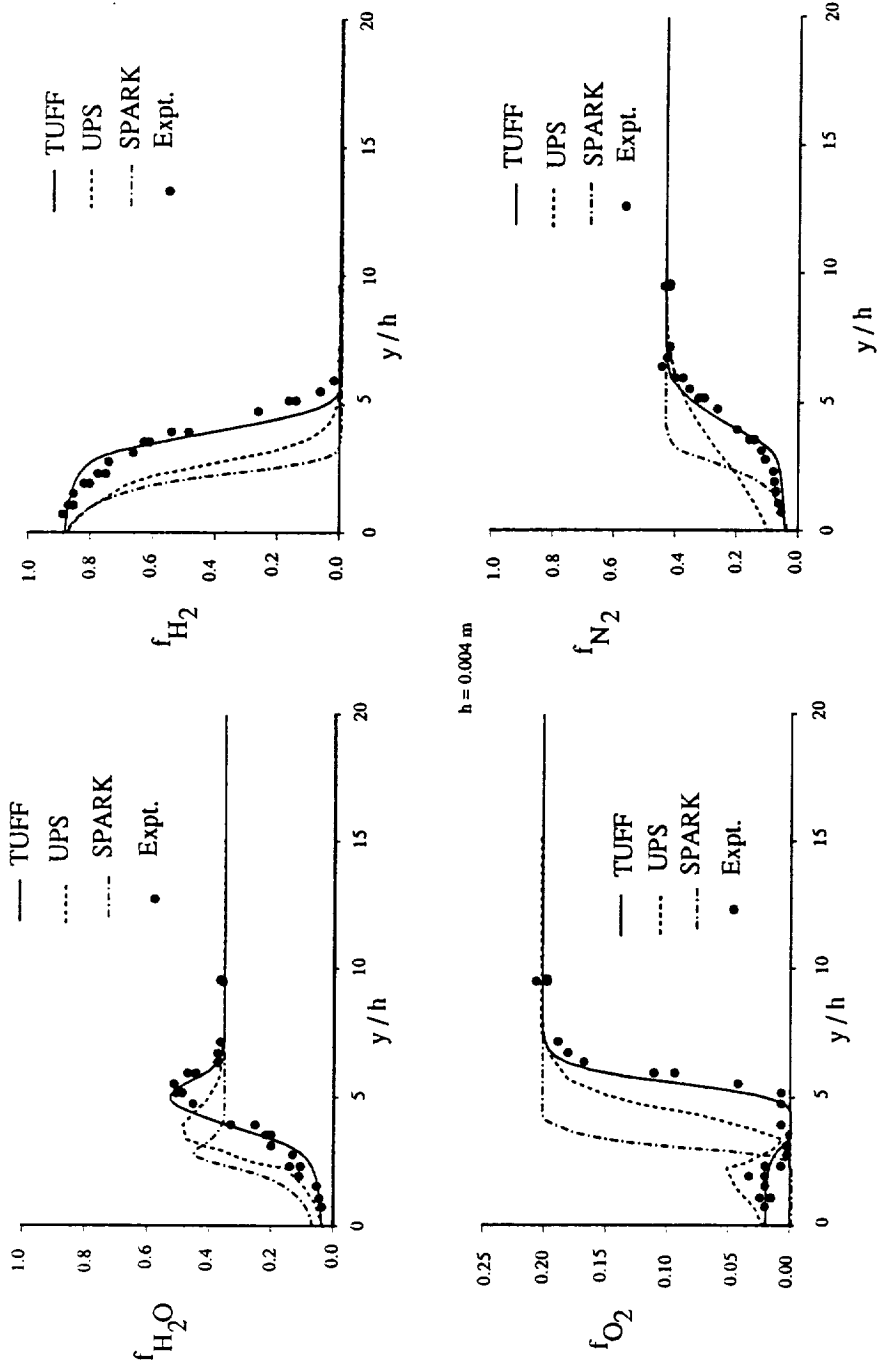


Fig. 2 Burrows-Kurkov expt. : species mole fractions at exit plane

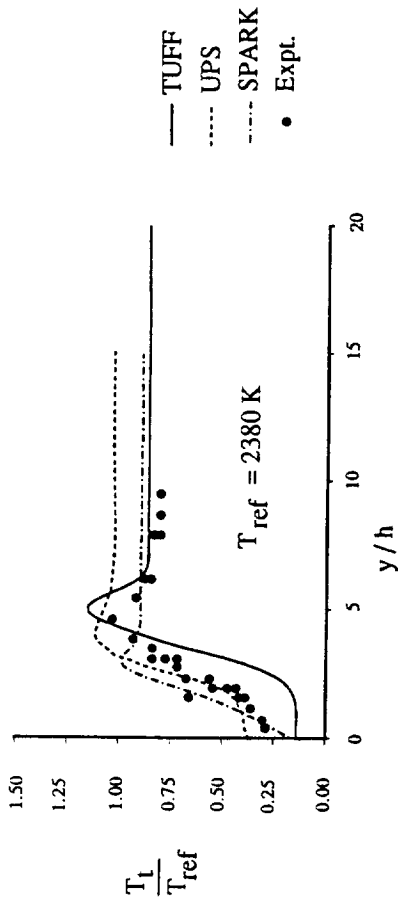


Fig. 3 Burrows-Kurkov expt.: Total temperature at exit

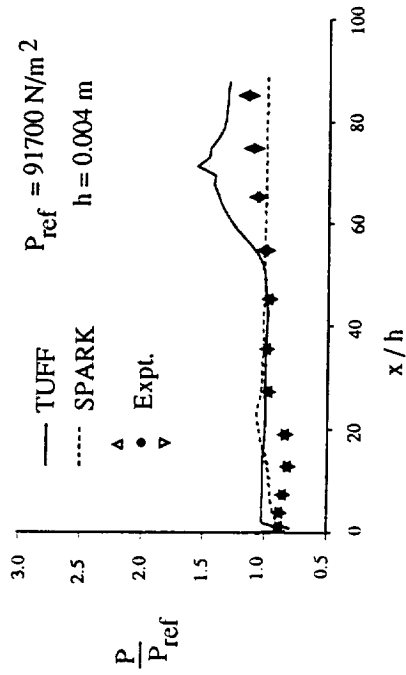


Fig. 4 Burrows-Kurkov expt.: wall pressure

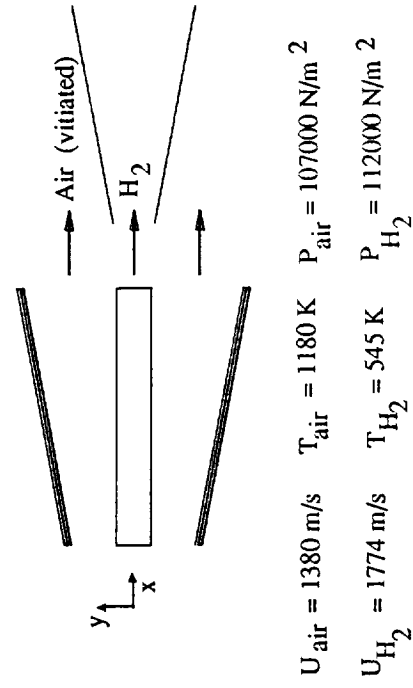


Fig. 5 Coaxial jet case : schematic view

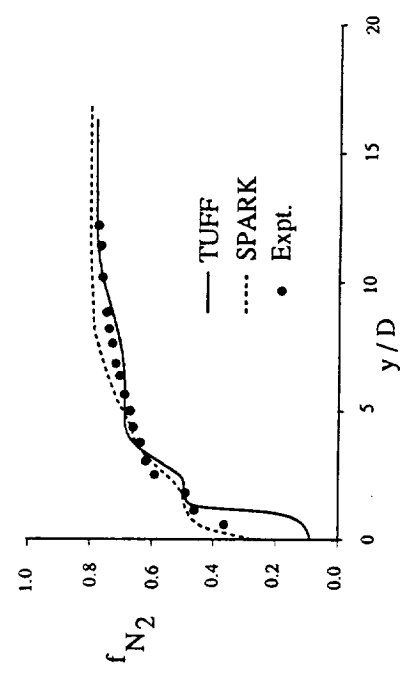
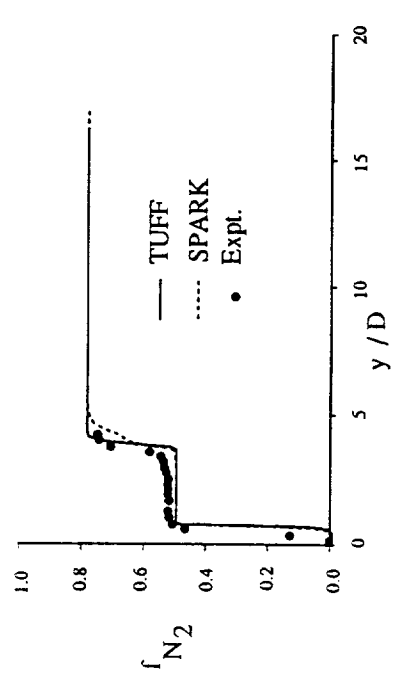
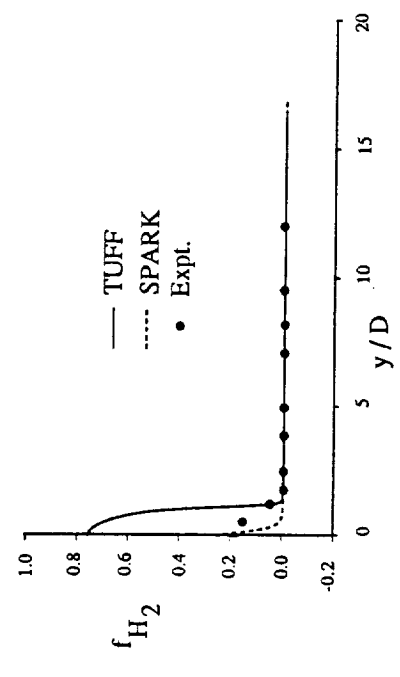
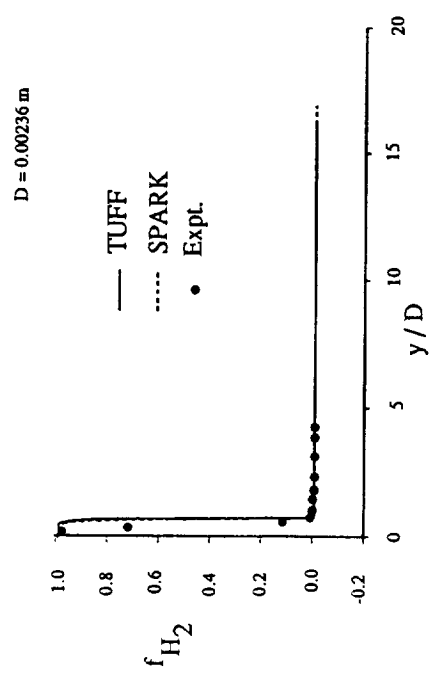
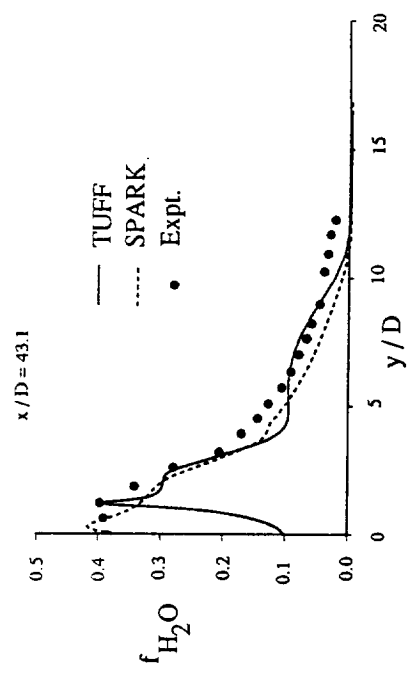
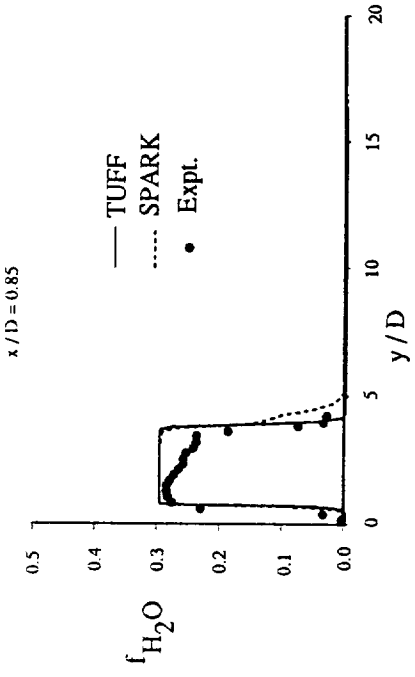


Fig. 6 Coaxial jet case : species mole fractions

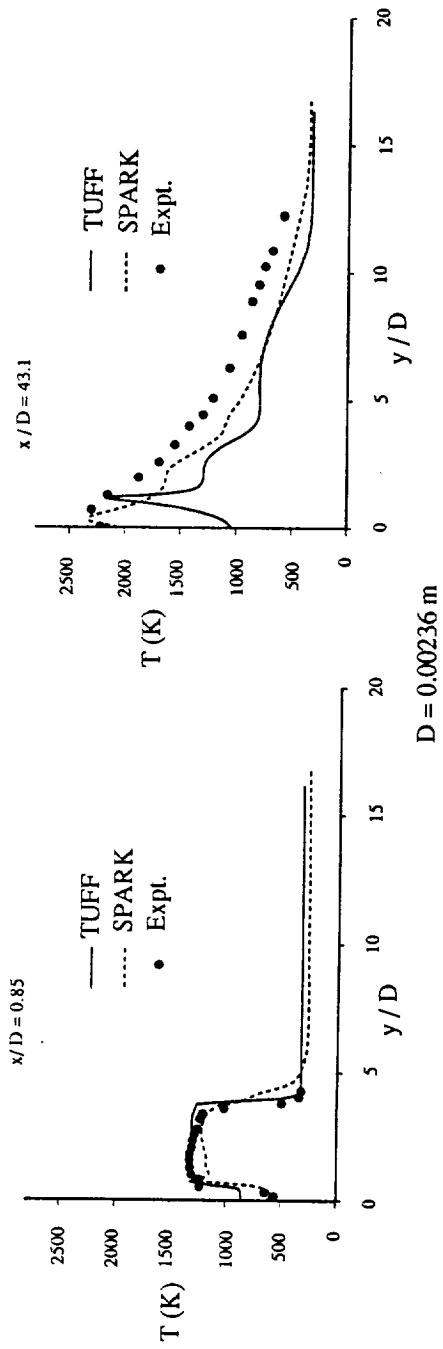


Fig. 7 Coaxial jet case : Temperature

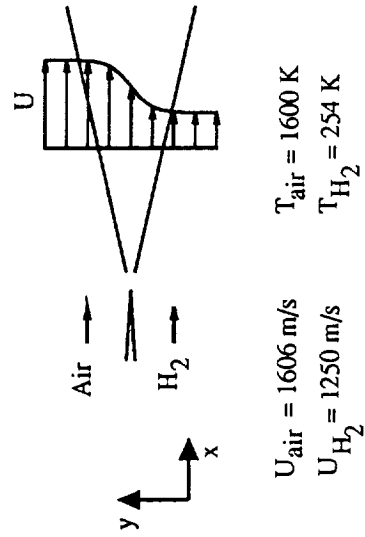


Fig. 8 Mixing layer (2-D) - schematic

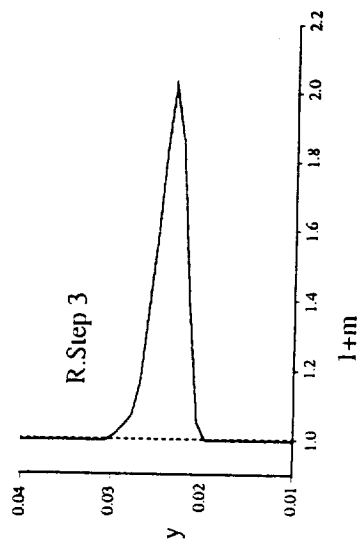
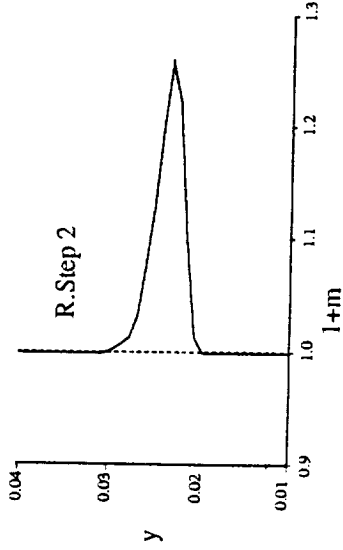
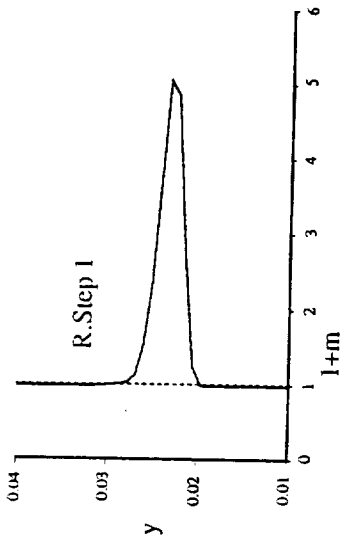


Fig. 9 Effect of temperature fluctuations

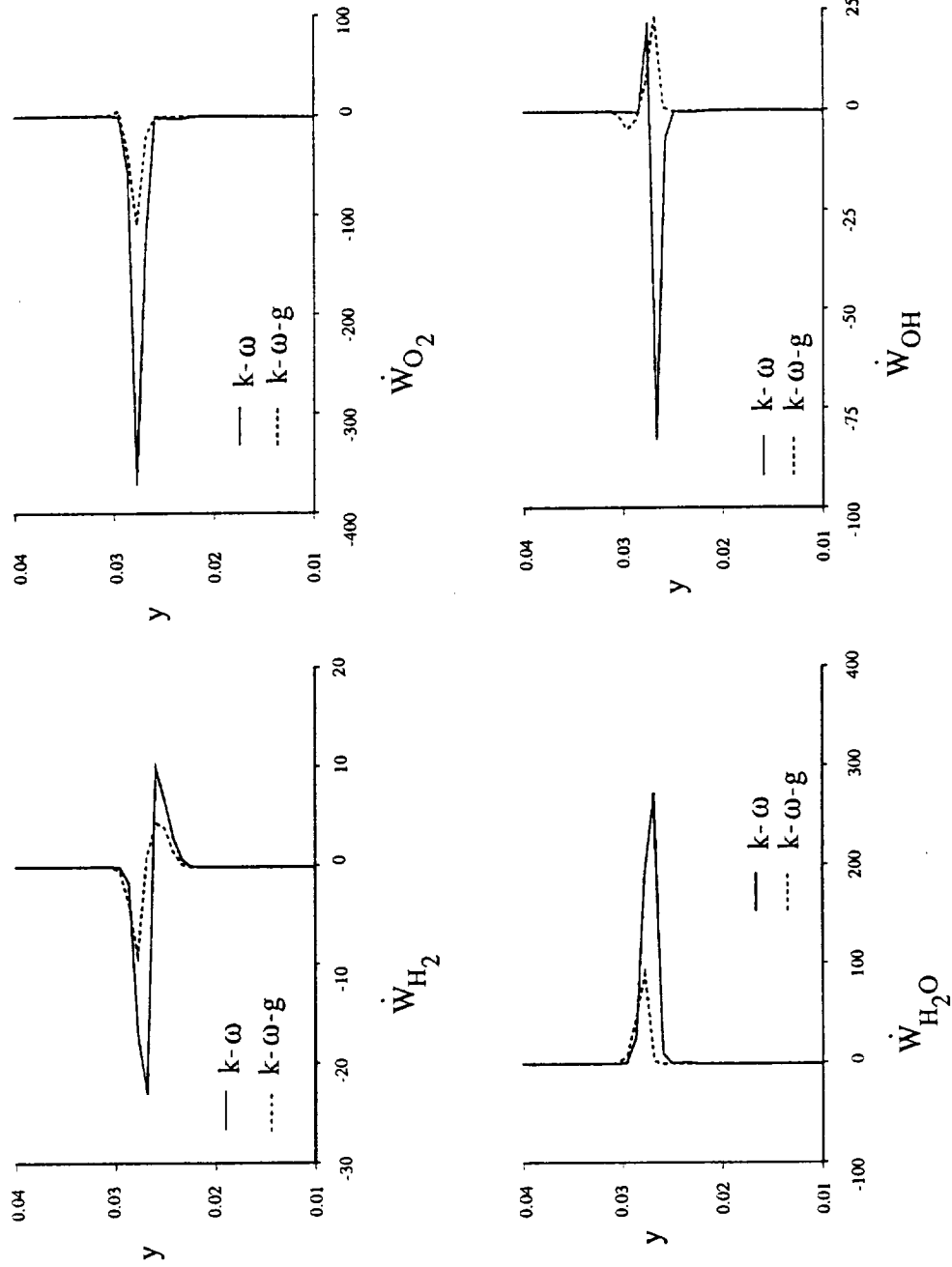


Fig. 10 Effect of Turbulence-Chemistry interactions on species production rate

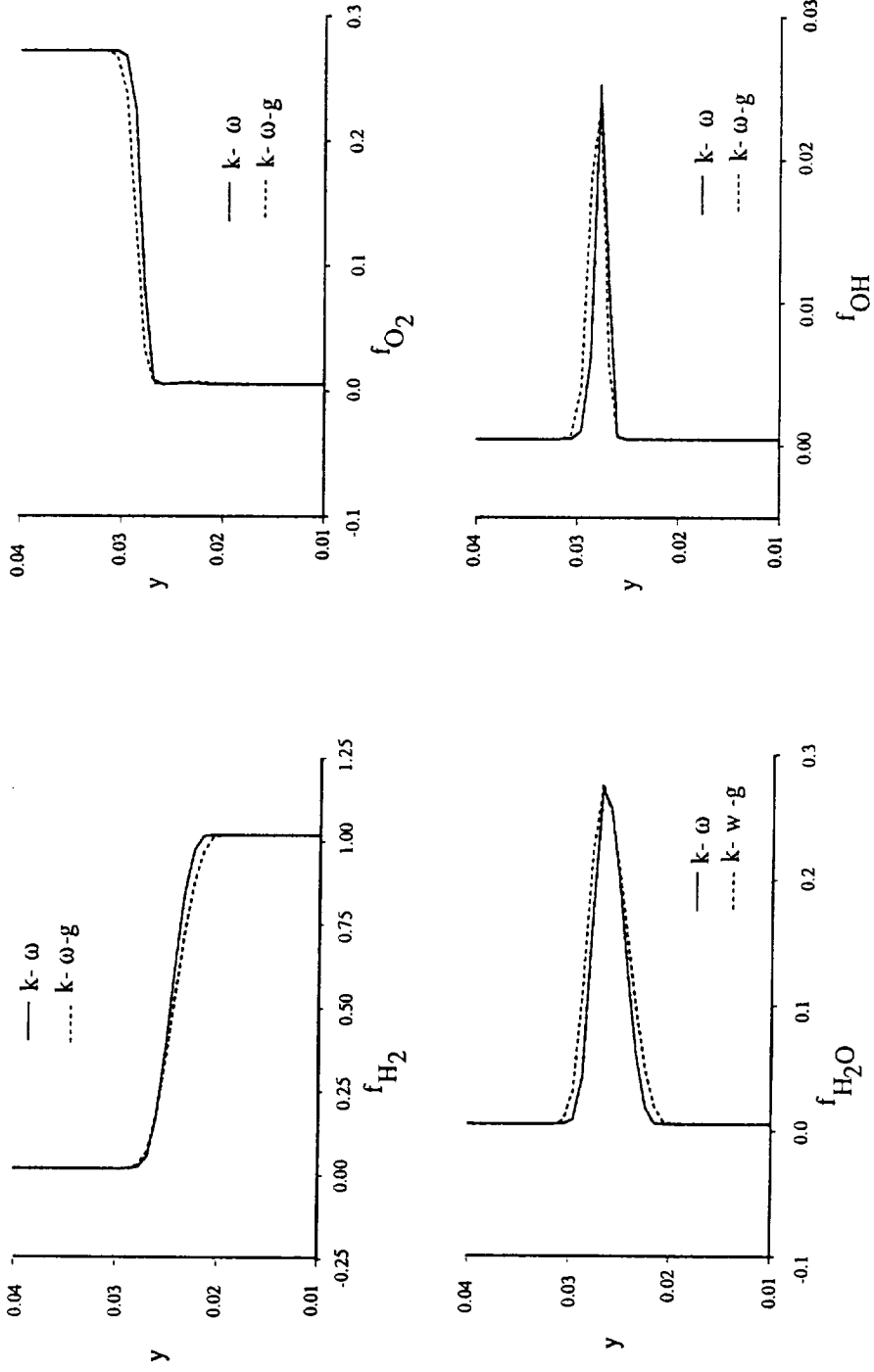


Fig. 11 Effect of interaction model - species mass fractions

APPENDIX - D

Two-Equation Turbulence Model for Compressible Reacting Flows

J. R. Narayan

Reprinted from

AIAA Journal

Volume 31, Number 2, February 1993, Pages 398-401



A publication of the
American Institute of Aeronautics and Astronautics, Inc.
The Aerospace Center, 370 L'Enfant Promenade, SW
Washington, DC 20024-2518

PRECEDING PAGE BLANK NOT FILMED

Two-Equation Turbulence Model for Compressible Reacting Flows

J. R. Narayan*
*NASA Ames Research Center,
Moffett Field, California 94035*

Introduction

ONE of the major areas of current interest where computational fluid dynamics (CFD) is used extensively is the development of advanced air-breathing propulsion systems for hypersonic vehicles. A hydrogen-fueled supersonic combus-

Received Jan. 13, 1992; revision received July 9, 1992; accepted for publication July 10, 1992. Copyright © 1992 by the American Institute of Aeronautics and Astronautics, Inc. All rights reserved.

*Research Scientist, MCAT Institute. Member AIAA.

comparison between the predictions and representative experimental data.^{6,7} Here, C_δ is defined as

$$C_\delta = \frac{d\delta}{dx} \frac{U_1 + U_2}{U_1 - U_2}$$

and C_{δ_0} is its value for incompressible flow. KEPS1 refers to the predictions with compressibility correction included, and KEPS2 refers to the predictions without the correction. RS refers to the Reynolds stress closure predictions.⁹ The scatter among the experimental data is indicative of the nature of available data. The effect of compressibility on the mixing-layer growth rate is to reduce the growth rate with increasing convective Mach number. The two-equation model without the compressibility correction does not predict the reduced growth rate with increasing compressibility. However, the compressible two-equation model does predict this trend very well. The close comparison between the Reynolds stress closure and the $k-\epsilon$ model is important because for complicated flowfields, such as that in the scramjet combustor, the higher-order Reynolds stress closure may be very expensive to use. The predictions agree well with experiment within the scatter in the available data. It must be pointed out that there are other compressibility correction models, similar to the one used here, available today. However, a detailed comparison between such models is beyond the scope of this report.

Mixing between fuel and air and the ensuing chemical reaction is the main focus of study for a configuration such as the scramjet combustor. The presence of turbulence and its effect on the flowfield, especially the mixing aspect of it, is an important part of such studies. A representative mixing dominated reacting flow (hydrogen and air) is considered here. A seven-step, seven-species H_2 -Air reaction model (Table 1) has been used for the finite rate chemistry system considered here.

The test case studied is the reacting coaxial jet problem (Figs. 3) for which the experimental data was obtained by

Evans et al.⁸ In the experiment, hydrogen at a temperature of 251 K was injected (Mach number = 2.0 and velocity = 2418 m/s) along the axis of a supersonic jet (Mach number 1.9, velocity = 1510 m/s) of vitiated air (temperature = 1495 K). The species mass fractions in the airstream are nitrogen = 0.478, oxygen = 0.241, and water = 0.281. The fuel injector has an inner diameter of 0.6525 cm and outer diameter of 0.9525 cm. The outer jet (air) diameter is 6.53 cm. The predicted centerline distribution of hydrogen and the profiles of the major species mass fractions (H_2 , O_2 , H_2O , N_2) at three axial locations are compared with experimental data in Figs. 3. In these figures, D is the fuel injector outer diameter. The predictions agree well with experiment in the region where the mixing effects dominate. The discrepancy between the predictions and experiment immediately downstream of the injector exit may be due to the fact that the conditions set at the inlet location (boundary condition for computations) in the calculations may not match the exact experimental conditions. These conditions are unknown and, hence, could not be used for the calculations. The predicted profiles of water vapor, which is an indication of the extent of reaction, agree reasonably well with the experiment. The location of the peak in the profile is farther into the airstream for the predictions than the experiment indicates. This may be because the interaction between turbulence and chemistry is not fully accounted for in the calculations. As mentioned earlier, the calculations account for only the effect of temperature fluctuations on the reaction rate. In addition, correlations of order higher than 2 were dropped from the model. Also, the experimental data itself may not be very accurate. Given that, the compressible turbulence model used here performs very well in predicting the turbulent reacting flow.

Conclusions

A two-equation turbulence model ($k-\epsilon$) has been modified to be applicable for compressible flows by adapting a compressibility correction model. Computation of compressible mixing layers indicate that the decrease in the growth rate of the mixing layer with increasing convective Mach number is well predicted by the model. Comparisons of the predictions agree very well with available experimental data and the predictions of a compressible Reynolds stress closure. Preliminary studies of reacting mixing problems involving dissimilar gases indicate that the model is well suited for application to such flows. The computations use a model for the effect of temperature fluctuations on the reaction rate in the finite rate chemistry model. Further improvement to the model, especially the effect of turbulent fluctuations in species concentrations on the production rate, is necessary.

Acknowledgments

This work was supported by Theoretical Flow Physics Branch, Fluid Mechanics Division, NASA Langley Research Center under Contract NAS1-18599. The Technical Monitor was J. P. Drummond.

References

- 1Carpenter, M. H., "Three-Dimensional Computations of Cross-Flow Injection and Combustion in a Supersonic Flow," AIAA Paper 89-1870, June 1989.
- 2Narayan, J. R., "A Two-Equation Turbulence Model for Compressible Reacting Flows," AIAA Paper 91-0755, 29th Aerospace Sciences Meeting, Reno, NV, Jan. 1991.
- 3Narayan, J. R., and Sekar, B., "Computation of Turbulent High Speed Mixing Layers Using a Two-Equation Turbulence Model," *Proceedings of the CFD Symposium on Aeropropulsion*, NASA Lewis Research Center, Cleveland, OH, April 1990.
- 4Sarkar, S., Erlebacher, G., Hussaini, M. Y., and Kreiss, H. O., "The Analysis and Modeling of Dilatational Terms in Compressible Turbulence," NASA CR 181959, Dec. 1989.
- 5Jachimowski, C. J., "An Analytical Study of the Hydrogen-Air Reaction Mechanism with Application to Scramjet Combustion," NASA TP 2791, 1988.

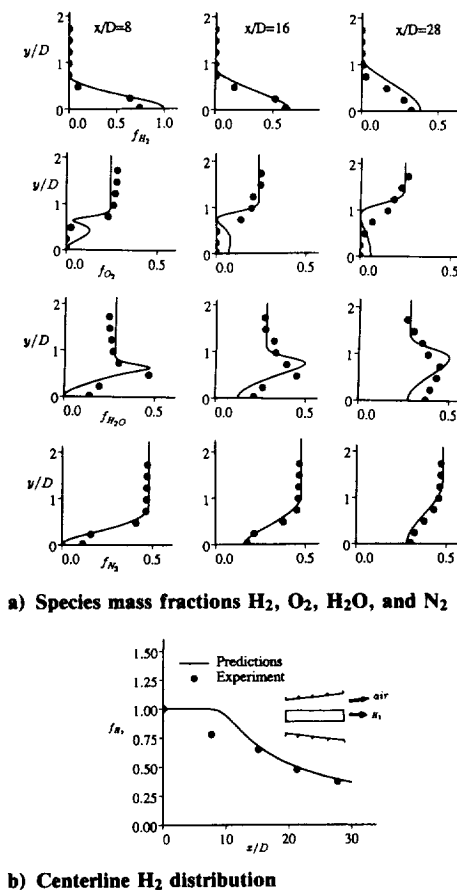


Fig. 3 Reacting flow: coaxial jets.